UNIVERSIDAD POLITÉCNICA DE MADRID
Escuela Técnica Superior de Ingenieros de Caminos, Canales y Puertos

Design, characterization, and testing of high-performance fibre reinforced concrete girders for road bridges

DOCTORAL THESIS

Submitted for the degree of Doctor by:

Rafael Ruiz Maestre
Ingeniero de Caminos, Canales y Puertos

Madrid, 2023

UNIVERSIDAD POLITÉCNICA DE MADRID
Escuela Técnica Superior de Ingenieros de Caminos, Canales y Puertos

Doctoral Degree in Engineering of Structures, Foundations and Materials

Design, characterization, and testing of high-performance fibre reinforced concrete girders for road bridges

D O C T O R A L T H E S I S

Submitted for the degree of Doctor by:

Rafael Ruiz Maestre
Ingeniero de Caminos, Canales y Puertos

Under the supervision of:
Dr. Hugo Corres
Dr. Leonardo Todisco

Madrid, 2023

Title: Design, characterization, and testing of high-performance fibre reinforced concrete girders for road bridges

Author: Rafael Ruiz Maestre

Doctoral Programme: Engineering of Structures, Foundations and Materials

Thesis Supervision:

Dr. Hugo Corres, Doctor Ingeniero de Caminos, Canales y Puertos(Supervisor)

Leonardo Todisco, Doctor Ingeniero de Caminos, Canales y Puertos

External Reviewers:

Thesis Defense Committee:

Thesis Defense Date:

Abstract

High and ultra high-performance steel fibre reinforced concrete (HPFRC and UHPFRC, respectively) exhibit potential for widespread application in bridge construction. These materials enable the use of increased prestressing levels, potentially resulting in a substantial reduction in the amount of concrete and mild steel reinforcement required. This material-saving feature is complemented by a notable enhancement in durability properties compared to conventional concrete. However, despite these potential advantages, the utilization of these materials in bridge construction remains uncommon.

In this context, the Universidad Politécnica de Madrid, in collaboration with ACCIONA's Construction Technology Centre, undertook a research project to explore the application of these materials in the construction of bridges. This thesis is the first result of this collaborative effort.

As first stage, a comprehensive review of the state-of-the-art was coupled with the expertise in bridge design possessed by the research team. This led to the development of different sound structural solutions for girder bridges made of HPFRC and UHPFRC. Subsequently, a 60-metre-span U-girder constructed from HPFRC was chosen as the most promising application for road bridges. Specifically, this U-girder comprised three segments prestressed by unbonded tendons, without the need for conventional shear reinforcement, thanks to the fibre's contribution to shear strength. ACCIONA's Special Concrete Team developed an economically viable HPFRC that met both performance and cost criteria. In fact, it showed a compressive strength of 100-120 MPa and a residual flexural strength ranging from 8 to 10 MPa, not exceeding three times the cost of conventional concrete. This achievement was made possible through a combination of a coarse aggregate fraction, a high content of long steel fibres, and a moderate amount of cement and silica fume.

The second stage focused on addressing the constructability challenges associated with the U-girder. The absence of vertical stirrups in the webs made the formation of a weak plane unacceptable. Therefore, a specific experimental campaign was carried out to investigate the impact of the waiting time between casting successive layers and the distribution of fibres on the performance of HPFRC while adhering to conventional construction techniques.

The third stage of this thesis was dedicated to the evaluation of the shear strength of U-beams without stirrups with unbonded tendons, combining theoretical analysis with experimental observations. Specifically, a comparison of established code provisions with experimental data drawn from technical literature revealed a significant underestimation of shear strength

in such structural elements. This finding prompted a detailed experimental investigation that focused on eight HPFRC I-beams without stirrups and featuring different levels of prestressing. Digital image correlation was employed to capture the exact kinematics of the cracks and, consequently, to gain insights into the various shear-transfer mechanisms influencing shear strength.

In conclusion, this research explored the substantial advantages of cost-affordable HPFRC, with the potential to transform bridge construction practices. This investigation has been conducted in a comprehensive approach, combining conceptual considerations, material development, and experimental testing. Nevertheless, the broader adoption of these materials in bridge construction may require overcoming practical challenges and reevaluating existing standards.

Resumen

El hormigón de altas, o muy altas prestaciones, reforzado con fibras metálicas (HPFRC o UHPFRC según sus siglas en inglés) muestran un alto potencial para su aplicación generalizada en la construcción de puentes. Estos materiales permiten el uso de elevados niveles de pretensado, y reducir la cuantía de acero y hormigón empleados. Este ahorro de material se complementa con una mejora notable en las propiedades de durabilidad en comparación con el hormigón convencional. Sin embargo, a pesar de estas ventajas, la utilización de estos materiales en la construcción de puentes sigue siendo poco común.

En este contexto, la Universidad Politécnica de Madrid, en colaboración con el Centro Tecnológico de Construcción de ACCIONA, llevó a cabo un proyecto de investigación para explorar la aplicación de estos materiales en la construcción de puentes. Esta tesis es el primer resultado de este esfuerzo colaborativo.

En la primera etapa se realizó una revisión exhaustiva del estado del arte desde la experiencia en el diseño de puentes que posee el equipo de investigación. Este análisis condujo al desarrollo de diferentes soluciones estructurales para puentes de vigas de HPFRC y UHPFRC. Posteriormente, se eligió una viga artesa de 60 metros de longitud construida con HPFRC como la aplicación más prometedora para puentes de carretera. En particular, esta viga artesa estaba compuesta por tres segmentos pretensados con tendones no adheridos, y no presentaba refuerzo a cortante convencional, gracias a la contribución de las fibras a la resistencia a cortante. El Equipo de Hormigones Especiales de ACCIONA desarrolló un HPFRC que cumplía con los criterios de rendimiento mecánico y coste. De hecho, mostraba una resistencia a la compresión de 100-120 MPa y una resistencia a flexión residual que oscilaba entre 8 y 10 MPa, sin superar tres veces el costo del hormigón convencional. Este logro fue posible gracias a la combinación de una fracción de árido grueso, un alto contenido de fibras de acero largas y una cantidad moderada de cemento y humo de sílice.

La segunda etapa se centró en abordar los desafíos constructivos asociados con la viga artesa. La ausencia de cercos verticales en el alma hacía inaceptable la formación de una junta fría. Por lo tanto, se llevó a cabo una campaña experimental específica para investigar el impacto del tiempo de espera entre el hormigonado de tongadas sucesivas, siguiendo técnicas de construcción convencionales, y la distribución de las fibras en el comportamiento del HPFRC.

La tercera etapa de esta tesis se dedicó a la evaluación de la resistencia a cortante de vigas artesa sin cercos con pretensado no adherido, contrastando un análisis teórico con

observaciones experimentales. Específicamente, una comparación entre las estimaciones de diferentes normativas con resultados experimentales objetidos de la literatura técnica reveló una subestimación significativa de la resistencia a cortante en estos elementos estructurales. Este hallazgo motivó una campaña experimental detallada que se centró en ocho vigas doble T de HPFRC sin cercos y con diferentes niveles de pretensado. Se utilizó la correlación de imágenes digitales para capturar la cinemática exacta de las fisuras y, utilizando dicha información, obtener las contribuciones de los diferentes mecanismos de transferencia de cortante que influyen en la resistencia al cortante.

En conclusión, esta investigación exploró las ventajas de un HPFRC asequible economicamente, con el potencial de transformar las prácticas habituales de construcción de puentes. Esta investigación se llevó a cabo de una manera integral, combinando consideraciones conceptuales, desarrollo de materiales y ensayos experimentales. Sin embargo, la adopción más amplia de estos materiales en la construcción de puentes podría requerir superar desafíos prácticos y reevaluar normas existentes.

Acknowledgments

En primer lugar, quiero agradecer a mis directos de tesis, Hugo Corres y Leonardo Todisco. Gracias por darme la oportunidad de investigar junto a vosotros, de aprender a pensar y desgranar los problemas hasta entenderlos, siendo consciente de que el resultado de encontrar una respuesta son nuevas preguntas. Vuestros ánimos y ejemplo me han motivado para superar y mejorar en las pruebas. Muchas gracias por vuestra exigencia, constancia e implicación, que me han ayudado a desarrollarme durante estos cuatro años tanto profesional como personalmente. Gracias también a Carmen Andrade por su ayuda en la caracterización de la durabilidad de la mezcla desarrollada, tanto a nivel conceptual como en el laboratorio. Gracias también a Miguel Fernández por ayudarnos a entender mejor el fenómeno del cortante, y de las contribuciones de los diferentes fenómenos físicos implicados.

Gracias al equipo de Acciona Construcción (Jose Poyato, Ignacio Calvo, Stefano Primi, Jose Vera y Antonio Urrecho) por la financiación, sugerencias y revisiones en las reuniones de seguimiento. Una mención especial por su implicación en este trabajo a Valle Chozas, por desarrollar la dosificación del hormigón, y a Jose David Jiménez por su ayuda en la definición de las campañas experimentales y análisis de resultados. Agradecer también al personal del Centro Tecnológico de Acciona por llevar a cabo parte de los ensayos experimentales y a Pretersa y Prenavisa por acceder a hormigonar en sus instalaciones las vigas de la campaña experimental.

Gracias a los profesores del Departamento de Mecánica de Medios Continuos y Teoría de Estructuras. A Javier León por su simpatía, sabiduría y su afán por despertar en nosotros la chispa de la curiosidad. A Alejandro Pérez por su buen humor, disponibilidad, y por ser el comodín a las preguntas más complejas. A Carlos Zanuy por su ayuda (tanto en el laboratorio como conceptual) y por su preocupación por nosotros. Gracias también a los profesores "dinámicos" Iván y Soria. Gracias a Hugo del Valle, por su simpatía y rápida integración.

Muchísimas gracias a los técnicos del laboratorio Isidro y Miguel Ángel, sin ellos el laboratorio se congelaría. Gracias por su paciencia y ayuda para la preparación y realización de los ensayos. Su buen humor y simpatía hacen divertidas las largas horas de laboratorio. También por supuesto muchísimas gracias a Beatriz, por su atención y cuidados a todo el que pasa por el laboratorio.

Muchas gracias también a los estudiantes de TFM que he tenido la suerte de apoyar. Gracias a vosotros esta investigación ha podido enriquecerse. Gracias a Biagio por su alta implicación

en el desarrollo de la herramienta de cálculo de vigas doble T. Gracias a Ligia por su ayuda en el montaje de la base de datos de ensayos a cortante y su simpatía. Gracias a Antonella por su dedicación y a Ignacio por su investigación sobre el DIC.

Muchas gracias a los amigos y compañeros del laboratorio. A Carlos, mi mejor colega, gracias por tu apoyo incondicional, tu buen humor, tu paciencia y tu disponibilidad para ayudarme con cada demostración analítica que se me atascaba, mil gracias. A Benny, la aguja que conseguía que no perdiéramos el norte. Gracias por tu alegría, consejos, bromas sorprendentes, y por tirar del grupo en tantísimas ocasiones. Gracias a Marck, el extremo tanto analítico como pasional, gracias por tu tranquilidad, por tu ejemplo de constancia, empeño y superación. Siempre nos quedará Enresa. Muchísimas gracias a los tres por vuestra amistad.

Gracias a Maleja por su implicación personal, simpatía hacia todos y empeño en crear familia, sin ti el laboratorio no sería el mismo. Gracias también a Javier Naranjo, con sus raquetas a la espalda, atento y tranquilo. Navjit Kaur, thank you for your friendship, for almost a year of sharing gossips, tips, failures and achievements in the department, you are the best. Gracias a Xavier Cárdenas, por compartir el despacho primigenio junto a Leonardo, por ser un ejemplo de investigador e ingeniero e iluminarme con consejos de toda índole. Gracias también a: Mar, Rolo, Borja, Gonzalo, Fernandito, Belen, Luis, Christian Barrera y Christian Gallegos, Alfi, Miriam, y tantos otros que habéis pasado por el departamento. Gracias a todos vosotros se ha sentido un hogar estos años.

Muchas gracias a mis amigos fuera de la Escuela: Enrique y Pedro, los ingenieros sevillanos, Luis y los médicos, los de siempre cordobeses y los madrileños. Gracias por interesaros siempre por mí a pesar de que tuviera muchas veces la cabeza llena de hormigón.

Muchísimas gracias también a Fr. Nacho y a la Comunidad del Santo Niño de Cebú, donde siempre me he sentido muy acogido. Millones de gracias a mis padres y hermanos. A mi madre por aguantar incrédula mis inseguridades. A mi padre por ser mi ejemplo profesional y personal. Gracias Bernardo por apoyarme en la distancia y Fátima gracias por haberte embarcado en tu aventura madrileña, gracias por vuestra gran ayuda. Vuestros abrazos me dan fuerzas para subir montañas. Por último, siempre agradecido en cada paso a Paloma. Por escuchar mis penas y alegrías, y esforzarte por entender las complejidades de esta tesis. Por quererme como soy, animándome a ser cada día un poco mejor. Ánimo ahora que te toca a ti la tesis. Y, por supuesto, gracias a Dios por ponerme esta oportunidad y a cada persona en mi vida.

Contents

List of Figures

List of Tables

Nomenclature

Latin lower case

a shear span

a_a dimension of support plate

$a_{cs,0}$ effective shear span with respect to the control section without considering effect of prestressing or external load

a_f dimension of loading plate

b width of flange

b_a distance between support axis and beam end

b_{ft} width of tension flange

b_w width of web

c cement quantity

c_c minimum concrete cover

c_p distance between point loads

d effective depth

d_f fibre diameter

d_{g0} reference size

d_{pbot} effective depth of bottom prestressing steel

d_{ptop} effective depth of top prestressing steel

d_{pweb} effective depth of prestressing steel in web

e_p eccentricity of the prestressing force or of the external load that produces the compressive axial force with respect to the centre of gravity of the cross-section considered as positive towards the tensile side.

f diameter of the flow table test

f_{1c} uniaxial compression strength of concrete

f_{1cm} mean value of the uniaxial compression strength of concrete

f_c compressive strength of concrete

f'_c specified minimum 28-day compressive strength

$f_{c,cu}$ cube concrete compressive strength

$f_{c,cyl}$ cylinder concrete compressive strength

f_{cd} design value of compressive strength of concrete

f_{ck} characteristic value of compressive strength of concrete

f_{cm} mean value of compressive strength of concrete

f_{ct} axial tensile strength of concrete

f_{ctd} design value of axial tensile strength of concrete

f_{ctk} characteristic value of axial tensile strength of concrete

f_{ctm} mean value of axial tensile strength of concrete

f_{Ftsk} characteristic value of post-cracking strength for seviceability crack opening for fibre reinforced concrete

f_{Ftu} ultimate post-cracking strength for fibre reinforced concrete

f_{Ftuk} characteristic value of the ultimate post-cracking strength for fibre reinforced concrete

f_L limit of proportionality for fibre reinforced concrete

f_{Lm} mean limit of proportionality for fibre reinforced concrete

f_{pd} design tensile strength of prestressing steel

f_{pu} ultimate tensile strength of prestressing steel

f_{py} yield strength of prestressing steel

f_R value of residual post-cracking strength

f_{R1} residual strength at a CMOD equal to 0.5 mm for fibre reinforced concrete

f_{R1k} characteristic value of residual strength at a CMOD equal to 0.5 mm for fibre reinforced concrete

f_{R1m} mean value of residual strength at a CMOD equal to 0.5 mm for fibre reinforced concrete

f_{R2} value of residual strength at a CMOD equal to 1.5 mm for fibre reinforced concrete

f_{R2m} mean value of residual strength at a CMOD equal to 1.5 mm for fibre reinforced concrete

f_{R3} residual strength at a CMOD equal to 2.5 mm for fibre reinforced concrete

f_{R3k} characteristic value of residual strength at a CMOD equal to 2.5 mm for fibre reinforced concrete

f_{R3m} mean value of residual strength at a CMOD equal to 2.5 mm for fibre reinforced concrete

f_{Rm} mean value of residual post-cracking strength as the mean value from CMOD equal to 0.5 to 2.5 mm for fibre reinforced concrete

f_{yk} characteristic value of yield strength of reinforcing steel in tension

h height of beam

h_c height of the beam and the slab

h_f height of flange

h_{ft} height of tension flange

h_{hbot} height of bottom haunch

h_{htop} height of top haunch

h_s height of the slab

h_w height of the web

k_{dg} aggregate size influence parameter

l_f fibre length

t_{eff} effective beam thickness

w/c water to cement ratio

x height of the neutral axis from the top fibre of the composite beam

z internal lever arm

z_{c2} distance of CGS from top fibre

z_{pbot} distance of bottom strands from CGS

z_{ptop} distance of top strands from CGS

z_{pweb} distance of web strands from CGS

Latin upper case

A_c gross area of concrete section

A_{cv} inclined shear crack area

A_p area of prestressing steel

A_{pbot} area of bottom prestressing steel

A_{ptop} area of top prestressing steel

A_{pweb} area of web prestressing steel

D_{low} declared value of the lower sieve size D of the coarsest fraction of aggregates in the concrete

D_{Max} declared value of the upper sieve size D of the coarsest fraction of aggregates in the concrete

E_c Young modulus of the concrete

E_p Young modulus of the prestressing steel

I second moment of inertia

L span length

M_{Ed} design value of applied moment at ULS

M_{Rd} design value of resistant moment

$M_{u,test}$ bending moment at failure with self-weight

P_{bot} prestressing force of strands at bottom flange

P_{top} prestressing force of strands at top flange

P_{web} prestressing force of strands at web

S first moment of area above and about the centroidal axis

V_{cr} shear force at bending crack initiation

V_{Ed} design value of applied shear at ULS

V_f fibre content

V_{Rd} design value of resistant shear

V_{sh} first shear cracking

$V_{u,cal}$ calculated shear strength

$V_{u,test}$ shear force at failure with self-weight (from report)

Greek lower case

ε_{c3} elastic limit strain of the bilinear diagram

ε_{cu3} ultimate strain of the bilinear diagram

ε_{fu} strain of non-metallic reinforcement at maximum force in tension

ε_{pu} ultimate strain of the prestressing steel

ε_{py} yield strain of the prestressing steel

ε_x longitudinal strain at the mid-depth of the effective shear depth

η strength reduction coefficient for the fibre strength contribution to shear

η_{cF} strength reduction coefficient for shear component of concrete

η_φ strength reduction coefficient for the passive reinforcement contribution due to the interaction between fibre and conventional reinforcement

γ_c partial safety factor for concrete material properties

γ_F partial safety factor for fibre reinforced concrete

γ_{mod} model safety factor (ratio between the $V_{u,test}$ and the $V_{u,cal}$)

κ shear span to effective depth ratio

λ slenderness ratio

λ_f shape factor (ratio between l_f and d_f)

ρ_{pw} geometrical reinforcement ratio of prestressing steel under tension related to b_w

σ_{cp} mean concrete compressive stress due to prestressing force

$\sigma_{ct,max}$ concrete tensile strength limit at SLS

σ_{fu} ultimate direct tensile strength of fibres

σ_{pp} prestressing stress

τ_{Ed} design value of applied shear stress

τ_u shear stress at failure

τ_{uagg} shear stress contribution of fibres

$\tau_{u,cal}$ calculated shear stress at failure

τ_{ucc} shear stress contribution of fibres

τ_{ucF} shear stress contribution of fibres

τ_{udow} shear stress contribution of fibres

$\tau_{u,test}$ experimental shear stress at failure with self-weight

Acronyms

AASHTO American Association of State Highway and Transportation Officials

CC Conventional Concrete

EC2 Eurocode 2

FHWA Federal Highway Administration

fib *Fédération internationale du béton*

FRC Fibre Reinforced Concrete

HPFRC High-Performance Fibre Reinforced Concrete

KITC Korean Institute of Civil Engineering and Building Technology

MC2010 Model Code 2010

PCI Precast/Prestressing Concrete Institute

SLS Serviceability Limit State

UHPFRC Ultra-High Performance Fibre Reinforced Concrete

ULS Ultimate Limit State

1

Introduction

1.1 Motivation

In 2015, the United Nations published "the 2030 Agenda for Sustainable Development", which highlights as one of its main objectives "...heal and secure our planet.", as articulated in its Preamble [1]. Figure 1.1 illustrates the sustainable development goals which define the role of a Civil Engineer by its responsibility to implant industry, innovation, and infrastructure, contributing to the creation of sustainable cities and communities through responsible consumption and production practices.

Figure 1.1: Sustainable development goals [1].

This thesis deals with concrete, the most employed material in the world, after water [2]. This is due to the widespread availability of its raw materials, its comparatively low production cost, high structural efficiency, and its potential for use in both high- and low-tech building contexts. These factors substantiate the expectation of a significant increase in its consumption in the coming decades, particularly in developing countries where there is a growing demand for infrastructure and improved housing conditions. As consequence, concrete serves as a fundamental cornerstone for global development. Figure 1.2 shows the historical production of cement per capita on a global scale. With concrete and cement

production being proportional, both have experienced a threefold increase in the last thirty years [3].

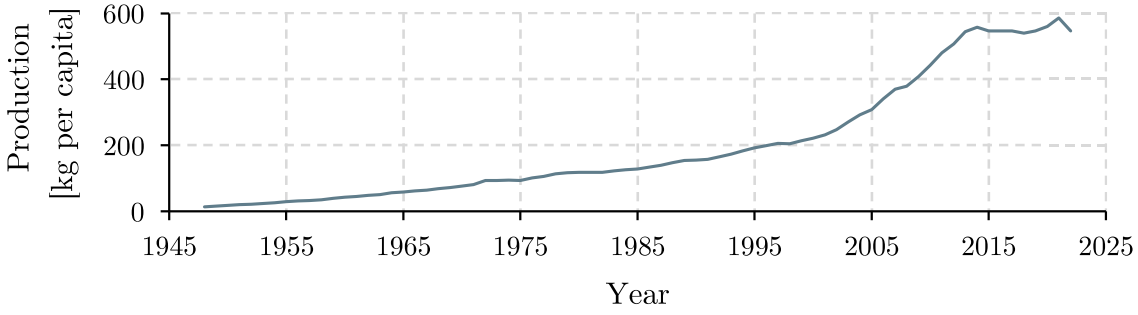

Figure 1.2: Historical growth in cement production per capita. Adapted from [3].

However, the concrete industry faces a significant drawback due to its substantial environmental impact, contributing between 5% and 8% of the total human CO2 footprint. Therefore, a markedly different approach to concrete construction is imperative to ensure its role as a sustainable driver of development. This represents a global undertaking necessitating a multidisciplinary effort at various levels, encompassing both material considerations and, notably, the development of efficient structures for practical applications. In this context, the utilization of high- and ultra-high performance fibre reinfroced concrete (HPFRC and UHPFRC) has emerged as a promising solution for mitigating the CO2 footprint associated with cement-based materials. Decades of research upon FRC and UHPFRC have culminated in the formulation of several standards, recommendations, and guidelines covering these materials. However, these materials are not widely employed in the construction of bridges.

In this context, in 2019 the Structural Engineering Research Group of the Universidad Politécnica de Madrid, in collaboration with ACCIONA, started a research project in which this thesis is framed. The multidisciplinary team, bringing together, structural designers, material developers, and researchers, was able to design a taylor-made concrete for the developed structural component. The primary objective was to explore novel structural solutions using UHPFRC. Following preliminary discussions, the team decided to focus on girders for road bridges, a choice driven by their repeatability and potential impact.

1.2 Objectives

The general objective of the thesis is to develop cost-competitive HPFRC and/or UHPFRC girders for road bridges compared to conventional solutions. To pursuit this goal, the study brings together insights from material developers, structural designers and execution experts.

In particular, the specific objectives of this thesis are as follows:

- To analyze standards, documents, and guidelines which cover the use of FRC, HPFRC, and UHPFRC in structural elements. This effort will mainly focus on identifying disparities among references that address distinct ranges of application, especially concerning compressive strength classes.
- To compile international experiences with the implementation of UHPFRC and HPFRC to road girder bridges, with the intent of drawing inspiration for the proposed solutions.
- Conceive different solutions for road girder bridges considering different cross-sections. In addition, carefully designing each solution regarding its longitudinal reinforcement. Employing a parametric analysis to study the influence in the material consumption of the girders of key factors (span length, concrete compressive class, slenderness, number of beams).
- To identify a road girder bridge solution that achieves, at a minimum, comparable initial cost and material consumption as a conventional concrete bridge with similar span length and deck width.
- To define a taylor-made concrete mix that fulfils the requirements for the selected road girder bridge solution.
- To detect potential risks in implementing the novel material into the proposed solution. These risks should be addressed by the research team in order to create guidance for practitioners.
- To critically analyze the formulations involved in the design of the proposed solution. This includes exploring analogous structural elements and emphasising databases collecting structural experimental campaigns made of FRC, HPFRC, and UHPFRC.

1.3 Methodology

In order to meet the objectives four methodological lines have been followed: the design of structural elements, the analysis of mixes at the material level, the study of the constructability aspects and the study of the shear strength of the structural elements.

The first line of research was centred around the design of road bridges. These bridges utilized girders made of UHPFRC or HPFRC instead of conventional concrete, aiming to reduce concrete consumption and replace, as far as possible, conventional reinforcement with steel fibres. This first design stage consisted of three distinct analyses.

The UPM team designed alternatives for each analysis, which were subsequently discussed in collaboration with the Acciona team. Following these discussions, the girder's cross-sections or the spans of the bridges were set for the next analysis.

In the first analysis, UHPFRC I-girders alternatives were proposed for a reference project with a span of 40 m with posttensioned I-girders of conventional concrete. In the second, a parametric analysis was carried out in which 81 road bridges with I-girders were designed. The parameters to be studied were compressive strength of the girders (C80, C100 and C120), slenderness (17, 20, 23), span (20, 40, 60 m) and number of beams (from 3 to 5).

In the third analysis, different post-tensioned U-beam alternatives for a span of 60 m were designed. To conclude the decision between the proposed alternatives, a comparison was made in terms of material consumption with conventional concrete solutions for similar spans and deck widths. The initial cost of the material consumption of each alternative allowed, finally, to accept or reject the solution as the object of study in the subsequent stages of the research.

Ultimately, the selected solution involved a 60 m span, divided into three segments of 20 m each, using two precast girders made from HPFRC. The precast beams would be externally postensioned by 6 external tendons. Finally, the conventional stirrups were replaced by steel fibres.

The second line of research aimed to characterize the different HPFRC mixes developed by Acciona's materials team, tailored specifically for the chosen structural solution. This taylor-made concrete was required not only to satisfy the strength requirements dictated by the structural solution but also to exhibit optimal workability to flow through the different containers and subsequent molding within the formwork.

Furthermore, a critical criterion was established mandating that the HPFRC remain within

a cost range of 2.5-3.0 times that of a C70/85. Using previous knowledge from manufacturing high-performance (C90/105) and ultra-high performance (C130/145) concretes (both without fibres) in conjunction with insights culled from an extensive collected database that included specifications for steel fibre reinforced cementitious materials, Acciona's materials team developed an HPC of C100/115.

Subsequently, varying the content and type of steel fibres added to the HPC, 9 different HPFRCs were developed. The compressive and flexural strengths of the 9 mixtures were characterised according to current standards, as well as their workability using the flow table test.

The third line of research addressed the analysis of the potential risks associated with the substitution of traditional stirrups with steel fibres. An inherent vulnerability could arise from the formation of a weakened plane, stemming either from a cold joint existing between layers resulting from successive concrete pourings or from inadequate distribution of the fibres. Therefore, a number of constructability aspects to be studied were identified regarding the casting of the U-girders: number of pours, pouring methodologies, waiting times between pours, and, if applicable, compaction procedures.

Through different experimental campaigns, the investigation ventured into gauging the impact of different waiting times between consecutive batches on the post-cracking flexural strength. This exploration commenced with prismatic specimens according to the EN 14651 [4] cast in varied orientations (both vertical and horizontal), where the positioning of the cold joint in relation to the notch was variably manipulated. After testing these specimens, their flexural post-cracking strengths suggested the use of poker vibrators in subsequent phases of the research to break the discontinuity planes between successive layers, to allow fibres to orientate perpendicular to this plane.

Furthermore, a judicious selection of permissible waiting periods was made to ensure that the flexural strength remained uncompromised. To utilise conventional formwork for concreting of U-beams, two L-shaped panels were cast, with varying waiting times between the casting of the bottom slab and the first layer of the web. The waiting time must allow the bottom slab to withstand the internal compaction of the second layer without liquefy, while the same compaction should allow fibres to locate through the layer between both pourings.

The third elements of this line of research were two rectangular panels representing the web of the U-girders. Thanks to the experience of concreting them, and the subsequent study of prismatic samples and cores extracted from them, it was possible to draw conclusions

regarding the post-cracking flexural strength of the panels, and the distribution and orientation of fibres.

The fourth line of investigation was raised during the first line of research. When collecting the formulations to obtain the shear strength of prestressed FRC, HPFRC and UHPFRC beams, notable disparities came to light between the formulations proposed for FRC and those tailored for UHPFRC. Moreover, there was no adequate transition between them. Furthermore, the utilization of certain formulations proved to be inadequate due to the application of an external unbonded prestressing system in the proposed solution.

Therefore, a comprehensive experimental campaign was devised, focusing on prestressed I-beams without stirrups. The central aim was to empirically determine their shear resistance, through the testing until failure in the laboratory of the UPM. The concreting of the beams was carried out in the precast factory of Pretersa and Prenavisa located in Teruel. The casting of these beams unfolded within the precincts of the Pretersa and Prenavisa precast factory located in Teruel.

The opportunity to extend the scope of this research to an operational precast facility, facilitating the casting process, yielded invaluable insights. This engagement afforded us a practical perspective, allowing for the synthesis of conclusions in accordance with the real-world dynamics of concrete production.

Throughout the research, emphasis was placed on a comprehensive review of the contemporary state-of-the-art prior to each successive phase. This diligent approach ensured a well-informed understanding that underpinned each step undertaken.

Moreover, recognizing the inherent significance of disseminating the acquired knowledge, different papers in scientific journals and congress were written.

1.4 Thesis organization

The main body of this thesis, Chapter 3 to 7, is organized as a compendium of papers published by the author (refer to Appendix F for further details). This main part is contextualized by an introduction (Chapter 1), and followed by a summary of the main conclusions of this work (Chapter 8).

The content of each chapter is described in the following.

- Chapter 1: Introduction

  This chapter presents the motivation of the thesis, states the research objectives, provides the methodology followed, and describes the state-of-the-art related with the implementation of HPFRC and UHPFRC into road bridges worldwide.

- Chapter 2: Conceptual design of UHPFRC and HPFRC girders for road bridges

  In this chapter, a typological analysis of I- and U-girder road bridges making use of HPFRC and UHPFRC is critically presented and discussed. The chapter also provides with the detailed structural analysis for the selected HPFRC U-girder bridge.

- Chapter 3: Parametric analysis of I-girder bridge decks

  This chapter investigates the influence of design variables on the material consumption of simply supported HPFRC I-girders for road bridges. The variables explored are: i) the concrete class (C80/95, C100/115, and C120/140); ii) the number of beams (from 3 to 5); iii) the girder span-to-depth ratio (17, 20, and 23); and iv) the bridge span (L) (20, 40, and 60).

- Chapter 4: Specific considerations on fibre reinforced concretes

  This chapter focuses first on the FRC, HPFRC, and UHPFRC mixes formulations. Examples are described in detailed and a database collected from the scientific literature is analysed. The second part of the chapter describes how conventional design of girder bridges is modified when adopting these new materials.

- Chapter 5: Mix development, material characterization and constructability aspects

  Chapter 5 describes the development of a cost-effective, HPFRC for the construction of the 60 m-span U-girder road bridge without stirrups in the webs described in Chapter 2. Furthermore, it is provided an extensive experimental campaign to cast the U-girder following the conventional casting techniques involving casting prismatic

samples, L-shaped and rectangular-shaped panels to represent different parts of the U-girder.

- Chapter 6: Database of shear tests for prestresses FRC beams without vertical stirrups

  This chapter presents a database collecting 80 experimental shear tests on prestressed fibre reinforced concrete beams without stirrups. This database is used to verify several codes and recommendations: i) Model Code 2010, ii) draft version of Model Code 2020, iii) draft version of the new Eurocode 2, and iv) Spanish National Code. Finally, results are compared with those achieved from two larger databases of beams with similar features but without prestress.

- Chapter 7: Experimental campaign of prestressed HPFRC beams without stirrups

  This chapter presents the results of an experimental investigation on seven full-scale prestressed HPFRC beams. The beams were tested with different levels of prestressing and were instrumented with refined optical DIC measurements. Using the experimental data, the crack development and kinematics are investigated in detail, as well as the associated contributions of the potential shear-transfer actions.

- Chapter 8: Conclusions and further research

  Chapter 8 remarks general conclusions and specific contributions of this work. Additionally, important directions for future studies are illustrated.

Six appendixes are included in this thesis. In Appendix A the technical drawings defining the HPFRC U-girder road bridge proposed in Chapter 2 are provided. Furthermore, in Appendix B the database of the mixes discussed in Chapter 4 is included. Also, in Appendix C the database collected of shear tests for prestresses FRC beams without vertical stirrups analyzed in Chapter 6 is presented, together with the results of the application of the formulations described in the same chapter presented in Appendix D. In addition, in Appendix E the technical drawings of the HPFRC I-beams without stirrups of the experimental campaign are given. Finally, the Appendix F collects the publications resulting from this thesis.

1.5 Background

1.5.1 Introduction

This section describes international experiences in the implementation of UHPFRC and HPFRC in road bridges, illustrating different approaches in material development, structural design solutions, and cooperation between designers, constructors, and local administrations.

It should be noted that certain pioneering countries have not been included in this state-of-the-art, such as Canada, China, or Japan. The following documents are recommended for readers who wish to expand their knowledge of their experiences and learn more about those already included here: Bulletin 105 Fibre Reinforced Concrete State-of-the-Art report [5], Ultra-High Performance Concrete UHPC Fundamentals - Design - Examples [6], International Perspective on UHPC in Bridge Engineering [7], and French recommendations for UHPFRC [8].

1.5.2 France

The first two road bridges with UHPFRC girders were the overpasses at Bourg-lès-Valence in France (OA6 and OA4). They were built in 2001 and each consists of two spans of approximately 22 m and a deck width of 12.70 m [9].

The French Government, being the owner of the bridges, supervised both their design and construction, with assistance from the Service d'Etudes Techniques des Routes et Autoroutes (SETRA) and the Centre d'Etudes Techniques de l'Equipement (CETE) of Lyon. The bridges were constructed by Eiffage Construction following a performance-based tender developed within the framework of an 'Innovation Charter' signed by the National Roads Department and the National Public Works Federation [9].

The material used was an UHPFRC named 'Béton Spécial Industriel' (BSI). In an effort to promote awareness of UHPFRCs, the publication for this application included the UHPFRC mix, as shown in the Table 1.1.

Table 1.1: Mix of BSI concrete [9].

Component	Content [kg/m^3]
Cement	1114
Silica fume	169
Aggregate (0-6 mm)	1072
Superplasticizer	40
Water	209
Steel straight fibre (l_f=20 mm, λ_f=66)	234

The use of high cement contents (about 4 times that used for a C30/37) in addition to a high silica fume content allows for an f_{ck} of 175 MPa to be achieved. Additionally, thanks to the addition of 3% steel fibres, direct cracking tensile strengths of f_{ctk}=8 MPa, and post-cracking f_{ctk}=9.1 MPa, are achieved.

Figure 1.3 depicts the cross-section of the bridge. The only passive reinforcement in the 5 girders is situated in their transverse and longitudinal joints as well as in the anchorages of the furniture. The 5 pi-beams are interconnected by joints, also built from UHPFRC. The slenderness of this application is 25. The web of the beams has a thickness of 110 mm, and the effective depth (t_{eff}) of these overpasses, thanks to the innovative pi-section and the use of UHPFRC, measures only 25 cm.

The longitudinal prestressing consists of bonded strands: 26 strands for OA6 and 30 strands for OA4, resulting in an amount of 11.7 kg/m^2 and 13.5 kg/m^2 per square metre of deck, respectively.

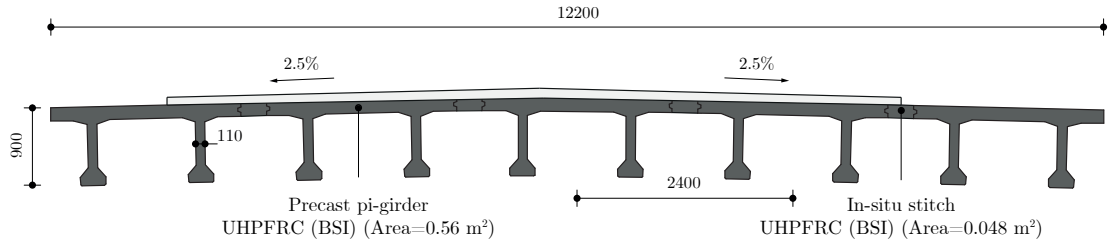

Figure 1.3: Cross-section of the Bourg-lés-Valence overpasses. Adapted from [9].

In 2004, the Chabotte bridge was built with a single span of 47.40 metres and a deck width of 4.40 metres [10]. To achieve this and ensure high durability in the harsh conditions of the region, BCV (Béton Composite Vicat), a proprietary mix with a f_{ck} of 130 MPa, was

used. By adding 2% steel fibres, a direct tensile strength of around 8 MPa was achieved, eliminating the need for passive reinforcement.

The girder consists of 22 segments: 18 standard segments, as depicted in Figure 1.4, and 2 segments which include the prestressing deviators. Additionally, there are 2 end segments dedicated to anchoring the 6 external tendons used for prestressing the girder. These 6 tendons are comprised of 19 strands, each measuring 150 mm^2, resulting in a prestressing steel quantity per square metre of deck of 30.5 kg/m^2.

The bridge's dimensioning was conducted by the Direction Scientifique de VINCI Construction Grands Projets (Alain CAPRA), following the recommendations of the AFGC [11]. This phase of the design encompassed assessments of longitudinal bending, shear strength, barrier anchorage, prestressing deviators and anchorages. Furthermore, COGECI developed two finite element models for the solution global and local.

The distribution and orientation of the fibres were examined in detail. To achieve this, prismatic specimens were extracted from additional segments to compare their bending strength with specimens tested for material characterization.

Thanks to the implementation of BCV and the design involving precast box segments with external prestressing, the target span can be achieved with a t_{eff}=29 cm. Only passive reinforcement was required due to the local effects of the deviation and anchorage of the prestressing.

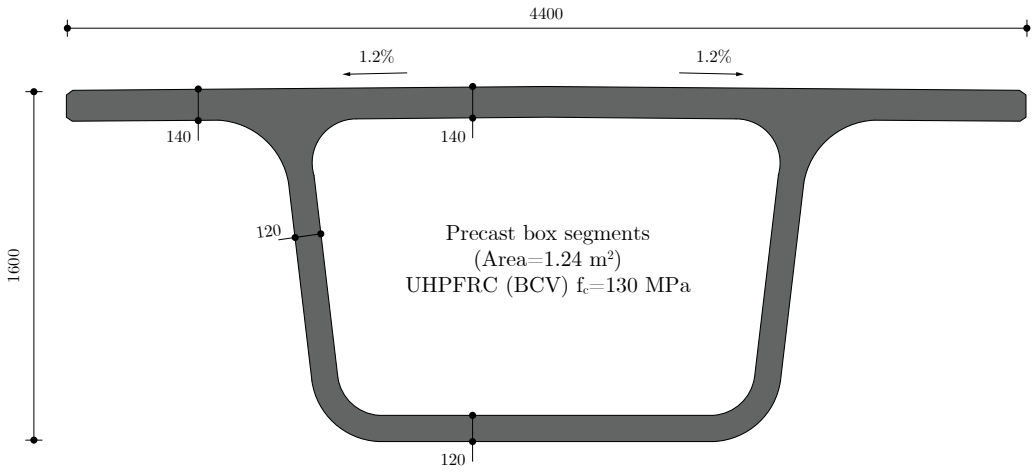

Figure 1.4: Cross-section of Chabotte Bridge. Adapted from [10].

1.5.3 Australia

After years of research, a guideline for the use of UHPFRC Ductal was developed at the University of New South Wales. It provides characteristic values for design, along with guidelines for calculating bending, shear, and torsional resistant forces of structural elements, as well as deflections, taking into consideration rheological effects. Additionally, it offers examples for a variety of prestressed beam designs [12].

In 2003, development commenced for mixes with a compressive strength of 180 MPa, utilizing local materials, with the exception of steel fibres. Subsequently, researchers investigated the performance of UHPFRC structural elements conducting tests on seven prestressed I-beams without stirrups with thin webs [13].

In 2004, the first road bridge using UHPFRC Ductal beams was constructed, the Shepherds Creek Ductal Bridge [14]. The bridge's cross-section, spanning 15 metres in a simply supported configuration, is depicted in Figure 1.5. It features 16 prestressed beams, each with a depth of 600 mm and a web thickness of 100 mm. Each beam presents 20 straight strands with a diameter of 15.2 mm (140 mm^2). On top of them, there is a 170 mm in-situ conventional concrete slab. Between the beams and the deck, serving as permanent formwork, are 25 mm thick UHPC panels spanning between the beams. The average thickness of the beams measures 8.62 cm, and the amount of prestressing per square metre of the deck is 16.91 kg/m^2.

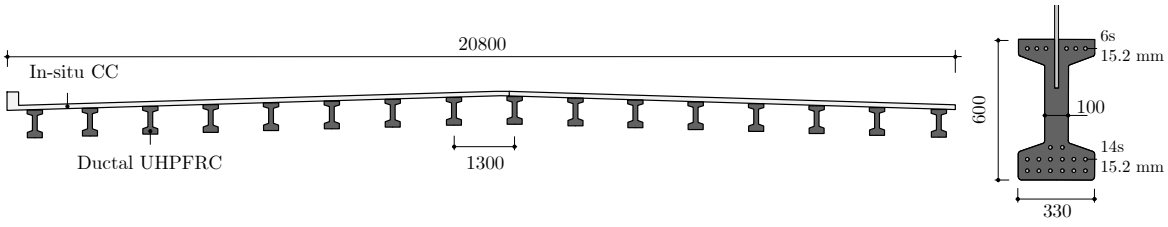

Figure 1.5: Shepherds Creek Road Bridge. Adapted from [14].

1.5.4 United States

In the United States, the integration of pioneering UHPFRC solutions within the bridge sector has been embraced by Precast/Prestressing Concrete Institute (PCI) in conjunction with the Federal Highway Administration (FHWA). A series of comprehensive documents and guidelines have been published by the FHWA concerning both the material level [15]

and its implementation within bridge structures [16]. Notably, the FHWA has compiled an online repository of UHPFRC applications in bridges within the United States [17].

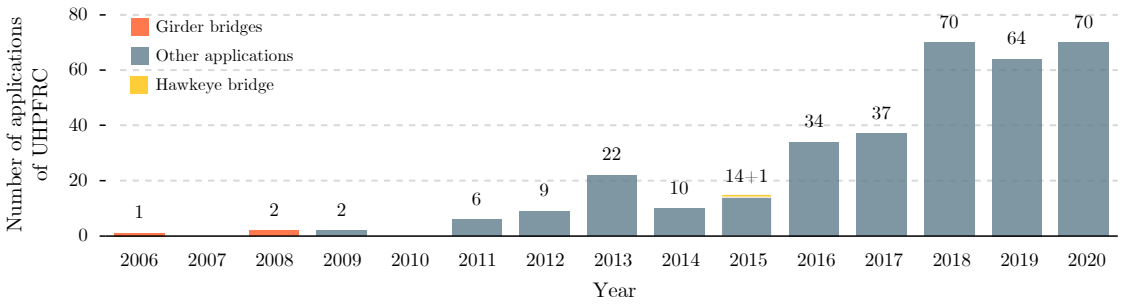

Figure 1.6: Number of applications with UHPFRC into the US by year (Data obtained from [17] and [18]).

Figure 1.7 illustrates the geographical distribution of all the UHPFRC applications carried out in the US. Notably, bridge beams built using UHPFRC are distinctly highlighted in orange. These particular applications assume a pioneering role, as the UHPFRC remains absent from the official American Association of State Highway and Transportation Officials (AASHTO), as evidenced by [19], and was less recognized at the time of the study.

The earliest application was in 2006 in Iowa at the Mars Hill Bridge (100th Avenue) in Wapello County [20]. The image at the left of Figure 1.7 shows the completed bridge, which spans, in a simply-supported manner, a length of 33.53 m. Prior to the construction of this bridge, four modified Iowa bulb-tee girders were cast with the UHPFRC supplied by Ductal [21] for empirical verification of their flexural and shear strengths by testing.

This particular road bridge consists of 3 UHPFRC girders whose cross-section was inspired by the standard Iowa Bulb Tee design, yet with notable modifications: shallower top and bottom flanges and a narrower web [22]. Notably, this design exhibits a rather high slenderness of 25, in contrast to the conventional value of 18 [23]. This increased slenderness increases the clearance beneath its span. Studying the cross-section of these girders, it can be deduced that the bottom flange dimensions are defined to give room to the strands, which are needed due to the high slenderness of these girders. Furthermore, the draped strands (useful to reduce the design value of the applied shear) crossing the web make it difficult to further reduce the web thickness.

This configuration serves as an initial experience for both client and the designer. Presenting this innovative UHPFRC solution should be a great incentive to gain confidence in the

implementation of this novel UHPFRC into road bridges.

Subsequent to these initial developments in Iowa, the research advanced with a concerted collaboration involving key entities: the Iowa Department of Transportation, the FHWA, the Bridge Engineering Center at Iowa State University and Lafarge North America. Together, their collective efforts were focused in the research and construction of the pi-girders in 2008 [24].

After testing and optimization of the initial proposed solution, a second-generation pi-girders emerged. Three pi-girders of the resulting second generation are shown in their final location in the right photograph of Figure 1.7, at the mid-span of the 136th street Jakway Park in Buchanan County [25].

This solution adopts an innovative cross-section which exploits the outstanding mechanical strengths of the UHPFRC. The top slab substitutes the conventional concrete deck (conventionally 200 mm [20]), significantly reducing the self-weight of the superstructure. This solution exemplifies the possible concrete reduction with an effective thickness (t_{eff}) equal to 22.3 cm. Furthermore, it shows a low prestressing steel quantity 10.3 kg/m^2. However, the practical adoption of this innovative configuration may encounter resistance from precasters, attributed to the required novel and intricate formwork.

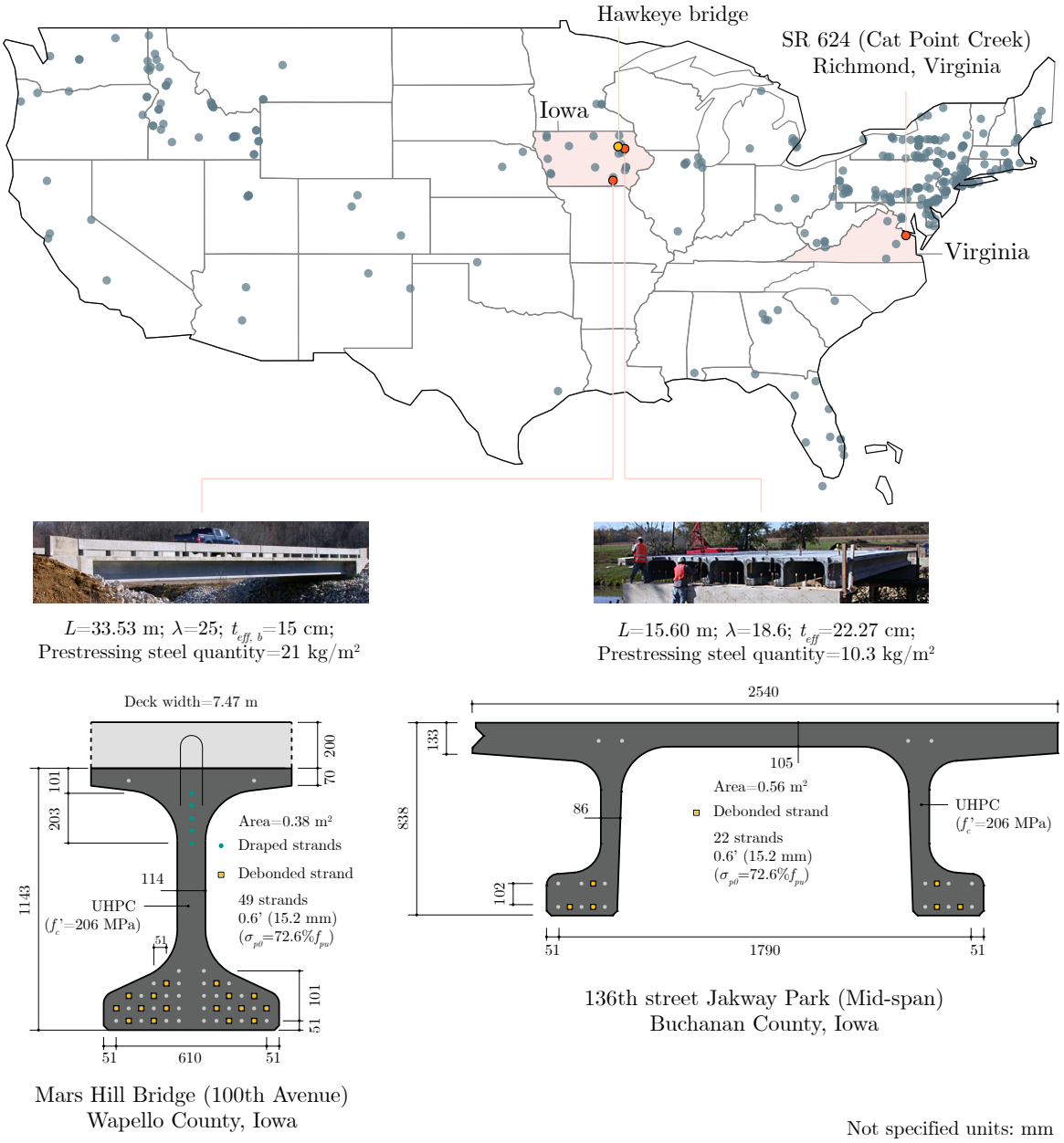

Figure 1.7: UHPFRC bridges in the U.S. [17, 18, 20, 24].

The third application was carried out in Virginia and consisted of concreting and placing five conventional bulb-T beams with a depth of 1143 mm using UHPFRC (f'_c=159 MPa). These beams were installed on one of the ten spans of the bridge on Route 624 over Cat Point Creek, spanning 24.84 metres. The Innovation and Research division of the Virginia Center for Transportation, as described in [26], aimed to study the casting process of the UHPFRC beams, characterize the material properties, conduct testing on one of the beams at FHWA's

Structures Laboratory, and monitor the bridge during its service life.

One of the conclusions drawn during the beam casting process was the project participants' concern about the potential occurrence of cold joints that might compromise the beams' integrity. Vibration was dismissed as an option due to their apprehension that it could disrupt the random distribution of the fibres.

The three presented applications confirm the feasibility of replacing stirrups with steel fibres to withstand the design shear. The conclusions drawn by those involved suggest that exploring innovative cross-sections is necessary to offer economically competitive solutions.

In the subsequent phase, PCI supported six precasters in formulating their own UHPFRC mixes. The primary goal was to disseminate, instruct, and advocate for the benefits of these materials. Furthermore, the formulated mixes aimed to incorporate local materials, thereby reducing costs when compared with the proprietary mix employed in Iowa's UHPFRC road bridges.

More recently, Tadros et al. [27] have developed the UHPFRC decked I-beams based on the use of concrete with a compressive strength between 117 and 152 MPa. This system allows the integration of girder and deck, taking advantage of the conventional concrete deck´s optimisation. The reduction of concrete in the deck allows a 50% reduction of the bridge superstructure's self-weight. Figure 1.8 shows the cross-section of UHPFRC's precast decked I-beams developed by Tadros et al. [28], which have already been used for both principal beam and slab for buildings, and now are being used in road bridges. As a drawback, its complex formwork implies a significant initial investment by the concrete manufacturer.

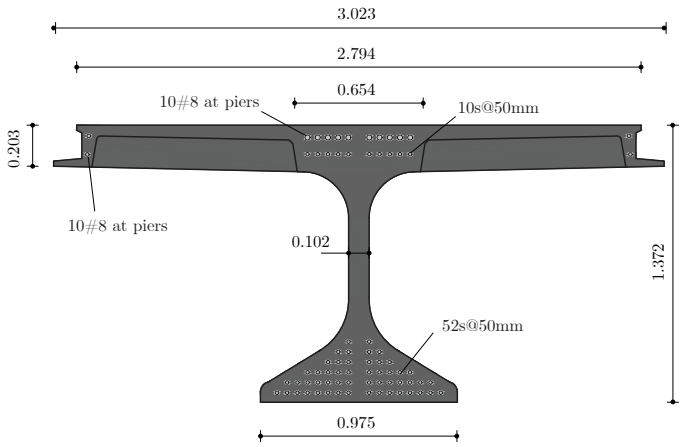

Figure 1.8: Decked I-beams [29].

As a conclusion to these two decades of the learning process, the publication titled "Implementation of Ultra-High-Performance Concrete in Long-Span Precast Pretensioned Elements for Concrete Buildings and Bridges" is currently in the final stages of preparation for publication. The UPM research team has had the opportunity to review the document in its draft stage. This document encompasses detailed accounts of the development and implementation experiences of the six precasters who formulated their own UHPFRC mixes. It also includes a comprehensive description of experimental tests, conducted at a 1:1 scale, on UHPFRC bridge beams until failure. Furthermore, the publication provides guidelines and recommendations for mix design, material placement, and structural design. Undoubtedly, this publication is poised to be of immense practical utility, as it consolidates all the essential knowledge required for carrying out applications with UHPFRC.

1.5.5 Malaysia

The company DURA Technology is the world's largest builder of UHPFRC road bridges. Its founder, Voo Yen Lei, studied, together with Stephen Foster [30], the characterization of UHPFRC mixtures in 2004. Furthermore, they performed experimental campaigns involving structural elements of the same material. The first elements under study were UHPFRC panels under transverse stresses, which represents the stress state caused by the local effects of prestressing and support anchorage. The conclusions highlighted that the cracking patterns were highly dependent on the support conditions and that the amount and type of fibres added to the UHPC influenced the ultimate load. The second experimental campaign studied the strength of prestressed UHPFRC beams without stirrups. In addition to highlighting the importance of fibre type and quantity on the failure type, it is emphasized that the ultimate failure load is more than twice the cracking load.

The strategy of the company started by developing various proprietary mixes of UHPFRC and UHPC. One mix was designed for application in precast, prestressed or post-tensioned concrete flexural members features an f_{ck}=140 MPa, coupled with cracking and post-cracking resistance of 7 and 8 MPa, respectively. Additionally, tailored for the connections between precast elements, the company also formulates a UHPC with an f_{ck} of 120 MPa. The French standards for UHPC were followed to characterize the mixes [31] and verify the design of these structural members [32].

Figure 1.9 shows the different types of road bridges built with these materials: Type 1, I-beam with UHPFRC deck; Type 2, UHPFRC I- or U-beam with conventional concrete composite deck; Type 3, UHPFRC box girder; and Type 4, UHPFRC U-beam.

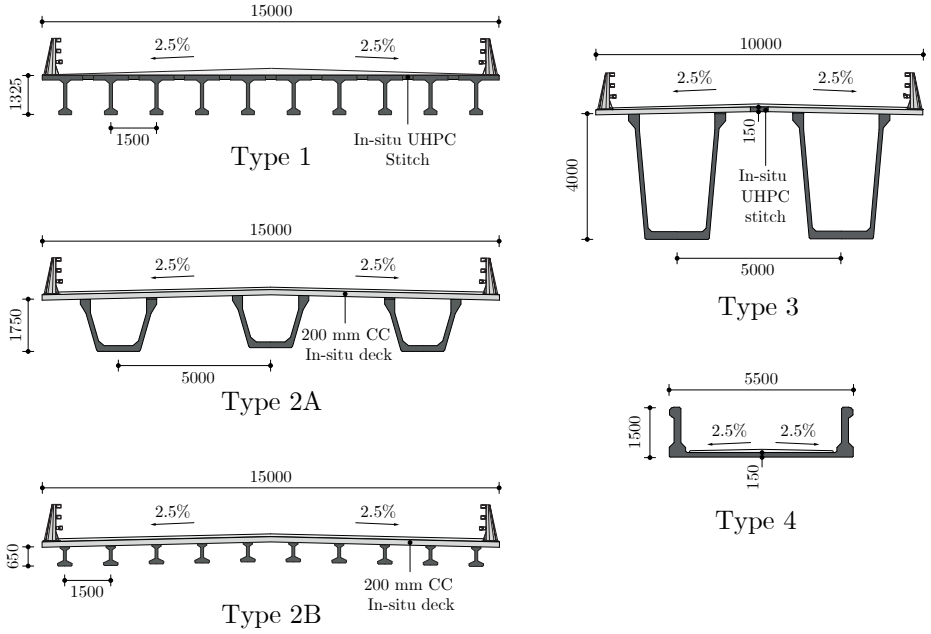

Figure 1.9: Typical UHPC bridge types used in Malaysia. Adapted from [7].

Figure 1.10 shows the area of decks built each year, which adds up to a total deck area of almost 150 thousand m^2 and 187 bridges. The percentage of bridges built according to the different typologies shown in Figure 1.9 is shown in the form of a cheese diagram. The most used are type 2 sections (83%) and the least, due to their significant longer span range, type 3 (1%).

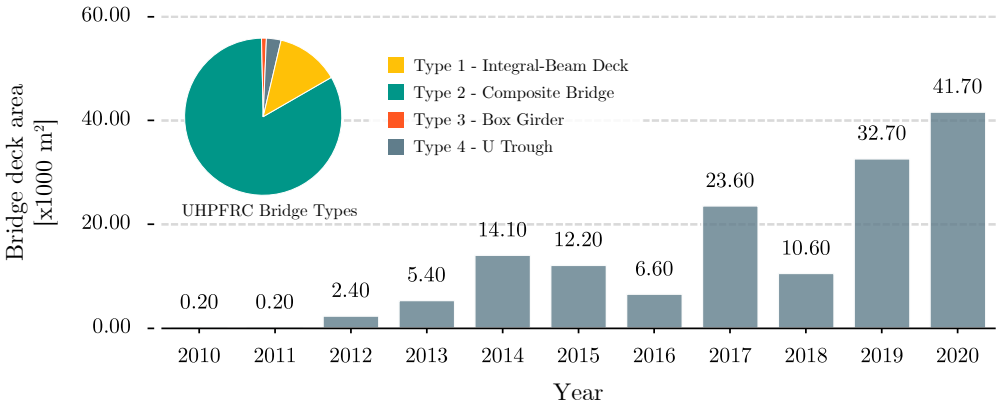

Figure 1.10: Malaysia UHPFRC bridge deck area, and their distribution according to their different cross-sections. Adapted from [7].

Figure 1.11 gathers the cross-sections of the solutions Type 2A of U-girders by DURA Technology and their corresponding span range.

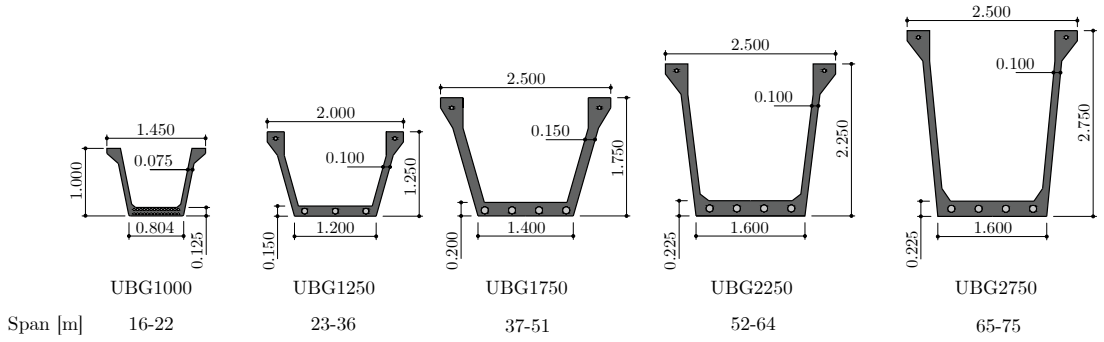

Figure 1.11: U-girders of the DURA Technology precast catalogue and its span range of application.

DURA Technology stands as a notable example of a company excelling in the formulation of its own proprietary mixes while seamlessly integrating its girder solutions into a multitude of road bridges. This achievement encompasses cost reduction, the development of adaptable solutions for diverse scenarios, and the successful encouragement of local authorities to recognize the enhanced durability offered by UHPFRC solutions compared to conventional alternatives.

1.5.6 Austria

The first bridge built using UHPFRC in Austria was the Feistritzbach Bridge in 2008, located in Carinthia. This road bridge is simply-supported, boasting a 9-metre span, and its cross-section, depicted in Figure 1.12, is upheld by a precast UHPFRC element classified as C165/185. This specific element serves as permanent formwork for the conventional C30/37 concrete. The precast element is prestressed longitudinally with 10 strands, distributed across the webs. In the transverse direction, it incorporates tendons with 10 strands each. The top slab comprises a cast-in-situ concrete slab of UHPFRC, also of C165/185. To enhance the bond between the in-situ concretes, the ”wet-on-wet method” has been applied [33, 34].

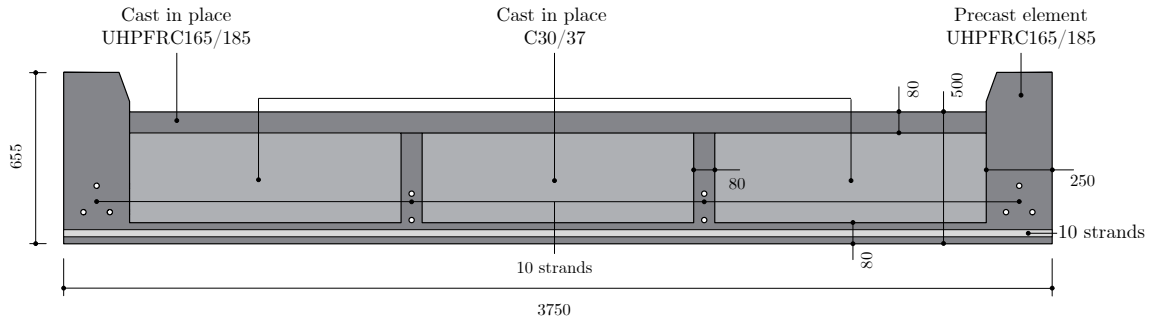

Figure 1.12: Feistritzbach bridge. Adapted from [34].

The WILD Bridge stands as the first precast road arch bridge built with UHPFRC. This remarkable bridge is located in Völkermarkt, in the southern part of Austria. Figure 1.13 presents the bridge's cross-section on the left and its longitudinal profile on the right. The suitability of selecting the arch bridge typology is evident when considering the topography of the valley in question.

The arch boasts a 69-metre span and features a polygonal design with twin parallel arches. The utilization of precast UHPFRC elements eliminates the need for passive reinforcement, resulting in elements with a reduced thickness of only 60 mm. This reduction in weight allows the arch's pressure lines to closely resemble the polygonal shape, with vertices aligned at the support points of the columns (C50/60), which introduce stabilizing forces thanks to the, according to the authors, rather heavy deck (C40/50) [34].

The project was realized through a design-by-testing approach involving elements representing the beam elements. At the University of Graz, 5-metre-long elements underwent testing [35]. Furthermore, cores from various mock-up elements were extracted to study the distribution and orientation of the fibres [36].

To prevent temperature gradients within the beam elements, they were subjected to heat treatment at 90°C and 100% relative humidity. This treatment not only promotes the gain of compressive strength but also accelerates the development of rheological deformations. Thanks to the heat treatment, the long-term deformations of the arch in its final position will be negligible, thereby preventing excessive stress increases in the arch elements.

Due to the use of dry joints between the precast elements, aiming to achieve the best possible load transfer between them, Computerized Numerical Control (CNC) technology was employed on the faces that would come into contact. This CNC process defined the geometry of these faces with an accuracy of $\leq$0.1 mm.

The initial arrangement of the arch was tri-articulated during construction, employing a technique inspired by Riccardo Morandi, as seen in examples such as the Morandi Bridge in Lucca, Italy, and later in the Paul Sauer Bridge over the Storm River. This approach allowed the precast elements to be assembled in a vertical position and then folded down around the arch supports' hinges until both half-arches met at the keystone node. The precast elements were prestressed using 150 mm^2 sheathed strands [34], which can be observed in the cross-section shown in Figure 1.13. Four of these strands were only used temporarily during construction. Once the bridge was completed, the hinges were locked to change the behaviour of the arch thereafter as fixed.

This application represents a significant milestone in the application of UHPFRCs, as it is the first road arch bridge using UHPFRC for a 69-metre span, requiring adaptation of precast elements to the characteristics of the material, and the application of specific techniques such as CNC and heat treatment. The successful completion of this remarkable project was made possible through the collaborative efforts of constructors, researchers, designers, and authorities [6, 34–37].

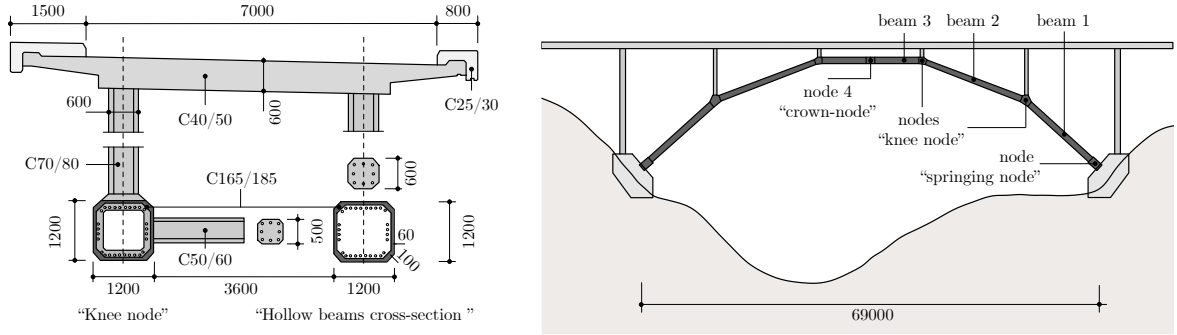

Figure 1.13: WILD-Bridge. Adapted from [37].

1.5.7 Italy

To optimize the overall cost of the structure along with reducing its carbon footprint, composite structures can be designed with UHPFRC only in specific locations of the cross-section, using conventional concretes or FRC for the rest of the structure. One example is the first P/R/SFRC bridge in Italy by di Prisco et al. [38]. Here precast UHPFRC plates are used as lateral inclined loose formworks to cast in place the rest of the slab bridge with FRC. In this application, according to the Model Code 2010 (MC2010) classification, the UHPFRC is a C120 14c while the FRC is a C40 5c.

1.5.8 Spain

A pioneering example can be found in the company RDC, which designed and constructed Spain's first UHPFRC road girder bridge. The replacement of a flood-damaged bridge led them to utilize UHPFRC girders, enhancing the solution's tenacity against potential impact loads. A picture of the bridge under service is shown in Figure 1.14. Moreover, this firm endeavors to promote the understanding of UHPFRC among practitioners [39].

Figure 1.14: Bridge over the Vernissa River (picture courtesy of RDC).

1.5.9 South Korea

Over the past twenty years, the Korean Institute of Civil Engineering and Building Technology (KITC) has undertaken three significant R&D projects dedicated to the development and implementation of UHPFRCs in bridge construction. The first of these projects, known as Bridge 200 (2002-2006), aimed to create UHPFRCs, referred to as "SUPER concretes". These SUPER concretes comprised UHPFRCs with a mean compressive strength (f_{cm}) of 180 MPa and very high strength concrete (VHSC) with f_{cm} ranging between 100 and 120 MPa. The intended applications for these materials were girder road bridges.

The second project, SUPER Bridge 200 (2007-2012), marked a significant milestone in the development of UHPFRC. During this phase, improvements were made to the previously developed UHPFRC, accompanied by the creation of design guidelines, production, and construction specifications for the application of UHPFRC in civil engineering structures. Notably, one of the outcomes of this project was the construction of the first UHPFRC cable-stayed footbridge [40].

Moving on to the third phase, named SUPER Structure 2020 (2013-2019), its primary goal was to develop concrete classes ranging from 80 to 180 MPa of f_{cm}. Furthermore, it aimed to expand the scope of application guidelines for these materials for the new concrete classes [41].

Notably, this phase sought to broaden the range of applications beyond bridges, including windmill towers, and buildings. The development of high-strength performance concretes addressing strengths between 80 and 120 MPa is relatively uncommon. From the author's knwoledge, there are few instances of HPFRC application sin bridge engineering, such as the Ogkwan Bridge (2014), featuring steel fibres and concrete with a compressive strength of 120 MPa.

In 2015, the Hawkeye Bridge was built in Buchanan County, Iowa, marking the fourth UHPFRC road girder bridge in the United States. The guidelines refined during the third phase of the project, as documented in [41], were successfully applied to this project. The concrete mix was developed by KITC, named as K-UHPC, after several years of in-depth research.

This particular mix incorporates two types of high-performance steel fibres: one with a fibre length (l_f) of 16 mm and the other with l_f of 20 mm. Approximately 39 kg/m^3 of the former fibres and 78 kg/m^3 of the latter were added, resulting in a fibre content of approximately V_f=1.5%. Through collaborative research between KITC and the University of Iowa, the mix was developed in the United States, utilizing local sands and cements, along with other constituents shipped from Korea [18].

The cross-section, as illustrated in Figure 1.15 (a), is a modification of the one previously employed for the 136th Street Jakway Park bridge, which had also been installed on the Andon Bridge, in South Korea, in 2012. In the case of the Hawkeye Bridge, each girder is prestressed by two longitudinal tendons, each consisting of 7 strands measuring 15.2 mm (140 mm^2) each, located at the bottom flanges. Additionally, to ensure transversal compatibility among the six beams, they were prestressed with 3-strand tendons on the five transversal girders, as detailed in [18]. A photograph depicting the six girders in their final position can be seen in Figure 1.15 (b).

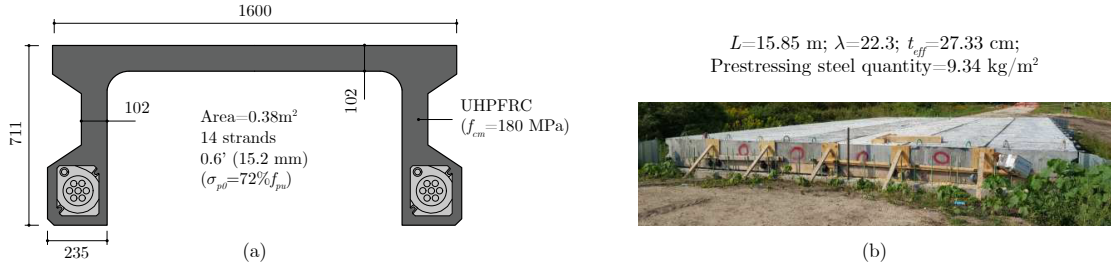

Figure 1.15: Hawkeye Bridge: (a) cross-section of the pi-girder design from the KITC, and (b) image of the six girders joint together. Adapted from [18].

The Chuncheon Bridge, providing access to Lego Park and completed in 2017, stands as a testament to the successful application of UHPFRC in cable-stayed bridges. This bridge boasts a span of 970 metres, with the cable-stayed bridge section extending across 200 metres and measuring 29.50 metres in width. Its distinctive circular pylon relies on the light-weight achieved thanks to the UHPFRC mechanical performance.

Currently, South Korea is one of the leading countries with the highest number of UHPFRC applications in integral bridge elements. Moreover, the nation's research efforts in developing more complex bridge typologies, such as cable-stayed bridges with longer spans, enable the full exploitation of the weight-reduction advantages afforded by UHPFRCs.

2

Conceptual design of UHPFRC and HPFRC girders for road bridges

2.1 Introduction

In this chapter, a typological analysis of I- and U-girder road bridges making use of HPFRC and UHPFRC is critically presented and discussed. The chapter also provides with the detailed structural analysis for the selected HPFRC U-girder bridge.

2.2 Case of study 1: I-girder

A 42 m-span I-girder bridge made with six NU2000 girders [42] spaced 3.70 m was selected as the reference project. Girders and deck were made of C50/60 (f_{ck}=50 MPa). The 4 different girder cases presented as alternatives use UHPFRC of C125/140 and PCC21c; the deck employs C50/60 in the case study 1 and C60/75 in the longitudinal joint of the case study 3. Case studies 2 and 4 emulate the decked I-beam system proposed by Tadros et al. [27][5]. Figure 2.1 shows the cross-sections of the reference project girder (on the left) and 4 different case studies considered as alternatives.

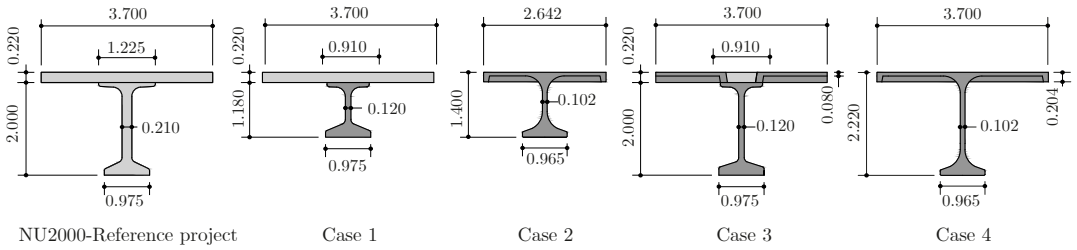

Figure 2.1: I-Girder scheme alternatives.

For every case of study, SLS and ULS conditions were verified for both shear and bending. The four design cases could bear shear loads without any passive reinforcement, which was 1016 kg (42% of the girder passive reinforcement) for the reference project. The prestressing of the reference girder consisted of four unbonded tendons. Two of them presented a parabolical longitudinal profile whereas the others were straight. The web width was defined to accommodate passive reinforcement, ducts, and concrete covers. Hence, in the different cases the prestressed has been kept away from the webs to minimize its thickness. When pre-tensioned strands are used, some of them must be debonded near the supports. In addition, strands may be required also at the top flange. Instead, when designing with post-tensioning, blisters above the bottom flanges should be designed to anchorage the prestressing tendons. Case study 1 and 2 present a higher span-to-depth ratio (slenderness) of 30 while case study 3 and 4 maintain the value of 18.9 as the reference design. The reduction of the mechanical arm in the first two cases entails an increase in prestressing steel. This effect is counteracted by the reduction of self-weight, as illustrated Table 2.1 where the material consumption of the different alternatives is compared with the reference project. The case study 4 represents the optimal solution regarding material savings, both in concrete and prestressing steel, but, as a drawback, its complex formwork requires higher investments from precasters. An intermediate alternative which combines simpler formwork with interesting material savings is represented by case study 3.

Table 2.1: Material consumption and comparison of I-girder bridge alternatives with reference.

Case of study	V_{CC50} [m^3]	V_{CC60} [m^3]	$V_{UHPFRC125}$ [m^3]	Prestressing steel [cm^2]	Concrete savings [%]	Prestressing savings [%]
NU2000-Ref.	64	-	-	60.0	-	-
Case study 1	35	18	-	88.5	↓18	↑50
Case study 2	-	27	-	54.0	↓44	↓10
Case study 3	-	37	6	49.5	↓32	↓18
Case study 4	-	33	-	40.5	↓48	↓32

Next, a cost comparison of the alternatives with respect to the reference project was performed. The UHPFRC cost was considered as 5 times the cost of a standard concrete. After discussing the results with a construction company, to achieve a clear economic benefit using UHPFRC for I-girder bridges, the main conclusion was that this material has not a clear advantage in economic savings for conventional spans. In view of this meeting, new goals were defined: (i) to achieve longer spans to reduce the number of bridge substructures, (ii) to reduce the cost of the concrete mix, (iii) to minimize modifications to the existing formworks, and (iv) to maintain a conventional deck. Transportation requirements limit the maximum girder length to 40-45 m [43]. Furthermore, from the craftsperson perspective, longer prestressed beds are unusual, and the arrangement of blisters at the top of the bottom flanges would require a modification of current formworks. In addition, the calculation of a new alternative with HPFRC of C100/115 and PCC12c revealed that a polygonal prestressing profile was required to avoid passive shear reinforcement. It has been highlighted the significant material savings and weight reductions when designing I-girder bridges with UHPFRC. However, professionals are yet reluctant to deviations from their current practices. For them to become familiar with high performance enhanced fibre reinforced concretes, the construction of HPFRC structures which overcome conventional span ranges is set as an initial mile-stone to accomplish.

2.3 Case of study 2: U-girder

2.3.1 Introduction

It is a common practice for precasters to arrange tendon deviators and anchorages on the free space inside U-girders, avoiding any interference between ducts and webs/bottom slab. Hence, U-girders could be a better typology to be designed with HPFRC.

Figure 2.2 shows the case of study, characterized by a 12.50 m-width deck with a 0.25 m-thick cast-in-place C30/37 slab. Two girders spaced 6.50 m bear the deck. The goal was to reach a 60 m-span and eliminate the passive shear reinforcement using an HPFRC mix of C100/115, with the minimum post-cracking strength requirement possible.

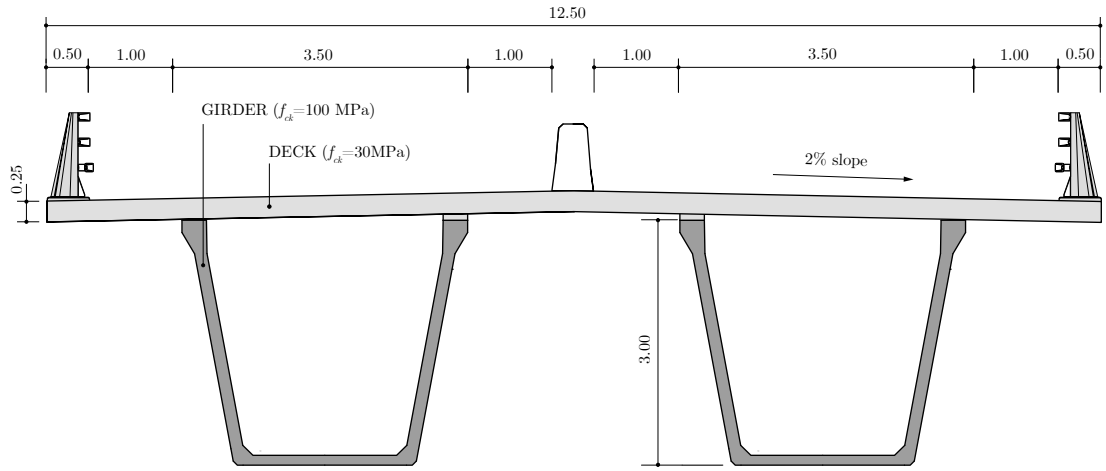

Figure 2.2: U-girder case of study.

To ease segments transportation and to avoid any undesired cold joint, Voo [44] designs short segments, 6-8 m long, to be able to pour them with one concrete batch. However, a scaffolding system must temporarily support the girder before the prestressing release. From the author's experience, the use of longer segments with the minimum number of temporary supports is a reasonable alternative. To experimentally ensure the avoidance of cold joints, a mock-up segment can be concreting and search for any planes of weakness without continuity of fibres.

2.3.2 Conceptual design of U-girder alternatives

Figure 2.3 (a) and (b) geometrically describe half of the longitudinal profile of the four designed alternatives, along with the cross-sections at the support and the mid-span, respectively. The main differences among the alternatives are as follows: (i) the girders are composed of two or three segments (2S or 3S), (ii) the prestressing steel is either considered unbonded or bonded to the concrete (U or B), and (iii) the tendons are either straight or deviated (S or D). As an illustration of the proposed nomenclature, the first alternative is named 2S-U-S, signifying that it consists of two segments, with straight and unbonded tendons.

The first alternative, 2S-U-S, is based on Voo's applications [44] but utilizes two 30 m segments. External prestressing within the U-beam leaves the webs and the bottom slab free. The thickness of the webs will, therefore, be determined to withstand the design shear applied load without the need for stirrups. In this alternative, straight longitudinal tendons are proposed, which implies the provision of two 7-strand tendons at the top to avoid cracking at the supports. The amount of longitudinal prestressing was estimated in a rough manner, but it provided the team with a preliminary idea of the expected magnitude.

This alternative was rejected due to the high cost of implementing an UHPFRC capable of withstanding the required design shear to eliminate the need for stirrups.

The second alternative, 2S-U-D, maintains the number of segments and the unbonded condition. However, by deviating two tendons, it effectively reduces the design shear by 50%. Furthermore, the application of two-stage prestressing, a thorough examination of the evolutionary load application process, and the utilization of precise sectional calculations for bending checks enable optimization of the prestressing. The amount of prestressing for this alternative, expressed as kilograms per square metre of the deck, is 32.35 kg/m^2.

As joints between segments must be under a compressive state, it is convenient to locate them far from sections of maximum bending moments. Consequently, the decision was made to install two temporary supports, enabling the utilization of three 20 m segments. This led to the development of the alternatives 3S-B-S and 3S-U-D. This decision results in a 16% reduction in prestressing when comparing the 3S-U-D alternative with the 2S-U-D alternative.

Lastly, the alternative involving bonded tendons within the bottom slab was investigated. As depicted in Figure 2.3, only 4T25S could be accommodated within the slab, causing an increase from 12 cm (as seen in the other alternatives) to 21 cm. This enlargement of the

bottom slab results in an additional 6% of concrete in the beam.

The decrease in prestressing steel at mid-span, comparing solutions 3S-B-S and 3S-U-D, was 3.6%. This reduction was constraining to this minor value because the most constraining criterion for prestress dimensioning at the span centre is the SLS. Consequently, the increase in prestressing stress due to bonding does not have a significant impact. Given the use of straight tendons, the τ_{Ed}=6.36 MPa.

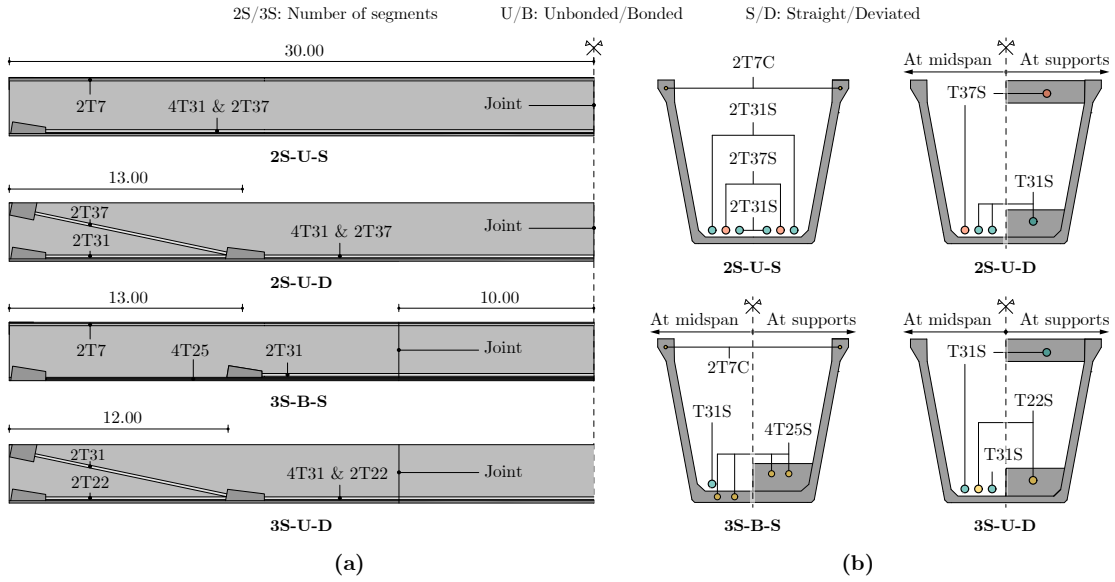

Figure 2.3: U-Girder scheme alternatives.

Table 2.2 presents the prestressing steel quantities along with the design applied shear stress τ_{Ed}, facilitating a comparison among the various alternatives. The advantages previously described for the 3S-U-D alternative, which was ultimately selected for further development, are significant.

Table 2.2: Comparison of the four alternatives of U-girders.

	2S-U-S	2S-U-D	3S-B-S	3S-U-D
Prestressing steel [kg/m^2]	39.94	32.35	28.10	27.08
τ_{Ed} [MPa]	6.84	3.42	6.36	3.55

2.3.3 Design procedure of the proposed alternative

Material properties

When designing the U-beams, HPFRC100/115 has been used, characterized by a f_{ck} of 100 MPa and a maximum aggregate size equal to 12 mm. The tensile strength at the SLS has been established at 4.5 MPa.

A conventional concrete C30/37 (f_{ck}=30 MPa) is used for the cast-in-place deck located on the top of the beams. However, it should be mentioned that a ribbed HPFRC deck could carry a reduction of the self-weight of the slab of approximately 30%, which would allow savings in the super and sub-structure. Furthermore, the durability of the bridge will also be improved as the HPFRC can present a permeability index 10 times lower compared to a conventional concrete. Nevertheless, a conventional slab was selected as this work focuses on the study of the girders.

Tendons with strands have been used as prestressing steel and they are characterized by an ultimate tensile strength (f_{pu}) of 1860 MPa and a Young Modulus (E_p) of 200 GPa. Its design strength (f_{pd}) is 1455 MPa and the ultimate strain (ε_{pu}) is 20‰. Prestressing losses are considered constant among alternatives, as 5% for the initial losses and 15% for the long-term losses. The passive reinforcement used is a BS500 (f_{yk}=500 MPa).

Loads and load combinations

It has been assumed that the material's specific weight will be 25 kN, equivalent to that of conventional reinforced concrete. Although the unutilized quantity of passive steel contributes to a reduction in weight, this will be counterbalanced by the greater density of high-performance concrete in conjunction with the steel fibre arrangement.

The external loads, as well as the load combinations, considered in this study, follow the EN 1992-1-1:2013 (EC2-2013) [45]. Pavement density is assumed to be 23 kN/m^3. The weight of each barrier is 2 kN/m, and it is considered to be equally distributed by all beams. The traffic loads defined by the EN 1991-1-2:2013 (EC1-13) [46] consist of distributed lanes and a series of heavy vehicles located in the most critical section for each check. The heavy vehicles were located at mid-span to obtain the critical bending moment, while they were located at an effective depth (d) from the support to calculate the critical shear load.

Prestressing is categorized as P1, encompassing the effect caused by elements positioned outside the concrete section but within the cross-section outside the perimeter (external prestressing). For external prestressing, a resistance factor of 1 is applied during strength verifications, and a factor of 0.9 or 1.1 is used for serviceability verifications depending on whether the effect is favorable or unfavorable, respectively.

For the SLS, two different combinations are considered:

- Quasi-permanent combination, Equation 2.1.

$$1.00 \cdot G \tag{2.1}$$

- Characteristic combination, Equation 2.2.

$$1.00 \cdot G + 1.00 \cdot UDL + 1.00 \cdot TS \tag{2.2}$$

- For the ULS, the persistent combination is considered, Equation 2.3:

$$1.35 \cdot G + 1.5 \cdot UDL + 1.5 \cdot TS \tag{2.3}$$

The following construction stages are also included: (i) first prestressing phase and girder self-weight, (ii) development of the long-term losses once the slab is installed but before its hardening, (iii) second prestressing phase (if needed) and installation of the barriers and pavement.

Flexural and shear analysis at ULS and SLS

The design loads, calculated in the previous Section, are numerically described in Table 2.3.

Table 2.3: Design loads of the proposed alternative.

Loads	Girder self-weigth	Deck self-weight	Additional load	Heavy vehicles (TS)	Distributed load (UDL)	ULS	SLS
Bending [kNm]	Variable	17550	5850	9000	13500	87000	62100
Shear [kN]	1080	1170	390	570	900	5770	4110

In the bending verifications, the progressive application of prestressing and loads was considered. Each effect was imposed upon the existing strain profile of the cross-section.

In each subsequent equilibrium state, no strains were allowed to exceed the ultimate strain of the materials. To determine the value of the design resistant bending moment M_{Rd}, the bending moment applied in the final stage was incrementally increased until one of the ultimate strains was reached.

The stresses verificatios under SLS are conducted with the following set of limits:

- Tensile stress must not exceed $0.45 f_{R1k}$ under characteristic combination.
- Sections with joints are required to be in compression under characteristic combination.
- Compressive stresses must not exceed $0.45 f_{ck}$(t) under the quasi-permanent combination. To prevent cracking, they must remain below $0.6 f_{ck}$ under the characteristic combination.

The longitudinal profile of the proposed solution is depicted in the lower section of Figure 2.4. Two 22-strand tendons span the entire length of the beam in a straight configuration. Within the L/5 sections near the support, one pair of tendons is anchored, while another pair, comprising four tendons each with 31 strands, is deviated. Prestressing is carried out in two stages: during the first stage, the tendons extending to the beam's ends are fully tensioned, and 30% of the final stress of the other two tendons is applied. Following the concrete slab's curing, the remaining 70% is tensioned in a second stage.

Figure 2.4 illustrates specific strain and stress conditions in the proposed U-girder solution. The left column presents those pertaining to the SLS, while the right column depicts those for the ULS. Beneath these cross-sectional conditions, the chart displays the ULS bending verifications conducted: a discontinuous line indicates the stage during the initial concrete pour of the top slab (with an efficiency of 96.3%), and with a continuous line the persistent combination (with an efficiency of 96.8%).

The increase of the prestressing stress in the ULS has been assumed to be 100 MPa, following the simplified assumption outlined in the document 'Design and Construction of Bridges and Structures with External Prestressing' by the Spanish Technical Prestressing Association (ATEP) [47].

Initially, prestressing is dimensioned based on the characteristic combination in SLS, as this results in a tensile stress of 4.50 MPa at the centre of the span. The remaining stress constraints are likewise met: the joint experiences compression (-1.06 MPa), and the maximum compression is observed at section C, amounting to -41.64 MPa.

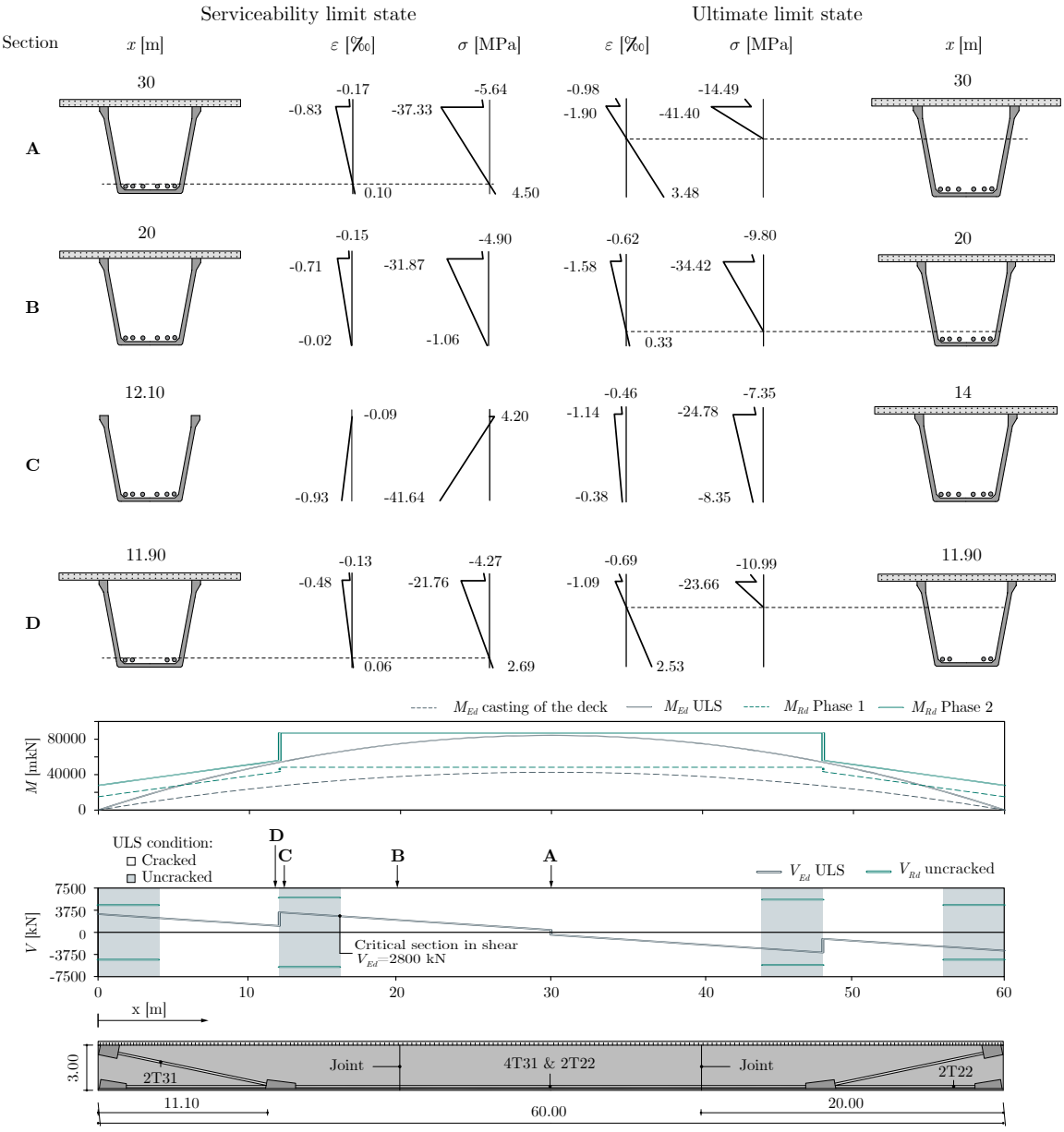

Figure 2.4: Graphical description of the structural analysis of the U-girder alternative.

The longitudinal profile in Figure 2.4 displays the design shears (V_{Ed}) in the ULS. It shows how the deviation contributes to a reduction in V_{Ed} near the supports. Furthermore, sections subject to compression under the persistent combination of ULS are shaded in grey. As per [45], the Collignon-Jourawski formulation can be applied to these sections in concrete beams without stirrups. The outcome of this formulation is depicted as a green line within the gray areas, denoted as V_{Rd} uncracked. Lastly, it's imperative to verify the critical design shear

V_{Ed} within the cracked zone, occurring at section x=16 m and equating to 2800 kN.

Various shear formulations in accordance with several standards have been applied to the critical cross-section. Figure 2.5 indicates the required characteristic value of the ultimate post-cracking tensile strength (f_{Ftuk}) to resist the τ_{Ed} according to the different applicable models. The outcomes exhibit significant variability; the latest version of the EC2 [48] predicts a 50% less ultimate shear strength than the ones obtained from MC2010 [49] and MC2020 [50]. This disparity stems from the EC2 draft not accounting for concrete contribution if the longitudinal reinforcement is unbonded. Such variations underscore a notable lack of consensus arising from the utilization of disparate shear models.

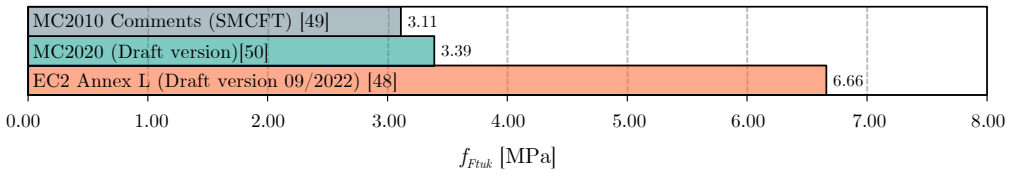

Figure 2.5: Shear formulations applied to HPFRC U-girder case.

3

Parametric analysis of I-girder bridge decks

3.1 Introduction

More than two decades have passed since the first applications of UHPFRC to precast girders of road bridges [51] [7]. Specifically, in Europe the first applications of UHPFRC in bridge engineering dates back to 2000. An example is found in the Bourg-lès-Valance bridge, whose deck was made continuous with in-situ UHPFRC between the two spans [9]. In Spain, the first UHPFRC road girder bridge, which crosses the Vernissa River, was designed and built by the firm RDC. Another type of application is found in Switzerland, where UHPFRC was applied for the refurbishment of deteriorated bridge decks [52]. The firm DURA Technology [53], a pioneer in the implementation of UHPFRC solutions, has already built more than 100 bridges in the last decade; all of them are based on the use of tailor-designed precast I and U girders. The increasing use of this material can be also detected in the USA, where the PCI, together with the FHWA, supported precast companies in developing their own UHPFRC mix design using local materials [54].

The advantages of UHPFRC compared with a conventional concrete are well known: i) compressive strength greater than 120 MPa; ii) ductility under direct tension stresses; iii) a matrix packaged that allows to support aggressive ambient conditions [55]. These characteristics might lead to a reduction in material consumption in the design of conventional structural elements [56]. Specifically, Tadros et al. [28] studied the possibility of applying UHPFRC to precast girders. As main finding, a UHPFRC decked-I beam was conceived,

and a 50% reduction in concrete consumption was achieved respect to a bridge made of conventional concrete (C50/60) with Nebraska girders as described in Chapter 4. In addition, the passive reinforcement was reduced to just one third of the amount used in the conventional solution. Finally, also savings in prestressing steel quantity was found due to self-weight reduction.

However, as main drawback, a UHPFRC can be around 12 times more expensive than a conventional concrete. This very high cost is limiting its wider application to the construction sector.

As an appealing alternative to UHPFRC, the HPFRC may represent a product compromising cost and benefits of the material [57]. Walraven et al. [58] proved that an HPFRC can reach post-cracking hardening behaviour under the bending test showing a smeared cracking. This behaviour might allow to replace conventional shear reinforcement with fibres [49]. In addition, the same fibres can control the development of cracks, possibly also replacing conventional longitudinal reinforcement.

Nowadays, the design of traditional precast girders for road bridges is optimized [43] using more refined calculations based on optimization techniques. The question arises to what extent the use of HPFRC may optimize classical solutions of precast girders. From a conceptual perspective, the high axial tensile strength of concrete (f_{ct}) of HPFRC is favourable for increasing the tensile stress limitation ($\sigma_{ct,max}$) at the SLS. Furthermore, the ultimate post-cracking strength for fibre reinforced concrete (f_{Ftu}) might increase the M_{Rd}. These two ideas suggest possible savings in the prestressing steel quantity. Furthermore, due to the high compressive strength, concrete consumption may also be reduced. Finally, fibres also provide a contribution to the shear strength of the girders [59]. In particular, Baby et al. [60] performed eleven tests on UHPFRC critical shear beams to study, among other aspects, the degree of additivity between the stirrups and the fibre shear contributions and the possibility of substituting stirrups for fibres. Therefore, the possibility of removing shear reinforcement and/or reducing web thickness must be considered in the overall evaluation.

Definitely, these few conceptual ideas suggest the HPFRC may lead to a relevant optimization of girders for road bridges. The goal of this Chapter is to quantify this potential material savings and to understand the role of the different design variables in the dimensioning of the solutions.

3.2 Research significance

UHPFRC is currently available for the construction of girders; its use is covered by several codes, leading to the fact that designers begin to be familiar with its use. However, the very high cost of this material prevents its wide application in the construction market. As a promising alternative to UHPFRC, this Chapter focuses on HPFRC, which combines high performances and affordable cost. This work presents a systematic study on the use of HPFRC to the design of precast simply supported girder bridges. After defining design criteria at SLS and ULS, a complete parametric analysis is performed considering different spans, number of beams, beam slenderness and concrete classes with the goal of investigating their role on the material consumption.

The Chapter is organized as follows. Section 3.3 focuses on the design principles and assumptions; specifically, it describes constitutive laws, load cases, and combinations followed in the design procedure. Section 3.4 defines the complete design methodology for one case of study. The analysis includes the evaluation of the capacity at the (ULS), as well as the study of the limits at the SLS. Also, the dimensioning criteria of the prestressing are analysed. In addition, different shear formulations are applied to define web thickness and shear reinforcement, and the results are critically discussed. Next, Section 3.5 presents the results of the parametric study. The variables under investigation are the class of concrete (C80/95, C100/115 and C120/140), the number of beams (3, 4 and 5), the span of the bridge (20, 40 and 60 m) and the span-to-depth ratio (λ) (17, 20 and 23). Finally, the results of the parametric analysis are analysed and discussed. The Chapter concludes with Section 3.6, where the main findings of this research are summarized.

3.3 Design principles and assumptions

3.3.1 Material properties and constitutive laws

The behaviour under direct tension of the fibre-reinforced cementitious materials is strongly affected by the fibre characteristics and fibre content. In general terms, UHPFRCs with short fibres and a fibre content (V_f) higher than 2% present a hardening response under direct tension [15], while FRCs are prompt to present a softening response [49]. Regarding HPFRC, in this Thesis, it was found a hardening response under bending with a HPFRC of class C120/140, and a V_f=1% of long steel fibres, as described in Chapter 5. In addition,

Walraven et al. [58] designed a HPFRC of class C80/95 with a V_f=0.75% of long fibres which also presented a hardening response under bending, and this behaviour can be exploited in the design. Consequently, as a hypothesis for simplification of the parametric analysis, the HPFRC considered in this study is supposed to have enough ductility to present a hardening post-cracking response under bending, which allows, at least, to consider in the design a horizontal plastic plateau after cracking with the same tensile strength of the concrete matrix. The ultimate limit strain considered in this work has been selected as 4‰according to El-Helou and Graybeal [61] designs recommendations for UHPFRC. However, as described in Section 4.4, this limit has a negligible effect on the M_{Rd}. In contrast, in this study, the possible increase of ductility in compression is not considered [49]. Three classes of HPFRC are considered in this study: C80/95 (f_{ck}=80 MPa), C100/115 (f_{ck}=100 MPa), and C120/140 (f_{ck}=120 MPa). A conventional concrete C30/37 (f_{ck}=30 MPa) is used in all cases for the cast-in-place deck located on the top of the beams. However, it should be mentioned that a ribbed HPFRC deck could carry a reduction of the self-weight of the slab of approximately 30%, which would allow savings in the super and sub-structure. Furthermore, the durability of the bridge will also be improved as the HPFRC can present a permeability index 10 times lower compared to a conventional concrete. Nevertheless, a conventional slab was selected as this work focuses on the study of the girders.

Figure 3.1 summarizes the constitutive laws used in design procedure. Figure 3.1 (a) and (b) shows the compression behaviour at ULS and SLS, respectively. Figure 3.1 (c) and (d) illustrates the constitutive laws under tension at ULS and SLS, respectively. For the reader's convenience, Table 3.1 collects the main parameters that define the constitutive laws. All these values have been obtained from Table 3.1 of EC2-2013 [45] which agrees with Table 7.2-1 of Model Code 2010 (MC-2010) [49].

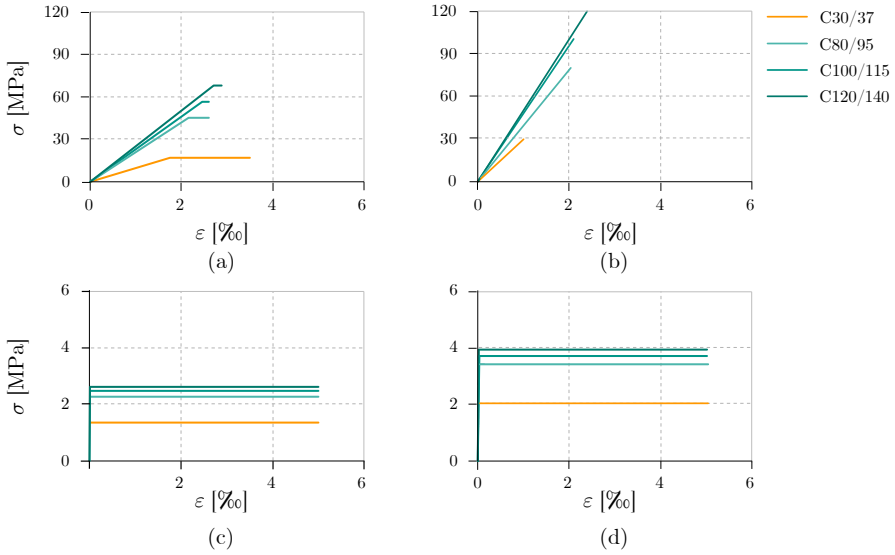

Figure 3.1: Constitutive laws for the concrete considered in the study.

Table 3.1: Concrete strength parameters.

Class	f_{ck} [MPa]	f_{cd} [MPa]	f_{ctk} [MPa]	f_{ctd} [MPa]	E_c [GPa]	ε_{c3} [‰]	ε_{cu3} [‰]
C120/140	120	68.00	3.9	2.60	50.30	2.71	2.88
C100/115	100	56.67	3.7	2.47	47.50	2.44	2.60
C80/95	80	45.33	3.4	2.27	44.40	2.16	2.60
C30/37	30	17.00	2.0	1.33	33.60	1.75	3.50

Pretensioned strands have been used as prestressing steel and they are characterized by an ultimate tensile strength (f_{pu}) of 1860 MPa and a Young Modulus (E_p) of 200 GPa. Its design strength (f_{pd}) is 1455 MPa and the ultimate strain (ε_{pu}) is 20‰. Prestressing losses are considered constant among cases, as 10% for the initial losses and 15% for the long-term losses. The passive reinforcement used for the shear reinforcement is a BS500 (f_{yk}=500 MPa).

3.3.2 Cross-section geometrical dimensioning

Figure 3.2 describes the dimensions of the deck and the girder cross-section. The different colours indicate which dimensions are fixed (black), variable (blue), or they are the output of the design process (red). The width of the deck is constant as 12 m, and two 0.50 m wide security barriers are considered at each side. The thicknesses of the deck and pavement are

0.25 m and 0.08 m, respectively. The number of girders is a variable of the parametric analysis, and it changes among case studies. Therefore, the girder spacing, as well as the length of the overhangs, which is half of the separation between the girders, varies accordingly. As the height of the beam (h) depends on its slenderness (span-to-depth ratio), it is automatically defined for a given slenderness and span.

Figure 3.2 right focuses on the girder cross-section. The procedure to define the dimensions of the beams is as follows: first, the upper flange width (b) is fixed for each girder spacing as follows: 3 girders lead to b=1.50 m; 4 girders lead to b=1.00 m; and 5 girders lead to b=0.50 m. When one case requires a larger top flange area, the upper flange top thickness (h_f) is increased. The thickness of the inclined part (h_{htop}) of the upper plate is fixed to control its slope, to facilitate the removal of the formwork [42]. With respect to the bottom flange, it must have enough space for arranging the strands. They are organized in a 50x50 mm grid, and each strand has an area of 150 mm^2. The inclined thickness of the bottom flange (h_{hbot}), the bottom part (h_{ft}), and the width of the bottom flange (b_{ft}) are increased whether the space for the strands is not enough, or the compression strength requirements are not satisfied. Finally, the thickness of the web (b_w) varies from 80 to 150 mm. Shear check is performed at each metre along the girder axis and, if necessary, ϕ16 single-legged stirrups are arranged at different spacing between 150 and 300 mm. The b_w is increased when a 150 mm leg spacing is not enough.

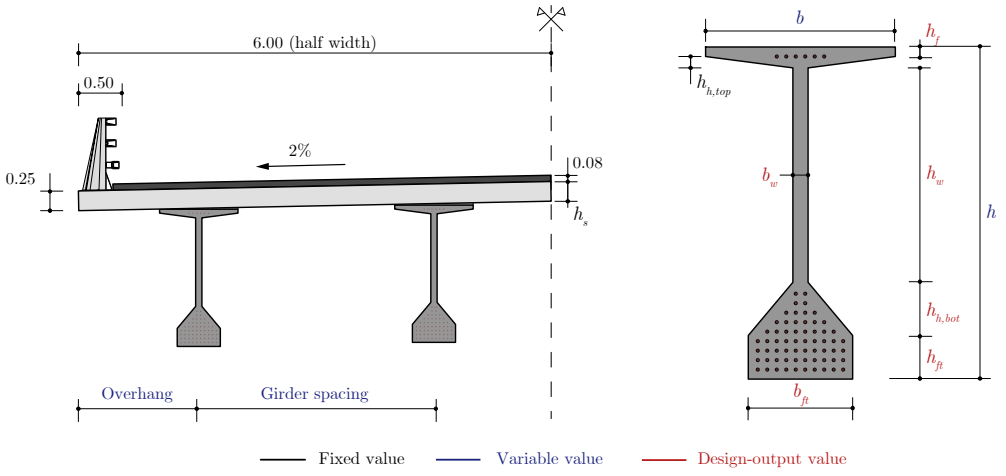

Figure 3.2: Cross-section of a bridge under study indicating the dimensions.

3.3.3 Loads and load combinations

The external loads, as well as the load combinations, considered in this study follow the EN 1992-1-1:2013 (EC2-2013) [45]. Concrete and pavement densities are assumed to be 25 kN/m^3 and 23 kN/m^3, respectively. The weight of each barrier is 2 kN/m, and it is considered to be equally distributed by all beams. The traffic loads defined by the EN 1991-1-2:2013 (EC1-13) [46] are applied to each case. They consist of distributed lanes and a series of heavy vehicles located in the most critical section for each check. To obtain the portion of the traffic load supported by the most loaded girder, 27 different two-dimensional finite element models were performed to calculate the distribution coefficients. The heavy vehicles were located at mid span to obtain the critical bending moment, while they were located at an effective depth (d) from the support to calculate the critical shear load.

For the SLS, three different combinations are considered:

- Quasi-permanent combination, Equation 3.1. The following construction stages are also included: (i) before the pouring of the concrete slab, (ii) once the slab is installed but before its hardening, and (iii) after the installation of the barriers and pavement.

$$1.00 \cdot G \tag{3.1}$$

- Frequent combination, 3.2.

$$1.00 \cdot G + 0.40 \cdot UDL + 0.75 \cdot TS \tag{3.2}$$

- Characteristic combination, Equation 3.3.

$$1.00 \cdot G + 1.00 \cdot UDL + 1.00 \cdot TS \tag{3.3}$$

According to EC2-2013 [45], the effect of prestressing at the SLS is multiplied by 1.05 or 0.95, whereas its action is considered as unfavourable or favourable.

- For the ULS, the persistent combination is considered, Equation 3.4:

$$1.35 \cdot G + 1.35 \cdot UDL + 1.35 \cdot TS \tag{3.4}$$

3.3.4 Serviceability limit state

According to EC2-2013 [45], several limits should be imposed to control cracking at SLS. As a simplification in this work no time-dependent effect has been considered for the calculation of stresses. With respect to the compression stresses, the limit of $0.6 f_{ck}$ could not be exceeded under the characteristic combination of loads. When this condition was not satisfied, the area of the compression flange was increased to fulfil this criterion.

In the design of prestressing conventional concrete structures, the stress limitation under tension is generally taken as zero under quasi-permanent SLS. Furthermore, the same value is considered in the frequent combination to avoid the checking of the fatigue phenomenon. However, for this parametric analysis, thanks to the ductility provided by the fibres, this limit was fixed as f_{ctk}, under quasi-permanent and frequent combinations. The tensile stress limit can be the determining condition for defining the prestressing steel area in the mid-span section. Therefore, in Section 3.4, the influence of different tensile limitations on the design of prestressed steel is studied. Near the supports, a certain amount of prestressing must be unbounded to avoid cracking of the upper flange. A day-to-day practice suggested by a partner construction company consists of limiting the maximum number of unbounded strands at the ends of the beams to a maximum of 30% of the total number of strands; furthermore, the unbounded strands are arranged in a distributed way. When these limits cannot be met, prestressing is introduced also in the upper flange. It should be noted that the local phenomena due to the introduction of the strands has not been checked.

3.3.5 Ultimate limit state

The values of the moment (M_{Ed}) and shear force (V_{Ed}) are the result of the application of the persistent combination (Equation 3.4). To obtain the design value of the resistant moment (M_{Rd}), the ultimate strain criteria were used. The sectional equilibrium was solved for an increasing bending moment until one of the materials reached its ultimate strain (as given in Subsection 3.3.1). Furthermore, to ensure enough ductility in the section for the concrete not crushing at ULS, the same criteria followed to design the Nebraska University (NU) girders [42] was employed; it consists in limiting the neutral axis position (x) as 0.36 of the depth of the section (h_c) [42] (Equation 3.5).

$$x \leq 0.36 h_c \tag{3.5}$$

There is not a common agreement on the expression to be used for proper estimating the shear strength of this kind of elements. Therefore, different shear formulations, published in different standards, are applied for the calculation of the design value of the shear strength (V_{Rd}). First, formulations applied when there is no conventional shear reinforcement are shown in Equations 3.6 to 3.21. The calculation process starts with the identification of the cracked section of the beam. According to the current version of EC2-2013 (EN 1992-1-1:2013 [45]), the Collignon-Jourawski formula, Equation 3.6 has to be used when the section is not cracked. For the cracked sections, the other formulations, from 3.7 to 3.21, apply according to the different codes. The stable version of the new EC2 (FprEN 1992-1-1:2022 (Date: 2022-09)) includes the fibre reinforced concrete (Annex L [48]), and a proper shear strength formulation is given (Equation 3.7 and 3.13). The shear contribution of concrete can be detected in a similar fashion to the König and Fisher formulation [62] in addition to the contribution of fibres, and an updated contribution of the compressive strength. When comparing this expression with the Model Code 2010 (MC-2010) [49] formulation (Equation 3.14), the fibre and concrete contributions were separated. The other two formulations, described through Equations from 3.14 to 3.21, have the same origin in the Vecchio and Collins investigations [63]. It seems that the new version of Model Code, (MC-2020) [50] will follow the Simplified Modified Compression Field Theory (SMCFT) [64] in the future (Equations from 3.18 to 3.21), but in the comments section of the MC-2020 also the approach of the new version of the Eurocode 2 (EC2-2022) [48] will also be given. The formulations to consider the contribution of shear reinforcement to shear strength are collected from Equations 3.22 to 3.26. The new version of the EC2-2022 [48] (Equation 3.22 and 3.23) does not consider any concrete contribution and sums the stirrup and the fibre shear contributions, each of them affected by an interaction factor η. In contrast, Equations 3.24 to 3.26 (MC-2010 and MC-2020, respectively) maintain the concrete contribution. When no further formulation is specifically given, the same as the case without stirrups applies.

EN 1992-1-1:2004 No-cracked section [45]

$$V_{Rd,c} = \frac{I b_w}{S}\sqrt{(f_{ctd})^2 + \alpha_1 \sigma_{cp} f_{ctd}} \tag{3.6}$$

FprEN 1992-1-1:2022 (Issue date: 2022-09) [48]

$$V_{Rd,cf} = \left(\eta_{cF}\frac{0.66}{\gamma_V}\left(100\rho_l f_{ck}\frac{d_{dg}}{d}\right)^{1/3} - k_1\sigma_{cp} + \ \eta_F f_{Ftud}\ \right) b_w z \tag{3.7}$$

$$V_{Rd,cf} \geq \ V_{Rd,min} = \left(\eta_{cF}\tau_{Rdc,min} \ + \ \eta_F f_{Ftud}\right) b_w z \tag{3.8}$$

$$\tau_{Rd,min} = \frac{11}{\gamma_V}\sqrt{\frac{f_{ck}}{f_{yd}}\frac{d_{dg}}{d}} \tag{3.9}$$

$$k_1 = \frac{0.5}{a_{cs,0}} \left(e_p + \frac{d}{3} \right) \frac{A_c}{b_w z} \leq 0.18 \frac{A_c}{b_w z} \tag{3.10}$$

$$a_{cs,0} = \left| \frac{M_{Ed}}{V_{Ed}} \right| \geq \ d \tag{3.11}$$

$$\eta_{cF} = max \left\{ 1.2 - 0.5 f_{Ftuk}; 0.4 \right\} \leq 1.0; \eta_F = 1.0 \tag{3.12}$$

$$d_{dg} = \begin{cases} 16 + D_{lower} \leq 40[\text{mm}] \text{ for concrete with } f_{ck} \leq 60[\text{MPa}] \\ 16 + D_{lower} \left(60/f_{ck}\right)^2 \leq 40[\text{mm}] \text{ for concrete with } f_{ck} > 60[\text{MPa}] \end{cases} \tag{3.13}$$

MC-2010 [65]

$$V_{Rd,c} = \ \left(\frac{0.18}{\gamma_c} k \left[100 \rho_l \left(1 + 7.5 \frac{f_{Ftuk}}{f_{ctk}} \right) f_{ck} \right]^{\frac{1}{3}} + 0.15 \sigma_{cp} \right) b_w d \tag{3.14}$$

MC-2010 based on SMCFT [49]

$$V_{Rd,F} = \frac{1}{\gamma_F} \left(k_v \sqrt{f_{ck}} + k_f f_{Ftuk} cot\theta \right) b_w z \tag{3.15}$$

$$k_v = \frac{0.4}{1 + 1500 \varepsilon_x} \frac{1300}{1000 + k_{dg} z} \tag{3.16}$$

$$\theta = 29 + 7000 \varepsilon_x \tag{3.17}$$

MC-2020 [50]

$$V_{Rd,F} = \frac{1}{\gamma_F} \left(k_v \sqrt{f_{ck}} + k_f f_{Ftuk} cot\theta \right) b_w z \tag{3.18}$$

$$k_v = \frac{0.4}{1 + 1500 \varepsilon_x + \xi} \frac{1300}{1000 + k_{dg} z} \tag{3.19}$$

$$\theta = 29 + 7000 \varepsilon_x \tag{3.20}$$

$$\xi = (20 - 14000 \varepsilon_x) \frac{K_s f_{Ftuk}}{f_{ck}} \tag{3.21}$$

FprEN 1992-1-1:2022 (Issue date: 2022-09) [48]

$$V_{Rd,cf} = \left(\eta_{sw} \rho_w f_{ywd} + \eta_F f_{Ftud} \right) cot(\theta) b_w z \tag{3.22}$$

$$cot\theta_{min} = 3 \text{ if } (|\sigma_{cp}| \geq 3 \text{ MPa and } x < 0.25d) \text{ else } cot\theta_{min} = 2.5 \tag{3.23}$$

MC-2010 [65]

$$V_{Rd} = V_{Rd,c} + \frac{A_{sw}}{S_w} z f_{ywd} cot\theta \tag{3.24}$$

MC-2010 based on SMCFT [49]

$$V_{Rd} = V_{Rd,F} + \frac{A_{sw}}{S_w} z f_{ywd} cot\theta \tag{3.25}$$

MC-2020 [50]

$$V_{Rd} = \frac{f_{Ftuk}}{tg\theta} \frac{1}{\gamma_c} z b_w + \frac{A_{sw}}{S_w} z f_{ywd} cot\theta \tag{3.26}$$

3.4 Detailed example of the design procedure

3.4.1 Geometrical and material definitions

This section describes the design procedure in full detail. It is applied to a case of study named as 40.17.3/100. This bridge has a span of 40 m and a slenderness of 17. It consists of three girders with a concrete C100/115 (f_{ck}=100 MPa), as shown in Figure 3. The deck, as mentioned before, consists in a 250 mm-thick slab made of concrete C30/37 (f_{ck}=30 MPa). Following the same colour rule presented before (black for fixed values, blue for variable values, and red for design-output values) the bottom part of Figure 3.3 illustrates the solution which fulfil all limit states. In this specific case, the web thickness was not increased from the minimum value of 80 mm. The bottom-right corner of the same figure illustrates the spaces available for the strands; a portion of them is full-bonded, and another portion are debonded at the beam end (different symbols correspond to different debonding lengths).

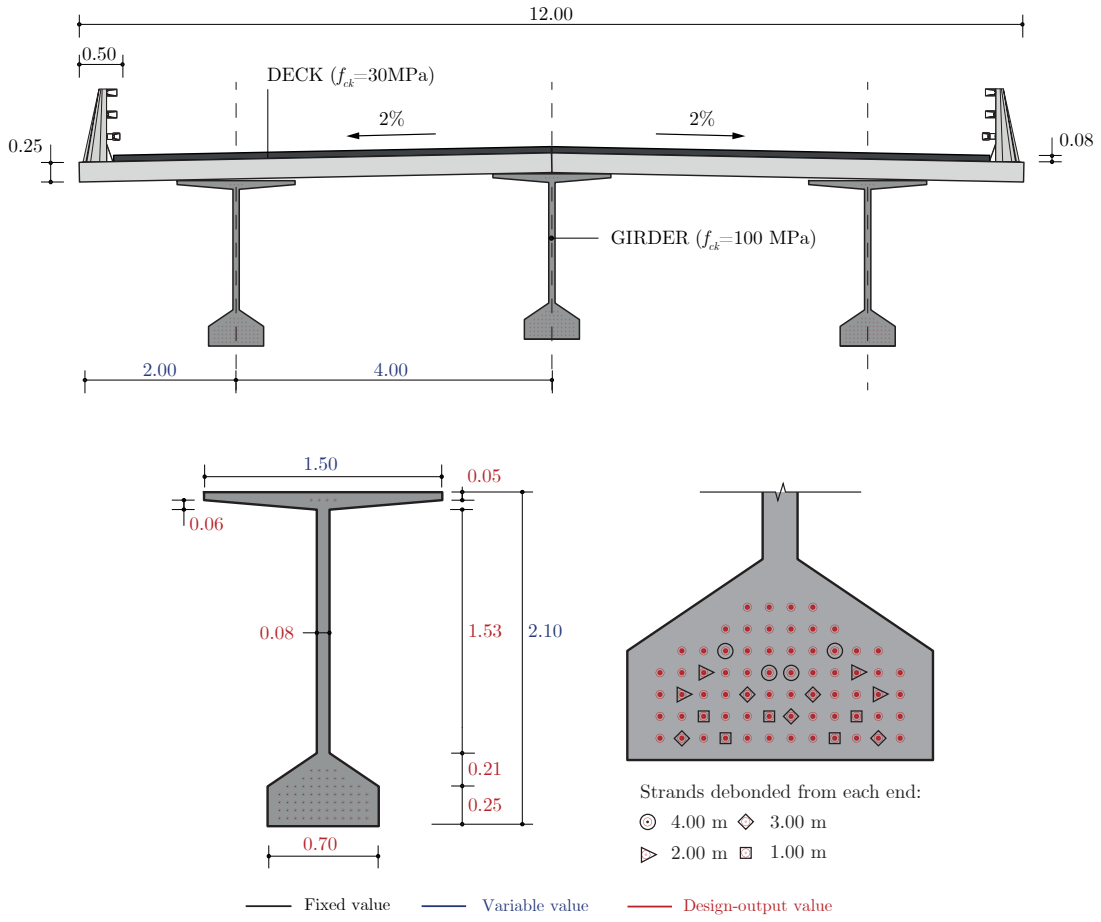

Figure 3.3: Geometrical description of detailed case 40.17.3/100: at the top the cross-section of the bridge, at the bottom left the cross-section of the girder, and at the bottom right the possible strands position and the debonded lengths.

3.4.2 Flexural analysis at ULS and SLS

The design bending moments at mid-span, calculated as described in Section 3.3, are numerically detailed in Table 3.2. In a simply supported structure, such as the case under study, the maximum prestressing steel area (A_p) is required at the mid-span section. Based on the day-to-day practice, the A_p is calculated at SLS using $\sigma_{ct,max}$ equal to f_{ctk}. Four different calculation hypotheses are examined: the first two (E) consider the construction stages, while the other two (NE) do not contemplate any step-by-step analysis. In addition, two calculations consider the stress increase in the prestressing steel due to the sectional compatibility with the concrete (B), while the other two neglect this effect (U). This totally

leads to 4 assumptions, which results, in terms of required prestressing steel, are shown in Figure 3.4, and numerically expressed in Table 3.3. The main finding is that to ignore the construction process in the calculations leads to an unsafe design. In contrast, there is almost no influence when considering section compatibility in the design.

Table 3.2: Bending moments considered in the design at mid-span.

Case	Girder self-weigth [kNm] - [%]	Deck self-weight [kNm] - [%]	Additional load [kNm] - [%]	Distributed load (UDL) [kNm] - [%]	Heavy vehicles (TS) [kNm] - [%]	Total
SLS	2510 - (11%)	5000 - (22%)	2475 - (11%)	5650 - (24%)	7436 - (32%)	23070 - (100%)
ULS	3388 - (11%)	6750 - (22%)	3341 - (11%)	7628 - (24%)	10039 - (32%)	31145 - (100%)

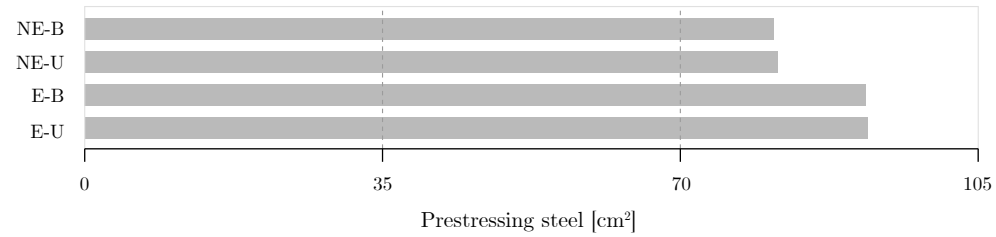

Figure 3.4: Prestressing steel dimensioned by the SLS stress condition under different calculation hypothesis at mid-span.

Table 3.3: Prestressing steel dimensioned at SLS following different calculation hypothesis.

Method	NE-B	NE-U	E-B	E-U
$A_p[cm^2]$	81.00	81.40	91.84	92.00

In the case of HPFRC, the question arises of which value of $\sigma_{ct,max}$ should be considered at SLS. To explore the relevance of this parameter in the design, the A_p is calculated considering three different assumptions: $\sigma_{ct,max}$=0, $\sigma_{ct,max}$=f_{ctk}, and $\sigma_{ct,max}$=f_{ctm}. Figure 3.5 shows the prestressing steel area required for three hypotheses, and the A_p required at ULS. This latter is depicted as a vertical dotted line as the tensile strength has a negligible effect on the M_{Rd} [10]. The results are numerically collected also in Table 3.4. The analysis proves that, for this specific case, the dimensioning of A_p at ULS is more restrictive than SLS, except if $\sigma_{ct,max}$ is lower than 1.33 MPa. The intersection of the two dimensioning criteria has been marked with a red dot in Figure 3.5. In order to complete the flexural analysis, Figure 6 illustrates the strain and stress distribution at the mid-span for the ultimate bending strength. The

small area of the web working at tensile stresses explains the small influence of f_{Ftu} on M_{Rd}. The neutral axis is marked with a dashed line, proving that the imposed criterion of ductility is fulfilled (i.e, $x< 0.36h$). The M_{Rd} is equal to 31879 kNm, higher than the M_{Ed} of 31145 kNm.

Table 3.4: Prestressing steel dimensioned at SLS, with different tensile stress limitations, and at ULS.

Method	SLS $\sigma_{ct,max}$=0	SLS $\sigma_{ct,max}=f_{ctk}$	SLS $\sigma_{ct,max}=f_{ctm}$	ULS
$A_p[cm^2]$	104.42	91.84	87.02	99.85

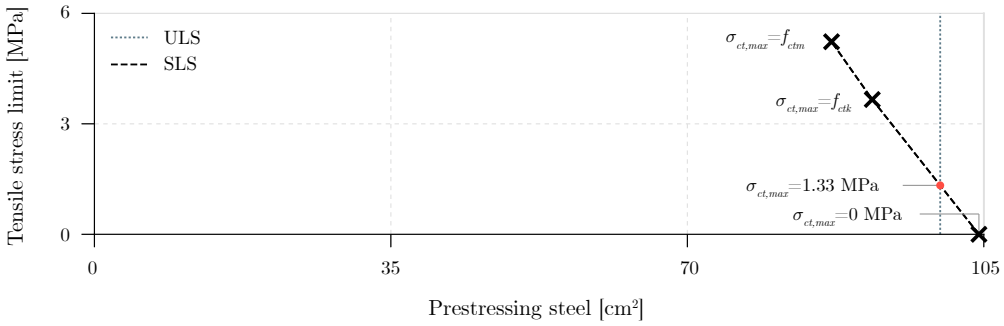

Figure 3.5: Prestressing steel dimensioned by SLS with different tensile stress limits and ULS at mid-span.

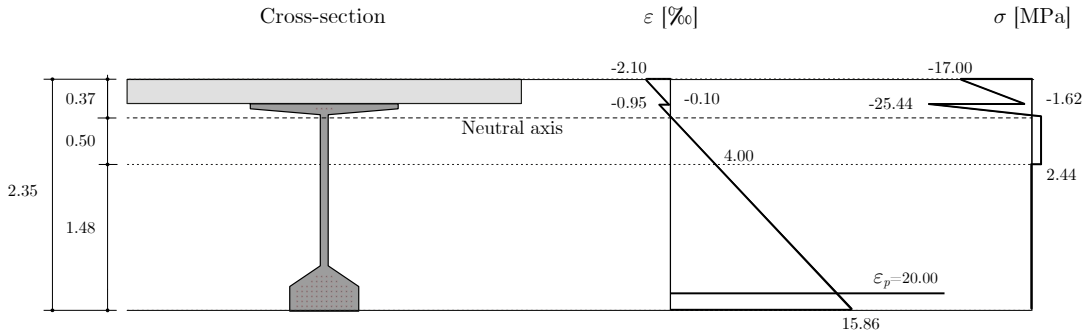

Figure 3.6: Strain and stress profiles at the calculation of the MRd at mid-span.

3.4.3 Shear analysis at ULS

Figure 3.7 shows the shear analysis of the girder at ULS. The plot compares the applied shear load (V_{Ed}) with the design shear strength (V_{Rd}) obtained according to several models,

as described in Subsection 3.3.5. The plot proves the great difference in terms of V_{Rd} among the applied formulations. A severe difference is observed between the formulation of the MC-2020 based on the SMCFT (green line) and the MC-2010 formulation (yellow line). As a general consideration, the MC-2010 formulation (yellow line) is the least restrictive. This model was conceived for lower compression classes and softening post-cracking under direct tension, which is not the case for this specific HPFRC. However, the MC-2020 approach is expected to consider higher compression classes and the hardening post-cracking response under tension.

After analysing all the relevant differences among shear formulations, the model included in the MC-2020, green line, (Equation 23) is chosen to design the different cases of study. As described in Subsection 3.3.5, one-leg ϕ16 stirrups are arranged when required, and their spacing is optimized along the girder, as detailed in Table 3.5. This variable stirrup separation can be also appreciated in the same Figure 3.7.

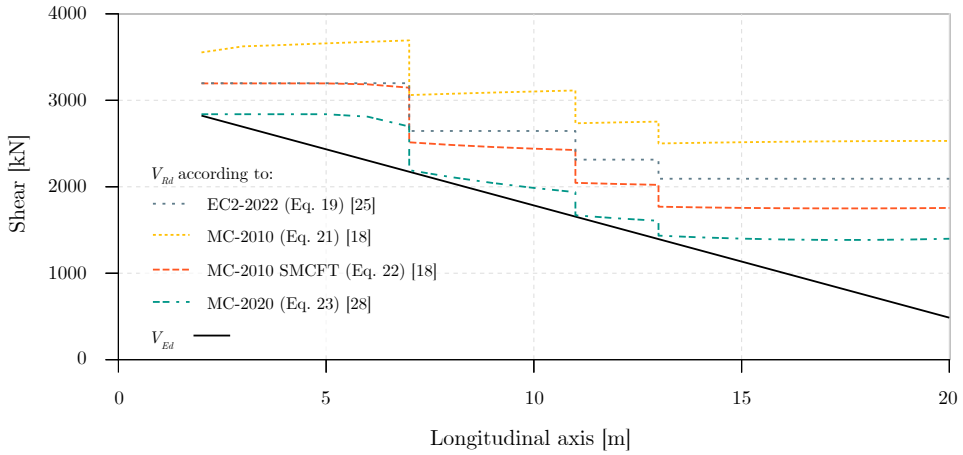

Figure 3.7: Shear load checks applying different formulations showed upon half of the girder length.

Table 3.5: Stirrups spacing according to the MC-2020 shear strength formulation.

x [m]	0-7	7-11	11-13	13-20
s [cm]	15	20	25	30

3.5 Parametric analysis

3.5.1 Definition of case studies

As briefly mentioned before, the parametric analysis presented in this work is based on 4 variables parametrically varied. First, three span lengths (L=20 m, L=40 m and L=60 m) are considered. Second, the slenderness (λ) which is defined as the relationship between the span (L) and the total height (h_c=h+h_s) is taken as 17, 20 and 23. For both variables, the first two values are within the conventional practice for precast girders, while a span of 60 m and a slenderness of 23 are driven to achieve out-of-the-trend results. The third variable under study is represented by the number of beams to support the slab, which takes the values of 3, 4, and 5. Lastly, three different HPFRCs are used for the girders: C80/95 (f_{ck}=80 MPa), C100/115 (f_{ck}=100 MPa), and C120/140 (f_{ck}=120 MPa).

A specific ID has been created for each case of study based on the following codification span-slenderness-number of beams/concrete class. Therefore, the case 40-20-4/80 presents a span length of L=40 m, a slenderness of λ=20, 4 beams in the cross-section, and a concrete class C80/95.

3.5.2 Effective beam thickness

A common parameter to evaluate the concrete consumption in a bridge is the effective thickness (t_{eff}), expressed as shown in Equation 3.27:

$$t_{eff} = \frac{V}{L \cdot b_{deck}} \tag{3.27}$$

where V is the total volume of precast concrete girders, bdeck is the width of the deck, and L is the span length of the bridge. Given that this study focuses on the precast girder design, the consumption of deck material is not included in the comparison of the results. Table 3.6 - 3.8 includes the material consumption per unit of deck area allowing for a comparison among cases. Figure 3.8 shows the differences of t_{eff} with respect to the span lengths; from left to right, each graph describes the cases characterized by a span of, respectively, 20 m, 40 m, and 60 m. The slenderness λ divides the subplot into three smaller groups. A specific colour is used to identify a different number of beams: indigo for 3 beams (B3), orange for 4 beams (B4), and green for 5 beams (B5). Finally, a tone is assigned to identify each HPFRC class, being C80/95 the lightest and C120/140 the darkest.

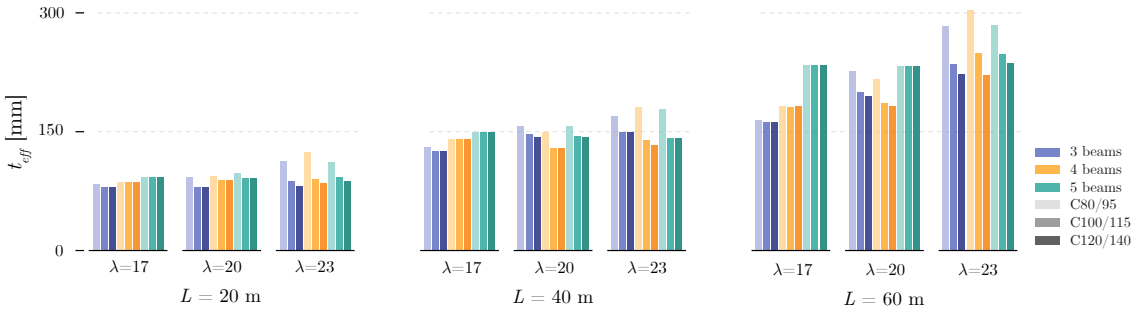

Figure 3.8: Effective beam thickness for all cases of the parameter study grouped by their span length, left L=20 m, centre L=40 m and right L= 60m.

Table 3.6: Results of the parametric analysis 1/3.

ID	Effective depth t_{eff} [mm]	Web thickness b_w [cm]	Stirrups [kg/m^2]	Bottom prest. [kg/m^2]	Top prest. [kg/m^2]	Total prest. [kg/m^2]	Cost [€/m^2]
20-17-3/80	84.10	8.00	1.64	10.89	1.18	12.07	26.52
20-17-3/100	80.70	8.00	1.61	10.89	0.88	11.78	28.08
20-17-3/120	80.70	8.00	1.61	10.89	0.88	11.78	30.50
20-17-4/80	87.00	8.00	1.56	11.78	1.18	12.95	27.75
20-17-4/100	87.00	8.00	1.52	11.78	1.18	12.95	30.33
20-17-4/120	87.00	8.00	1.49	11.78	1.18	12.95	32.91
20-17-5/80	93.40	8.00	1.72	11.78	0.98	12.76	28.78
20-17-5/100	92.50	8.00	1.64	11.78	0.98	12.76	31.35
20-17-5/120	92.50	8.00	1.64	11.78	0.98	12.76	34.12
20-20-3/80	92.50	9.00	1.14	12.66	1.47	14.13	29.39
20-20-3/100	80.60	8.00	1.22	12.36	1.47	13.84	29.58
20-20-3/120	80.60	8.00	1.14	12.36	1.47	13.84	31.94
20-20-4/80	93.90	8.00	1.27	13.74	1.57	15.31	30.80
20-20-4/100	88.70	8.00	1.23	13.74	1.57	15.31	32.54
20-20-4/120	88.70	8.00	1.21	13.74	1.57	15.31	35.18
20-20-5/80	97.70	8.00	1.39	14.23	1.47	15.70	31.89
20-20-5/100	91.10	8.00	1.24	14.23	1.47	15.70	33.38
20-20-5/120	91.10	8.00	1.18	14.23	1.47	15.70	36.07
20-23-3/80	112.70	11.00	0.86	15.60	2.65	18.25	36.30
20-23-3/100	87.20	10.00	0.86	14.13	2.06	16.19	32.73
20-23-3/120	81.70	9.00	0.93	13.84	2.06	15.90	33.88
20-23-4/80	124.70	8.00	1.05	16.49	3.14	19.63	39.72
20-23-4/100	90.10	8.00	1.05	15.31	2.36	17.66	34.78
20-23-4/120	84.80	8.00	0.95	15.31	2.36	17.66	36.18
20-23-5/80	111.30	8.00	1.05	16.68	2.45	19.13	37.02
20-23-5/100	92.60	8.00	1.03	16.19	2.45	18.64	36.15
20-23-5/120	87.70	8.00	1.03	15.70	2.45	18.15	37.37
40-17-3/80	130.40	9.00	3.41	20.02	1.47	21.49	44.34
40-17-3/100	125.50	8.00	3.47	19.72	1.18	20.90	46.79
40-17-3/120	125.50	8.00	3.35	19.72	1.18	20.90	50.45
40-17-4/80	140.50	8.00	3.55	20.80	1.57	22.37	46.97
40-17-4/100	140.50	8.00	3.55	20.80	1.18	21.98	50.84
40-17-4/120	140.50	8.00	3.30	20.80	1.18	21.98	54.85
40-17-5/80	149.90	8.00	3.82	21.10	1.96	23.06	49.41
40-17-5/100	149.90	8.00	3.53	21.10	1.96	23.06	53.66
40-17-5/120	149.90	8.00	3.53	21.10	1.47	22.57	57.72

Table 3.7: Results of the parametric analysis 2/3.

ID	Effective depth t_{eff} [mm]	Web thickness b_w [cm]	Stirrups [kg/m^2]	Bottom prest. [kg/m^2]	Top prest. [kg/m^2]	Total prest. [kg/m^2]	Cost [€/m^2]
40-20-3/80	157.10	15.00	2.44	24.14	2.36	26.49	52.58
40-20-3/100	147.00	14.00	2.44	23.84	2.36	26.20	55.01
40-20-3/120	143.70	13.00	2.44	23.55	2.06	25.61	58.14
40-20-4/80	149.30	8.00	3.47	24.73	1.96	26.69	52.28
40-20-4/100	129.20	8.00	3.30	24.34	2.36	26.69	52.59
40-20-4/120	129.20	8.00	3.30	24.34	2.36	26.69	56.47
40-20-5/80	156.80	8.00	3.43	25.02	2.45	27.48	54.23
40-20-5/100	145.00	8.00	3.35	25.02	1.96	26.98	56.06
40-20-5/120	143.00	8.00	3.35	24.53	1.96	26.49	59.52
40-23-3/80	169.50	15.00	2.59	28.26	2.65	30.91	58.79
40-23-3/100	149.40	15.00	2.41	27.67	2.94	30.62	59.44
40-23-3/120	149.40	15.00	2.26	27.67	2.94	30.62	63.79
40-23-4/80	181.30	11.00	2.87	29.83	3.14	32.97	62.87
40-23-4/100	139.20	9.00	2.89	28.65	2.75	31.40	58.51
40-23-4/120	132.60	8.00	3.04	28.26	2.75	31.01	60.94
40-23-5/80	179.10	8.00	3.29	29.93	2.94	32.87	62.76
40-23-5/100	142.20	8.00	3.00	28.95	2.94	31.89	59.62
40-23-5/120	142.20	8.00	3.00	28.95	2.94	31.89	63.89
60-17-3/80	165.10	8.00	5.06	27.67	1.47	29.14	58.49
60-17-3/100	162.30	8.00	5.02	27.67	1.47	29.14	62.86
60-17-3/120	162.30	8.00	4.93	27.67	1.47	29.14	67.65
60-17-4/80	182.30	8.00	5.19	28.65	2.36	31.01	63.20
60-17-4/100	181.30	8.00	5.11	28.26	1.96	30.22	67.70
60-17-4/120	182.30	8.00	4.85	28.26	1.96	30.22	73.15
60-17-5/80	234.70	8.00	5.73	29.93	1.96	31.89	73.37
60-17-5/100	234.70	8.00	5.48	29.93	1.96	31.89	80.19
60-17-5/120	233.60	8.00	5.39	29.44	1.96	31.40	86.47
60-20-3/80	226.90	15.00	3.97	35.03	2.65	37.68	75.79
60-20-3/100	200.40	14.00	3.64	34.15	2.94	37.09	76.49
60-20-3/120	194.70	13.00	3.64	33.85	2.65	36.50	80.65
60-20-4/80	216.40	8.00	5.39	35.72	1.96	37.68	75.17
60-20-4/100	185.80	8.00	4.92	34.54	2.36	36.90	74.45
60-20-4/120	182.70	8.00	4.89	34.54	2.36	36.90	79.29
60-20-5/80	233.10	8.00	5.17	36.31	2.45	38.76	78.81
60-20-5/100	233.10	8.00	5.08	35.82	2.45	38.27	85.28
60-20-5/120	233.10	8.00	4.99	35.82	2.45	38.27	92.20

Table 3.8: Results of the parametric analysis 3/3.

ID	Effective depth t_{eff} [mm]	Web thickness b_w [cm]	Stirrups [kg/m^2]	Bottom prest. [kg/m^2]	Top prest. [kg/m^2]	Total prest. [kg/m^2]	Cost [€/m^2]
60-23-3/80	283.20	15.00	4.36	42.98	2.94	45.92	93.10
60-23-3/100	235.50	15.00	3.87	40.92	3.24	44.16	90.04
60-23-3/120	223.00	15.00	3.68	40.62	3.24	43.86	93.81
60-23-4/80	303.50	13.00	4.23	45.53	3.53	49.06	99.26
60-23-4/100	249.20	11.00	4.29	42.78	3.14	45.92	94.73
60-23-4/120	221.20	9.00	4.45	41.61	2.75	44.35	94.50
60-23-5/80	285.20	8.00	5.12	44.16	2.94	47.10	95.12
60-23-5/100	248.10	8.00	5.06	42.68	2.94	45.63	94.89
60-23-5/120	236.10	8.00	4.75	42.19	2.45	44.65	98.43

As general finding, to higher concrete class correspond lower values of t_{eff}. This tendency is not significant for bridges with a span of 20 meters, where the material consumption is almost the same, independently on the concrete class. The trend is more noticeable for intermediate spans (i.e. 40 m) and clearly significant for long-span girders of 60 meters, where the concrete-savings achieve a -17% when a slenderness of 23 is considered, and a C120/140 is used instead of a C80/95. These results shed light on the fact that higher concrete classes lead to significant reduction of concrete if employed for slender and long girder bridges. Potential material savings are found when looking at the differences between the maximum and minimum values of each group defined by the same span. This difference is accentuated for the 60-m cases, where depending on the number of beams, slenderness and concrete class, the difference can be up to 50% (t_{eff}=162 mm for 40-17-3/120 vs t_{eff}=304 mm for 40-23-4/80). The minimum values of t_{eff} obtained for each span fit a linear trend defined by Equation 3.28 (R^2= 0.997).

$$t_{eff}\ [\text{mm}] = 2.043L\ [\text{m}] + 41.100 \tag{3.28}$$

3.5.3 Prestressing steel quantity

Figure 3.9 presents the prestressing steel quantity per square metre of bridge deck for each case of study. The prestressing steel consumption clearly shows a linear increase with the span and with slenderness.

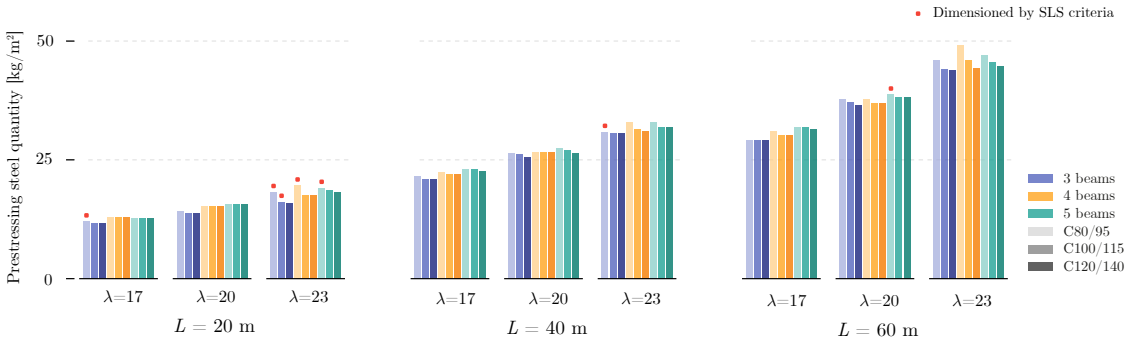

Figure 3.9: Prestressing steel quantity for all cases of the parameter study grouped by their span length, left L=20 m, centre L=40 m and right L= 60.

Within the cases with the same span, the minimum prestressing steel quantities are the cases defined as 20-17-3/100, 40-17-3/100, and 60-17-3/80, all of them with a λ=17 and 3 beams to support the deck. A linear relationship among these cases is provided in Equation 3.29 (R^2=0.999):

$$\text{Prestressing steel quantity} \left[\frac{kg}{m^2}\right] = 0.434L \text{ [m]} + 3.247 \tag{3.29}$$

Differences in concrete classes are generally not significant leading to small variations of prestressing quantity, regardless girder length and slenderness. However, for slenderness 23, this difference increases to 11-15%, indicating the convenience of using higher concrete class to reduce the prestressing steel for high slenderness.

As a general design rule, the tensile stress limitation at SLS in the midspan is the most restrictive condition for dimensioning the prestressing steel area. Unexpectedly, this happens only in 8.6% of the cases, which are marked in Figure 3.9 with a red square located at the bar top. This is explained by the fact that since f_{ctm} grows with the concrete class, the limitation at SLS is less restrictive for C80, C100, and C120 than for conventional concretes. On the contrary, as bending moment check at ULS is not significantly affected by the concrete class, there is no case with a C120 which prestressing steel is dimensioned due to the stress limitations at SLS.

3.5.4 Stirrup's quantity

One of the most attractive advantages of the use of HPFRC in bridge engineering is the contribution of fibres to the shear resistance, which allows to reduce the web thickness, and even to eliminate the conventional shear reinforcement in some cases. Figure 3.10 shows, on the top, the stirrups quantity per square metre of the deck and, on the bottom, the corresponding web thickness (b_w). Both plots must be analysed simultaneously.

If a specific span is selected, it is interesting to observe that to a higher concrete class corresponds a lower quantity of stirrups, maintaining unchanged the web thickness. The minimum thicknesses of the webs range from 80 to 150 mm depending on span and slenderness. The optimal solution can be defined as the case with the minimum quantity of stirrups, also maintaining a minimum value of b_w (80 mm). Independently on the span, these optimal case studies (20-23-4/120, 40-23-4/120 and 60-23-5/120) have a slenderness of 23 and a concrete class equal to C120/140.

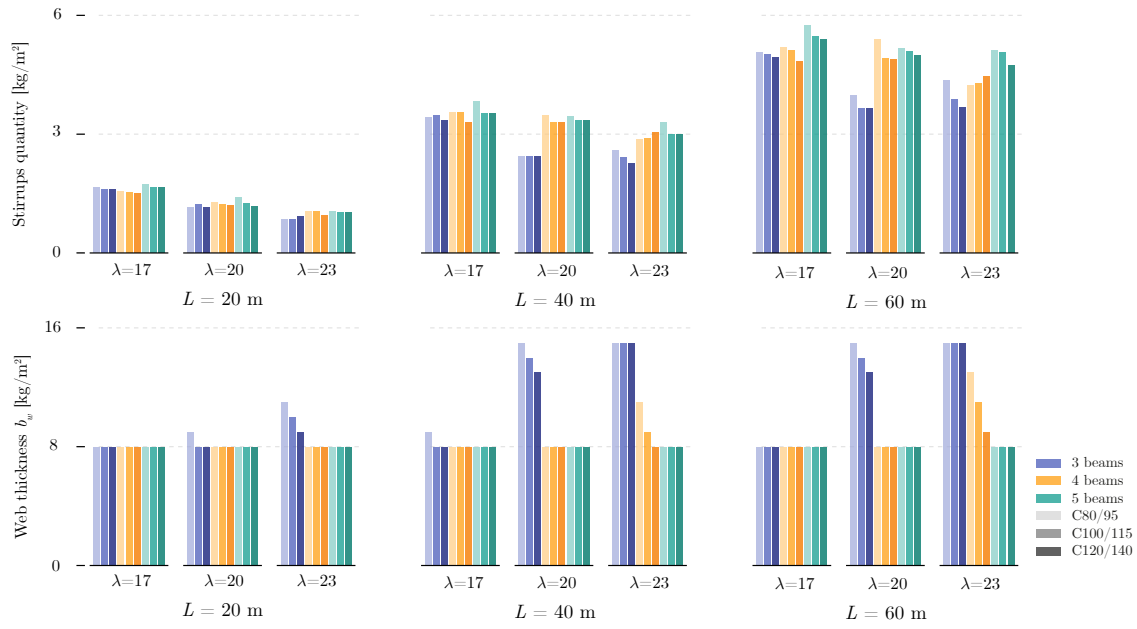

Figure 3.10: At the top, the stirrups quantity and bottom the web thickness for all cases of the parameter study grouped by their span length, left L=20 m, centre L=40 m and right L= 60m.

3.5.5 Cases of study with minimum material consumption

Table 3.9 summarizes the cases studies associated with a minimal consumption of each material (concrete, prestressing, and shear reinforcement), and the cases with the minimum material cost. The cross-sections of these optimal solutions are illustrated in the left part of Figure 3.11. Each row is characterised by a fixed span length, while each column gathers the optimal cases of study corresponding to a specific material (concrete on left, prestressing on centre, stirrups on the right). The different tones of the cross-sections indicate a different concrete class. The same Figure 3.11, on the right, illustrates three-column graphs that show the amount of material per deck area of each optimal case. At the top, the concrete, at the centre the prestressing steel, and at the bottom the stirrups. The 9 optimal cases are ordered by their span length in 3 smaller groups. In addition, Table 3.9 shows the material cost of the materials calculated in this work for each case between brackets. The unitary cost used are: C80/95=170 €/m^3, C100/115=200 €/m^3, C120/140=230 €/m^3 (including the cost of the steel fibres), stirrups=0.83 €/kg, and prestressing steel=0.90 €/kg.

Table 3.9: Optimum cases for each span and aspect under consideration, case (cost [€/m^2]).

	Concrete	Prestressing steel	Stirrups steel	Cost
L=20 m	20-20-3/100 (29.58)	20-17-3/100 (28.08)	20-23-4/120 (36.18)	20-17-3/80 (26.52)
L=40 m	40-17-3/100 (46.79)	40-17-3/100 (46.79)	40-23-4/120 (60.94)	40-17-3/80 (44.34)
L=60 m	60-17-3/100 (62.86)	60-17-3/80 (58.49)	60-23-5/120 (98.43)	60-17-3/80 (58.49)

As main finding, the optimal cases for minimizing concrete and prestressing steel consumption are generally characterized by 3 beams to support the slab and a slenderness of 17. For girders with these characteristics, the influence of the concrete class is low. For example, case 20-20-3/100 presents the same t_{eff} as case 20-17-3/100 since a higher mechanical arm reduces the prestressing steel quantity and the bottom flange, dimensioned to give room to the strands, is reduced. In contrast, cases with lower consumption of stirrups are characterized by the highest concrete class (C120/140) and the highest slenderness (23). Furthermore, the three case studies present four or five beams, which is detrimental for minimizing the consumption of concrete and prestressing. It is also remarkable that the minimum concrete consumption is found for the three span cases for a concrete class C100/115, being equal for their respective C120/140 cases. It can be concluded that for these cases the cross-section dimensions cannot be further reduced increasing the concrete strength due to

other considerations governing its design or because the minimum values have been reached (e.g. $h_f \geq 50$ mm).

The Lynch bridge (built in Asunción, Paraguay) has been selected as a reference ordinary bridge for comparison purpose. This bridge is made of a conventional C35/45 and presents a simply supported beams with a span of 35 m. The cross-section is based on 9 I-beams with a separation of 2.20 m; each of them presents a parabolic prestressing profile with three tendons of 13 strands. This bridge is characterized by a t_{eff}=336 mm, and material consumptions of 7.65 kg/m^2 and 19.48 kg/m^2, respectively, for stirrups and prestressing steel. Passive reinforcement due to local phenomena was disregarded in this comparison. Considering a unitary cost for the strands of post-tensioning tendons of 1.10 €/kg, and 79 €/m^3 for the C35/45, the material cost is estimated in 54.23 €/m^2.

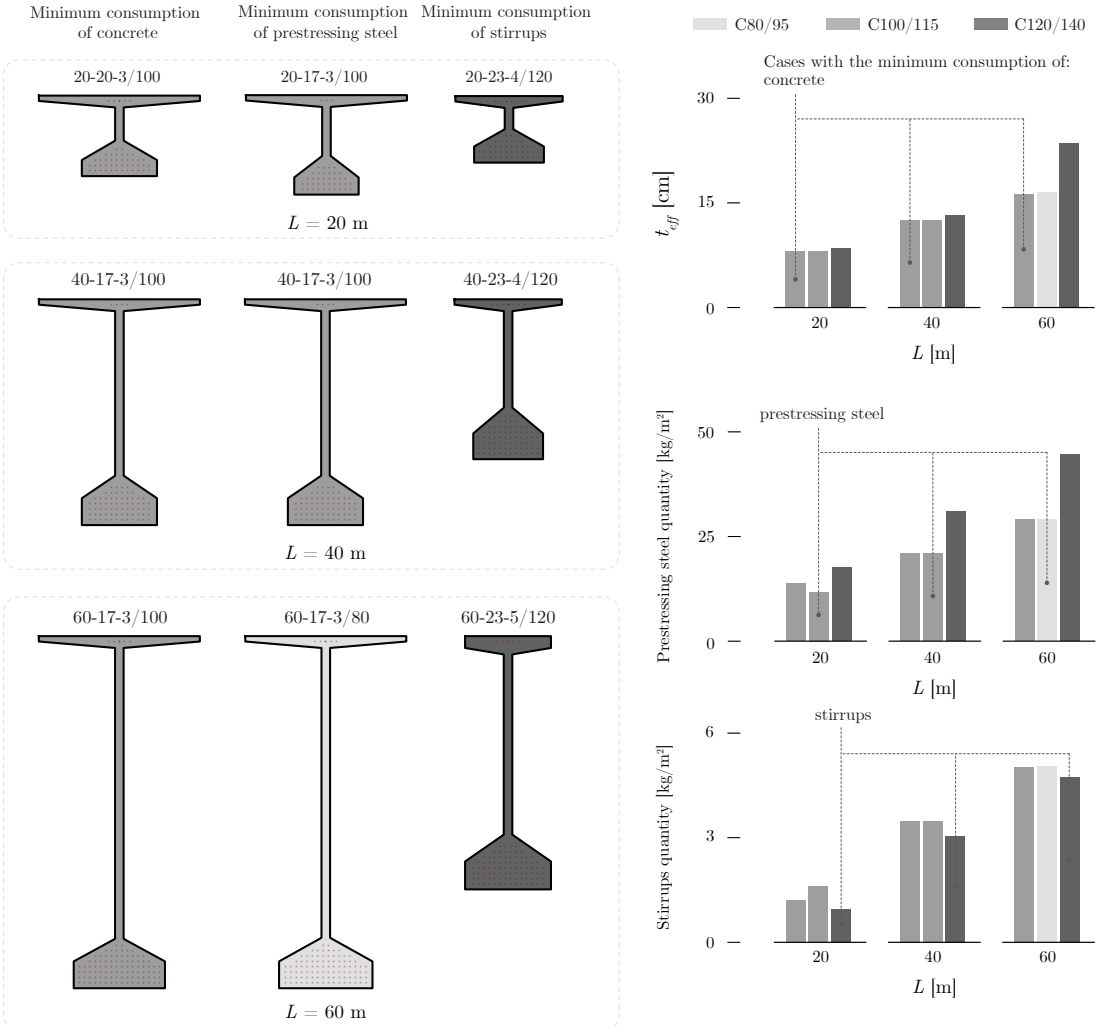

Figure 3.11: Optimum cases according to the concrete, prestressing, and stirrups consumption, at the left the 8 cross-sections are showed grouped by their span length; at the right, the material consumption of each case is case is showed.

3.6 Conclusions

3.6.1 Conclusions

This Chapter focused on the use of HPFRC for I-girder bridge decks. Different design variables (concrete class, slenderness, span and number of beams) have been parametrically analysed to assess their influence in terms of consumption of concrete, prestressing and stirrups. The design procedure was detailed for a specific case of study, pointing out relevant

differences by using specific formulation or assumptions, and then applied to all the case studies. The main findings of this study are:

- In contrast to common practice, when working with HPFRC the fulfilment of ULS conditions is generally more restrictive than the ones at SLS for the dimensioning the prestressing. This is because higher values of the tensile strength associated to HPFRC are more effective at SLS than ULS, where its contribution is almost negligible.
- The application of different shear formulations leads to relevant differences in terms of shear resistance. According to authors, the approach based on Model Code 2020 should be followed to cover with the same formulation all concrete types.
- Once a specific bridge span is selected, the concrete class has a strong influence on the effective thickness of the girder. Specifically, this effect is significant in bridges with long span and high slenderness. For example, for a 60 m-girder with a slenderness of 23, the use of C120/140 instead of C80/95 leads to a reduction of material consumption of around 26%. Therefore, the use of higher concrete classes is recommended for bridges with high spans and slendernesses.
- A similar influence, although in a less pronounced effect, has been detected with the quantity of the prestressing steel.
- The contribution of fibres to shear leads to very slender webs also for girder with a span of 60 meters. In addition, in most cases ϕ16 single-legged stirrups with a separation varying between 15 and 30 cm is sufficient for providing enough shear strength. The stirrups quantity is significantly lower than the material consumption that would be required by a standard concrete.
- The case studies with the lowest overall material cost are based on the same number of beams (3), slenderness (17), and concrete class (C80/95). All cases with minimum consumption of concrete and prestressing steel also are based on the same number of beams, and five out of six are characterized by the same slenderness. Regarding concrete class, concrete savings comparing C100/115 with C80/95 are not enough to compensate for the differences between their costs.
- Optimum cases for a L=40 m achieved significant savings regarding concrete and stirrups compared to the reference case study. In fact, considering the case 40-17-3/100, the reduction in teff reaches 63%. Comparing the reference bridge with the case 40-23-4/120, savings in stirrups quantity equals 60%. Lastly, the analysis of the material

cost considered for the girders, the optimum solution 40-17-3/80 costs around 44.34 €/m2, 23% less than the reference bridge.

This Chapter has analysed how different variables affect the dimensioning of the optimized I-shaped road girder. Intentionally, the authors have avoided the definition of a global optimal solution in terms of slenderness, concrete class, and number of beams for a given span. In fact, the exact definition of this overall optimized solution depends on many variables such as the cost of materials (which are largely different depending on the geographical location and time), cost of labour (also strongly related on geography), optimization target (CO2, cost, standardization, etc.). In addition, any variation of girder self-weight has consequences in terms of crane cost, and pier and foundation dimensioning. Any assumption in that direction would lead to an incomplete and superficial result. On the contrary, the presented results are objective and indicate clear trends to identify the effect of such variables in girder dimensioning. It is part of the designer's role to evaluate case by case the optimal solution for each specific situation.

4

Specific considerations on fibre reinforced concretes

4.1 Introduction

Since the French patent of H. Alfsen (1918) on the addition of fibre to concrete, the use of fibre reinforced concrete (FRC) has gained popularity over time. Today, it is commonly applied, for example, to tunnel segments [66] and industrial building slabs [67]. More recently, Braunauer et al. [68] developed Ultra High Performance Concrete (UHPC) with a water-to-cement ratio (w/c) between 0.2 and 0.3, achieving a f_{cm} up to 200 MPa. However, the developed UHPC had low workability, which prevented their implementation in the construction sector. As consequence, a decade later, pozzolanic additions and superplasticisers were added to the mix to improve the UHPCs' workability. Finally, between the 1980s and 2000, the addition of fibres to the UHPC matrix led to the implementation of the UHPFRC in civil engineering [7]. This work focuses on girders casted in precast factories, which guarantees and adequate control during casting. Different examples prove the wide application of UHPFRC to precast elements for bridge construction. As an example, the company DURA Technology [53] has pioneering implemented several UHPFRC solutions leading to the construction of more than 100 bridges in the last decade based on precast I- and U-girders. A growing number of UHPFRC applications can be also observed in the USA where institutions such as the PCI, together with the FHWA, support precast companies in developing their own UHPFRC mixes using local materials [54]. However, as the main drawback, UHPFRC is around 12 times more expensive than conventional concrete. This very high cost limits the widespread

implementation of UHPFRC in the construction sector.

As an appealing intermediate option between FRC and UHPFRC, the HPFRC may represent a product that compromises cost and material benefits [57]. Walraven et al. [58] proved that an HPFRC could achieve post-cracking hardening behaviour under bending tests with smeared cracking. This behaviour might allow to account for fibre contribution to shear strength and to avoid the use of conventional shear reinforcement [49], which represents around 40% of passive reinforcement in conventional girder bridges. Different proposals regarding steel fibre reinforced concrete beams without stirrups are found in the scientific literature, such as the one recently published by Marì Bernat et al. [69]. Furthermore, the same fibres can control the development of cracks, possibly also replacing part of the conventional longitudinal reinforcement.

Figure 4.1 collects three plots to contextualize the fibre reinforced mixes. The top graph shows on the horizontal axis the f_{ck}. Each horizontal bar limits the application field of a code or design recommendation regarding Conventional Concrete (CC), high-performance concrete (HPC), and/or ultra-high performance concrete (UHPC). These three material classes are coloured with different tones, with the darker one corresponding to higher f_{ck}. Furthermore, orange is used if the document does not consider fibres, teal if it considers fibres and yellow if it takes both into account. The specific designation used in each document is shown inside each bar. A global overview of Figure 4.1 shows the existence of two main groups of standards for fibre reinforced concretes:

- The first group includes the international standards, such as Spanish national standard [70], MC2010 [49], and the draft version of the new Eurocode 2 (EC2) [48]. These documents introduce fibre-reinforced and high-performance concrete as a variety of conventional concrete, but there is no specific consideration for the UHPFRC.
- The second group gathers national standards and guidelines for UHPFRC: French national annex to the Eurocode [31, 32], Swiss code SIA 2052 [71], documents from the FHWA [15], Walraven et al. UHPC textbook [6], and the recommendations by the *Fédération internationale du béton* (*fib*) about UHPFRC [5]. These documents focus on fine-grained cementitious materials with high compressive strength and a predominant hardening response at the post-cracking stage under tensile stresses.

The international standards are based on well accepted and rooted documents such as the previous version of the Spanish standard [72], the Eurocode 2, Part 1.1 [45], and Part 2 [73], and the AASHTO [19]. However, they require a longer time to incorporate recent advances in

concrete development. For example, AASHTO report 595 [74] provides some adjustments to AASHTO [19] to design concrete structures with HPC, but fibres are not taken into account. On the contrary, the second group defines UHPFRC as a different material. Due to this fact, they take advantage of the outstanding properties of the material more than the first ones. As a matter of fact, the shear strength model of the French code [32] provides a strength three times higher than the new draft version of the new EC2 [48]. As a detrimental aspect of specific national standards for UHPFRCs, they are not so well diffused among the practitioners. As a final remark, the KITC merges both approaches in the SUPER concrete documentation [41]. This approach will also be followed in the new Model Code 2020 [50], which aims to be a common framework for all concrete classes. According to the authors, this example should be followed, as it would carry a better acceptance and diffusion of this new material.

The middle plot of Figure 4.1 shows the common ranges of V_f for each type of concrete. The minimum value is defined as the fibre content required to achieve a non-neglectable concrete ductility under bending tests. The maximum fibre content is fixed due to workability problems, which can be related to the formation of fibre balls or the blocking of the concrete flow. This aspect will be further discussed in the next section.

Finally, the bottom plot of Figure 4.1 illustrates on the vertical axis the relative cost of the mixes compared to a conventional concrete (C60/75). On the horizontal axis, the characteristic compressive strength of the concrete is shown. Four different compressive classes are compared: C60/75 (conventional concrete), C100/115 (high-performance concrete), C150/165 and C200/215 (ultra-high-performance concrete). The material cost is given for the mix without fibre (in orange) and with a typical fibre content selected for each mix (teal). The relative cost of a HPFRC with $V_f = 1\%$ is equal to 3.6, while this value increases to 10 for UHPFRC with $V_f = 2\%$. This research focuses on high-strength concrete mixes with a f_{cm} between 100 and 120 MPa, with a V_f lower than 1%. Unfortunately, as already observed by Walraven [57], and confirmed by the top plot of Figure 4.1, there is a lack of normative covering the use of HPFRC.

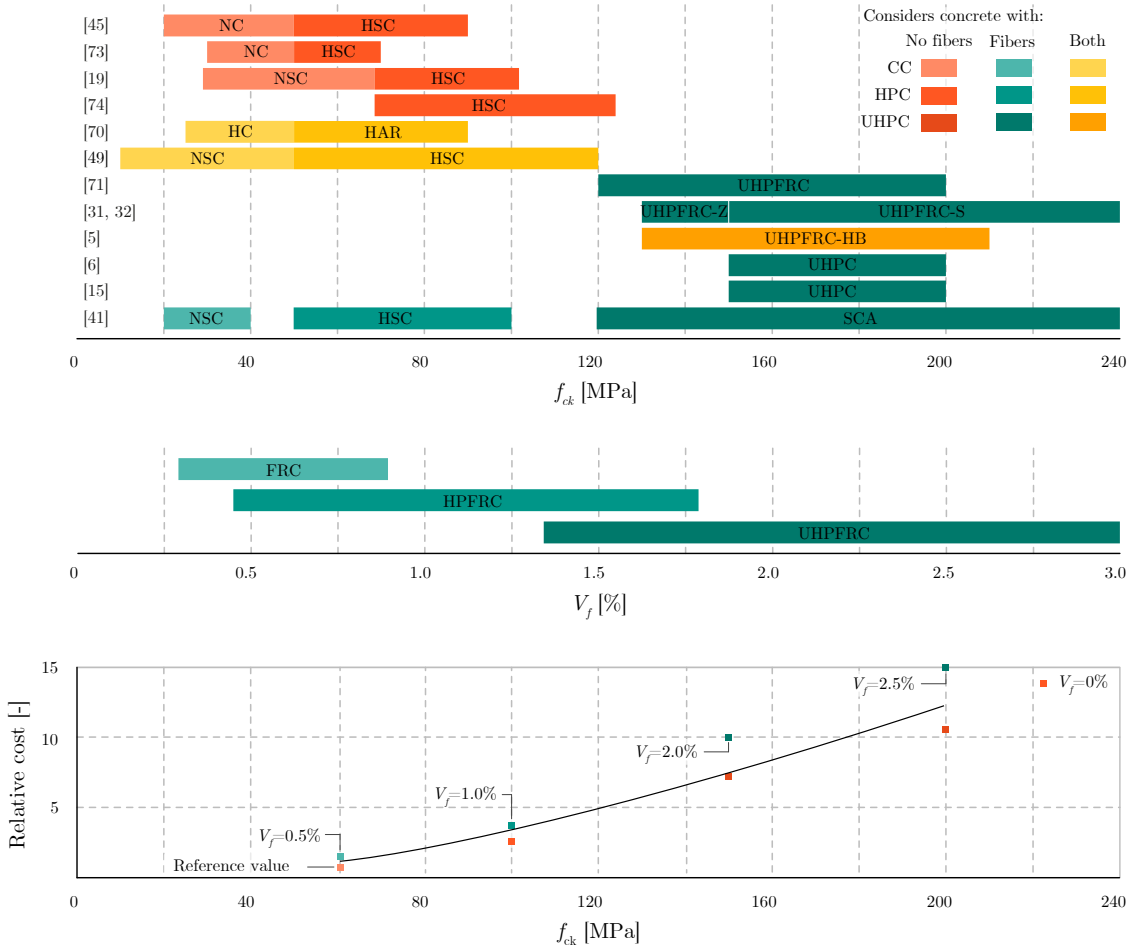

Figure 4.1: Fibre-reinforced concrete classes: at the top the applicability compressive strength ranges of different standards and recommendations, adding the corresponding terminology used in each document and the type of material considered, at the centre of the figure the typical fibre content for every type of fibre-reinforced concrete type, and at the lower part, a comparison of the prizes of different concrete classes according to its compressive class and whether they are reinforced with fibres or not.

4.2 Research significance

Although FRCs and UHPFRCs are not predominantly used in the construction sector, they are often employed for specific applications. As an intermediate solution between these materials, this research focuses on the potential of HPFRC for a wide application in the construction of girders for road bridges. This Chapter first describes and compares dosages of FRCs, UHPFRCs, self-compacting fine aggregate HPFRCs and a mixture of coarse aggregate

HPFRCs developed by the authors. Then, it provides a collection of FRC, HPFRC and UHPFRC mixes published in the scientific literature and describes trends observed in each of the groups. The advantages of using HPFRCs in bridge construction are presented and critically discussed, and its application to a case study is illustrated. Finally, the material consumption of the HPFRC-based alternative is compared with the conventional concrete solution.

4.3 Taylor-made concretes

4.3.1 Description of different fibre reinforced concrete classes

The mix composition of a FRC is very similar to the CC, although, in some cases, an additional 15 kg/m^3 of cement is added. An example of a FRC mix used for slab construction is described in Table 4.1 (Martinelli et al. [67]).

Table 4.1: Mix of a FRC by Martinelli et al. [67].

Component	Content [kg/m^3]
Cement (CEM II/A-LL 42.5 R)	370
Calcareous filler	150
Aggregate 1 (0-2 mm)	244
Aggregate 2 (8-16 mm)	993
Aggregate 3 (11-22 mm)	409
Water	185
Super-plasticizer	7.8
Straight cut-sheet indented steel fibre	35

In contrast, UHPFRCs are more analogous to mortars, where a higher degree of packing is achieved by an optimized gradation of granular constituents, without the conventional coarse fraction of the aggregates. The high degree of packing implies an increase of the specific surface area, requiring higher amount of cement than conventional concretes. Table 4.2 presents the UHPFRC mix used for the Las Ovejas footbridge in Alicante [75]; it proves that the cement content is almost three times the one used for the previous presented FRC. In many cases, additions, such as silica fume, are also included into the mix. Furthermore, these mixes are characterised by a w/c of around 0.2. The used fibres are usually high-performance short fibres with a V_f of about 2% (160 kg/m^3). Finally, plasticizers and superplasticizers are also included in UHPFRC mixes to facilitate the casting process. These concretes are

usually designed to be self-compacting, and it is recommended to avoid internal vibrating, as this can lead to inadequate fibre distribution [76].

Table 4.2: Mix of a UHPFRC by López et al. [75].

Component	Content [kg/m^3]
Cement	1000
Silica fume	150
Silica sand 0.5 mm	300.5
Silica sand 1.8 mm	700.5
Water	201.3
Super-plasticizer	11.22
Fibres OL 13/0,16	78.1
Fibres RC80/30BP	78.1

As an intermediate alternative between FRC and UHPFRC, the self-compacting HPFRC recently published by Walraven et al. [58] is shown in Table 4.3. This HPFRC has only 50% more cement than the previous FRC, but it achieves almost four times higher f_{cm}. As a drawback, it presents high contents of silica fume and blast furnace slag, which increase its cost. Regarding its D_{Max}, it is similar to a UHPFRC, and quite far from conventional concretes. The water-to-cement ratio is 0.34.

Table 4.3: Mix of a fine aggregate HPFRC by Walraven et al. [58].

Component	Content [kg/m^3]
Cement (CEM I 52.5R)	566.5
Blast furnace slag	170
Silica fume	40.2
BASF Glennium 51	6.2
Sand (0-4 mm)	757.1
Porphyry (2-6 mm)	633.5
Water	191.6
Steel fibres l/d = 30/0.38	61.8

Finally, the tailor-made mix developed by ACCIONA in a research program with the authors is described in Table 4.4. While having a cement content comparable to Walraven's HPFRC (Table 4.3), the blast furnace slag is not required due to the increasing of the D_{Max} to 12 mm. The fibre content is increased to 80 kg/^{3} to fulfil characteristic value of residual strength at a CMOD equal to 2.5 mm for fibre reinforced concrete (f_{R3k}) design requirements. Both aspects hinder the workability of the mix; this is counteracted by the addition of super- and

plasticiser.

Table 4.4: Mix of a coarse-grained HPFRC by Acciona in partnership with authors.

Component	Content [kg/m^3]
Cement (CEM I 52.5R)	500
Silica fume	50
Quartzite sand (0-6 mm)	978
Quartzite coarse (6-12 mm)	796
Superplasticizer (Sikaviscocrete 90 NG)	8.5
Plasticizer (Sikament 3003 NG)	3.75
Water	150
Steel fibre (Bekaert 4D Plus 80/60)	80

Figure 4.2 summarizes, in a graphical way, the component percentages of the 4 fibre reinforced concretes previously described. The mix developed by ACCIONA is the second, from the left. Figure 4.2 shows how the coarse fraction of the aggregate decreases in size and quantity until it disappears in the UHPFRC. On the other hand, cement content and additions increase with compressive strength. The addition of silica fume is also enlarged, while plasticizers and superplasticizers are necessary for the 4 mixes presented.

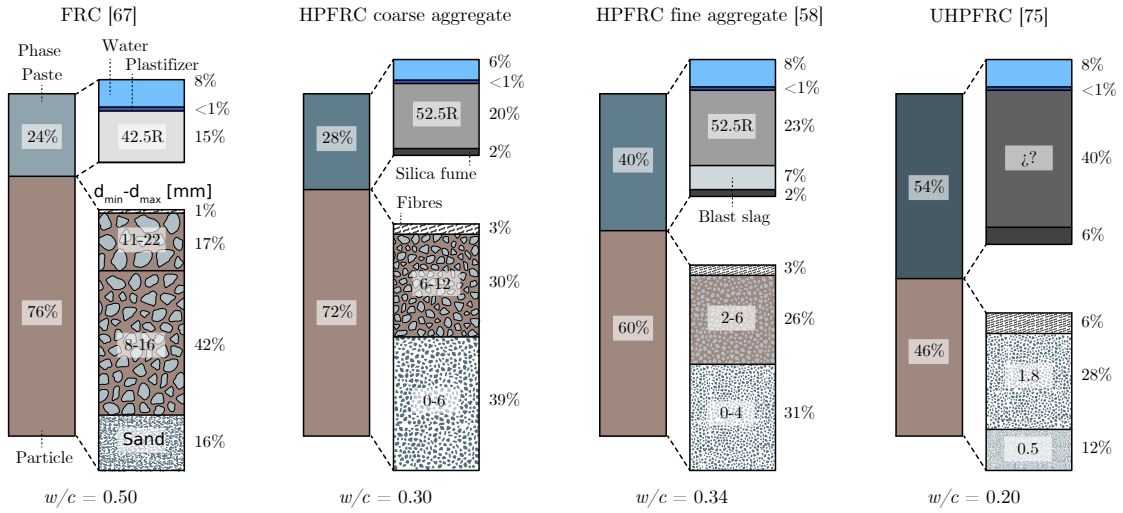

Figure 4.2: Components proportions of the four mix design presented. SP joins plastifizer and superplastifizer. SF means silica fume.

4.3.2 Analysis of fibre reinforced concretes in technical literature

The comparison made in the previous section is complemented by the analysis of 227 concretes collected from 26 different references [13, 29, 58, 65, 77–98]. Figure 3 shows the relations between f_{cm} and other relevant parameters: c (Figure 3 (a)), w/c (Figure 3 (b)), and D_{Max} (Figure 3 (c)). Randl et al. [37] demonstrated that it is possible to develop concretes that achieve compressive strength in the range of UHPFRC by replacing cement with additions such as silica fume, fly ash or blast furnace slag. To illustrate this aspect, the total binder content of each dosage, considering cement plus the additions, is proportional to the area of the circle that represents them. The tensile strength associated with the fibres plays a fundamental role in the design. Therefore, below the compressive strength graphs, f_{Rm} is added for the batches for which this value has been published. The mix developed by ACCIONA is represented by the red circles. Figure 3 (a) shows the cement content versus the compressive strength. Although it is difficult to classify the different dosages, certain trends can be observed. Drawing an imaginary horizontal line at f_{cm}=100 MPa, all the FRCs have less than 600 kg/m^3 of cement. In contrast, almost all the UHPFRCs have a cement content greater than 750 kg/m^3. Exceptions are found, such as the concrete by Randl et al., but it presents almost 450 kg/m^3 of additions [37] (the circle has a bigger area). The bottom part of Figure 3 (a) shows a similar trend when studying the distribution of f_{Rm}. Figure 3 (b) identifies the classical reduction in the w/c as the compressive strength increases. Furthermore, the dosages with the highest number of additions are found in the UHPC group. On the other hand, since the cementitious matrix affects the flexural strength as it is related to the anchoring strength of the fibres in the matrix, a growth of f_{Rm} is also observed as the w/c decreases. Figure 3 (c) agrees with the physical explanation behind the first two observed trends. First, as the D_{Max} grows, the specific surface area that needs to be surrounded by water decreases, and, therefore, the amount of water can be reduced. As a consequence, also the amount of cement decreases [55]. Figure 3 (c) illustrates that there are two subgroups separated by an imaginary horizontal line at f_{cm}=100 MPa. Most of the mixtures below this limit have a D_{Max} greater than 12 mm. On the contrary, those that exceed them have a D_{Max} lower than 2 mm. The HPFRC developed in the ongoing research (red circles) presents one of the lowest D_{Max} values of the coarse aggregate subgroup, a strength comparable to that of the UHPFRC while keeping a feasible binder content.

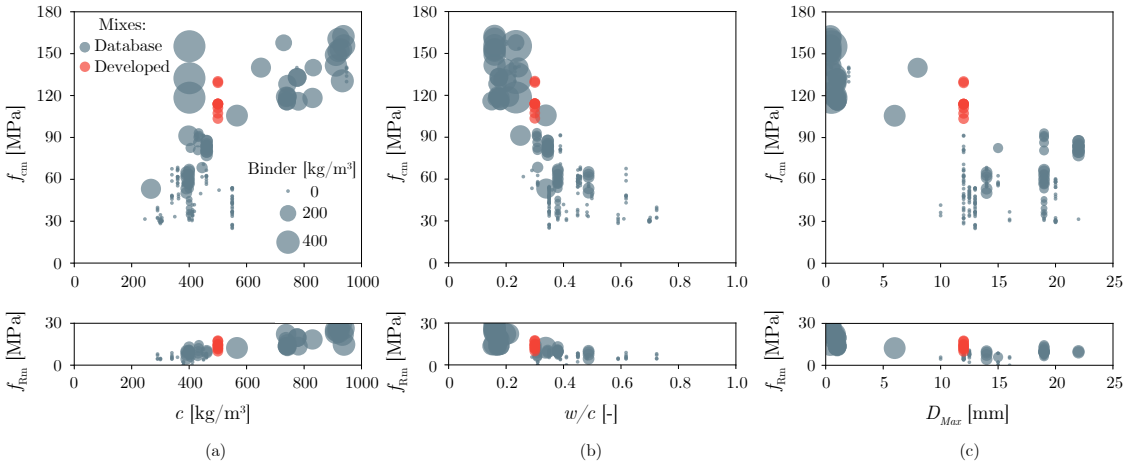

Figure 4.3: f_{cm} and f_{Rm} against: (a) c, (b) w/c and (c) D_{Max}.

Figure 4.4 presents a similar analysis applied to the l_f and σ_{fu} of the metallic fibres employed in each concrete. In addition, the V_f is represented by different areas of the circles. Figure 4.4 (a) shows that, normally, microfibres (shorter than 20 mm) are used in UHPFRCs, allowing a better interaction with fine aggregates by sewing small crack openings. On the other hand, macrofibres are usually used for FRC and HPFRC, with larger aggregate sizes. Even though fibres do not increase compressive strength, it is common for UHPFRCs to have a fibre content of 2%, while this value drops down to 1% in FRCs and HPFRCs. Next, looking at the plot of l_f versus f_{Rm} in the bottom part of Figure 4.4 (a), the highest f_{Rm} corresponds in most cases to the UHPFRCs. Finally, Figure 4.4 (b) relates the σ_{fu} of the metallic fibres to the compressive concrete strengths. Two main groups are identified: one with a σ_{fu} in a range between 700 and 1300 MPa, and another with σ_{fu} higher than 1500 MPa. There is also a small group of mixes with σ_{fu}=3000 MPa and conventional values of f_{cm} and f_{Rm}. Only increasing σ_{fu} is not enough to produce a HPFRC or UHPFRC mix.

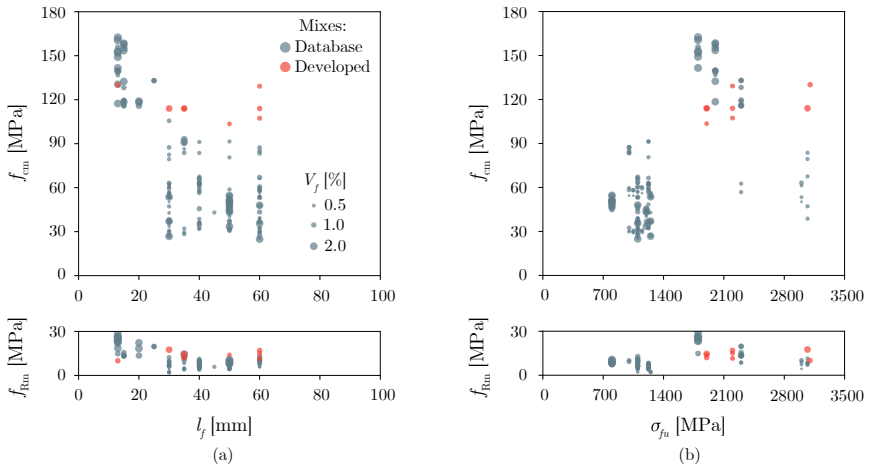

Figure 4.4: f_{cm} and f_{Rm} against: (a) l_f and (b) σ_{fu}.

4.4 Application of HPFRC for the design of precast concrete girders

4.4.1 Conceptual analysis of the advantages from the design perspective

This section describes the potential advantages associated with the application of HPFRCs in the design of bridge girders. First, their compressive strength is almost double that of conventional concretes used for standard precast bridge girders. Due to this higher compressive strength, also the allowable stress limit at SLS increases. Hence, the span lengths can be higher than usual as more prestressing can be provided. At the material level, a concrete matrix with a high f_{ck} also brings a high f_{ctk}. Furthermore, fibres provide ductility to the concrete, allowing designers to consider a certain f_{Ftu} in the analysis. Generally, the prestressed quantity is governed by the SLS tensile limit. To a higher concrete class corresponds a higher tensile strength. This may lead to ULS governing the material quantity, leading to a reduction of around 5%. In addition, the fast gain in strength of the cementitious matrix allows the prestressing force to be transmitted earlier, accelerating the production of these elements. This rapid gain in strength is linked to a quicker development of rheological deformations, thereby reducing long-term effects, as delayed prestress losses. Fibres provide ductility under tension [6] even after concrete cracks. However, a hybrid reinforcement with fibres and passive reinforcement is recommended for localized stresses, while only fibres would be enough for bearing distributed stresses. The top part of Figure 4.5 compares three different M_{Rd} of a prestressed I-girder bridge made of HPFRC characterized by a

concrete compressive and post-cracking tensile classes, respectively, 100 and 12c according to the MC2010 [49]. Three different results with different values of the strain of non-metallic reinforcement at maximum force in tension (ε_{fu}) are presented, darker colours indicate a more ductile behaviour of the HPFRC. Comparing the M_{Rd}, it can be stated that fibres present a negligible effect on the ultimate bending moment for this kind of cross-section; in fact, the M_{Rd} increases only 0.8% if the fibres are considered in the calculation (see last column). On the contrary, Figure 4.5, bottom, shows the same comparison, applied to the negative bending moment calculation of a ribbed deck. In this case, as the area under tension is larger, the M_{Rd} increases 62% when considering fibre contribution. As main finding, the fibre contribution to the ultimate bending moment is strongly dependent on the cross-section and the applied bending moment [99].

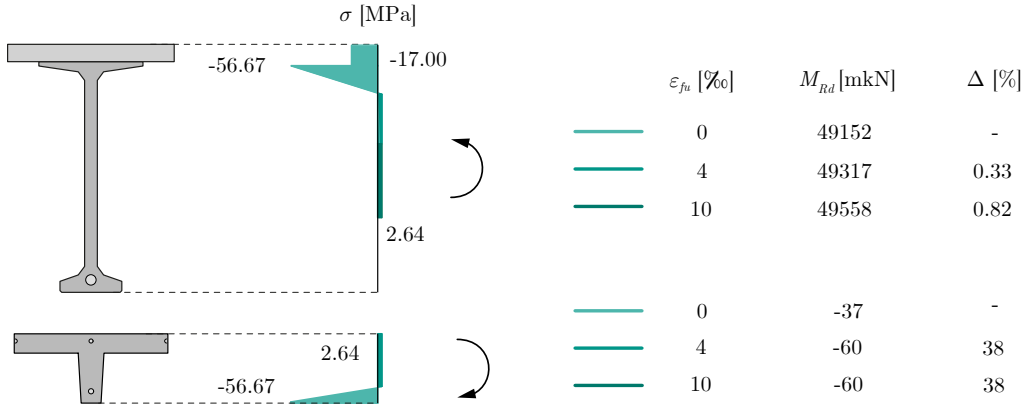

Figure 4.5: Ultimate bending moment strength calculation varying the ultimate tensile strain: (top) 3 m high I-girder bridge with conventional 0.25 m slab, (bottom) 0.25 m thick and 0.60 m wide lightened deck.

The shear strength provided by fibres may allow to replace the passive shear reinforcement, which represents around 40% of the passive steel in conventional girder bridges. To ensure enough ductility when stirrups are eliminated, MC2010 Eq. 7.7-15, expressed by Equation 4.1, limits the minimum characteristic value of the f_{Ftuk}. To illustrate this limit, for the HPFRC C100 this would be $f_{Ftuk} \geq 0.08 \cdot 10 = 0.8$ MPa; considering a 12c, with $f_{R1k} = f_{R3k}$, $f_{Ftuk} = f_{R3k}/3 = 4$ MPa. Therefore, this criterion is largely fulfilled with a fibre content of around 80 kg/m^3 ($V_f \approx 1\%$).

$$f_{Ftuk} \geq 0.08\sqrt{f_{ck}} \tag{4.1}$$

Whereas there are different mechanical models to account for the fibre contribution into the ultimate shear calculation, the basic concept is illustrated in Figure 4.6. V_{cf} stands for the vertical component of the tensile stress supported by the fibres along the inclined shear crack area (A_{cv}). Theoretically, the main difference between shear models lays in the consideration of the fibre contribution to shear strength together with the concrete contribution, or as a separate term. In the developed examples, substantial differences are observed when applying different formulations. Regarding shear verification at SLS, cracking must be avoided by limiting the principal tensile stresses to the same limit as bending SLS verification, fFtsk = $0.45 f_{R1k}$. Furthermore, as a high compressive level is possible with HPFRC, this would benefit both SLS and ULS verifications. Even though the positive effect of the compressive level on the calculation of the ultimate shear strength is accepted in several standards, the draft of the new EC2 [48] (Annex L for fibres) does not consider it. Finally, it worths mentioning that the authors are carrying out an experimental campaign on the durability properties of the developed HPFRC. The preliminary result indicates a very low porosity and a slow chloride intrusion. Hence it is confirmed that the coarse aggregate HPFRC has a very high durability and show that the tensile strength will not be reduced by possible corrosion of the fibres.

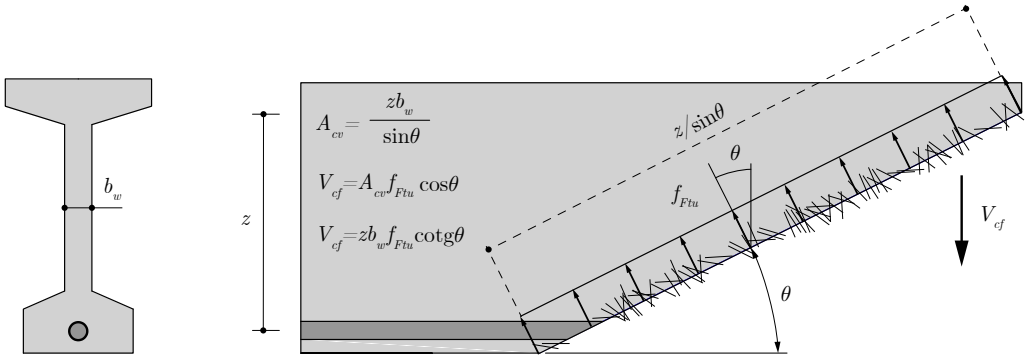

Figure 4.6: Shear contribution by the fibres.

4.4.2 International applications of FRC, HPFRC and UHPFRC to bridges

As mentioned above, there are several international successful examples in the application of UHPFRC to road bridges. DURA Technology has developed a catalogue of precast girders, which have been installed in the last decade on more than 100 bridges, predominantly in Malaysia. Figure 4.7 gathers the cross-sections of the solutions by DURA Technology and their corresponding span range.

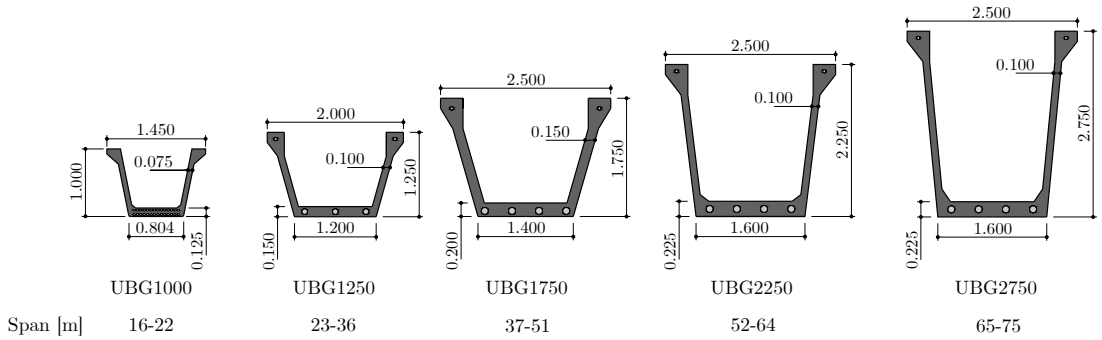

Figure 4.7: U-girders of the DURA Technology precast catalogue and its span range of applications.

In the United States, Tadros et al. [27] have developed the UHPFRC decked I-beams based on the use of concrete with a compressive strength between 117 and 152 MPa. This system allows the integration of girder and deck, taking advantage of the conventional concrete deck´s optimisation. The reduction of concrete in the deck allows a 50% reduction of the bridge superstructure's self-weight. Figure 4.8 shows the cross-section of UHPFRC's precast decked I-beams developed by Tadros et al. [28], which have already been used for both principal beam and slab for buildings, and now are being used in road bridges. As a drawback, its complex formwork implies a significant initial investment by the concrete manufacturer. To optimize the overall cost of the structure along with reducing its carbon footprint, composite structures can be designed with UHPFRC only in specific locations of the cross-section, using conventional concretes or FRC for the rest of the structure. One example is the first P/R/SFRC bridge in Italy by di Prisco et al. [38]. Here precast UHPFRC plates are used as lateral inclined loose formworks to cast in place the rest of the slab bridge with FRC. In this application, according to the MC2010 classification, the UHPFRC is a C120 14c while the FRC is a C40 5c. Finally, as far as authors know, there are few cases of HPFRC applications in bridge engineering, mainly in Korea, by KICT, such as the Ogkwan bridge with metallic fibres and concrete with a compressive strength of 120 MPa. These bridges follow other applications that use the HPFRC for precast girders as the Axe bridge and the Muyi bridge; in these cases, no fibres were added. These HPFRCs belong to the self-compacting category, differing from the coarse aggregate HPFRCs described in Section 4.3.

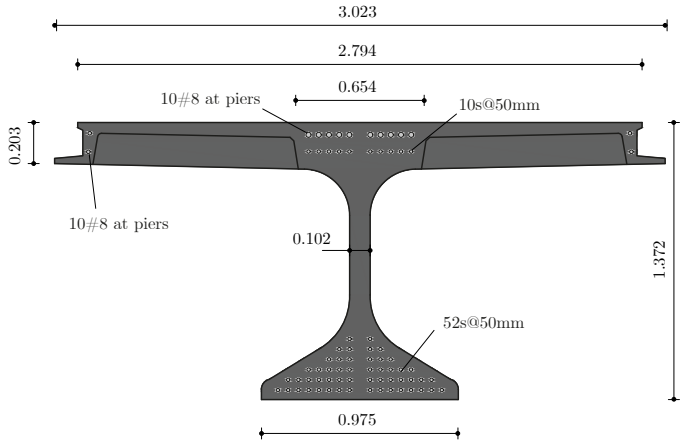

Figure 4.8: Decked I-beams [29].

4.4.3 Comparison of girder solutions for a 60 m-span bridge

This section describes the design of a coarse aggregate HPFRC U-girder for a bridge characterized by a span of 60 m and a deck width of 12.50 m. This structural solution is then compared with conventional alternatives made of standard prestressed concrete. Figure 4.9 (a) shows the cross-section of the optimized design for the HPFRC solution. The U-girders use a HPFRC100/115 (f_{ck}=100 MPa), while the deck adopts a standard C30/37 (f_{ck}=30 MPa). A conventional span-to-depth ratio for U-girders equal to 18.5 was selected to allow a better comparison with reference bridges. To ease segments transportation and to avoid any undesired cold joint, Voo and Tadros [44] propose the design of short segments (6-8 m long) to pour them with one concrete batch. However, a scaffolding system must temporarily give support to the girder before the prestressing release. According to authors' experience, the use of longer segments with the minimum number of temporary supports is also a reasonable alternative. Long segments may suffer planes of weakness caused by discontinuity of fibres across the cold joints between batches. In these cases, the use of mock-up segments is advisable to guarantee the lack of cold joints. According to EC2-2013 [45], several stress limits should be considered at Serviceability Limit State. Regarding compression stresses, the limits of $0.6f_{ck}$ and $0.45f_{ck}$ could not be exceeded under the characteristic combination of loads, and the quasi permanent combination of loads, respectively. Respect to the position of joints between segments it is recommendable to locate them far from sections of maximum bending moment. This is because segment joints must be under compression for any loading scenario at SLS $\sigma_{ct,max}$=0. In contrast, for a general section, the $\sigma_{ct,max}$ at SLS is characteristic value of post-cracking strength for seviceability crack opening for fibre reinforced concrete (f_{Ftsk}).

Therefore, the 60 m-span solution proposed in this Chapter accounts for two temporary supports arranged to bear three 20 m-length segments. This design choice saves 14% of prestressing respect to the 2-segment alternative with a joint at midspan. The prestressing distribution is illustrated in the 3D representation of half bridge in Figure 4.9 (b). It is a common practice for precasters to arrange tendon deviators and anchorages on the free space inside the U-girders, avoiding any interference between ducts and webs/bottom slab. Accordingly, prestressing steel was designed as 6 unbonded tendons. Specifically, two of them deviates at a distance of $L/5$ from the supports for a better approximation to the bending moment distribution. Furthermore, these tendons cause an uplift force in the area close to the support, which reduces the design shear and, therefore, decreases the tensile requirement to f_{R3k}=12 MPa. Other two tendons are anchored at a distance of $L/5$ from the support to fulfil the SLS stress limits near the supports. Respect to the ULS checks, the bending moment was verified in the different construction stages of the bridge, while different shear formulations were applied to obtain a thickness of 15 cm of the webs, and the material requirement of f_{R3k}=12 MPa. This allowed to eliminate the conventional shear reinforcement. Further details have been addressed in Section 2.3. As a final data, the proposed bridge has an average depth of 450 mm (200 mm corresponding to the girders and 250 mm to the slab).

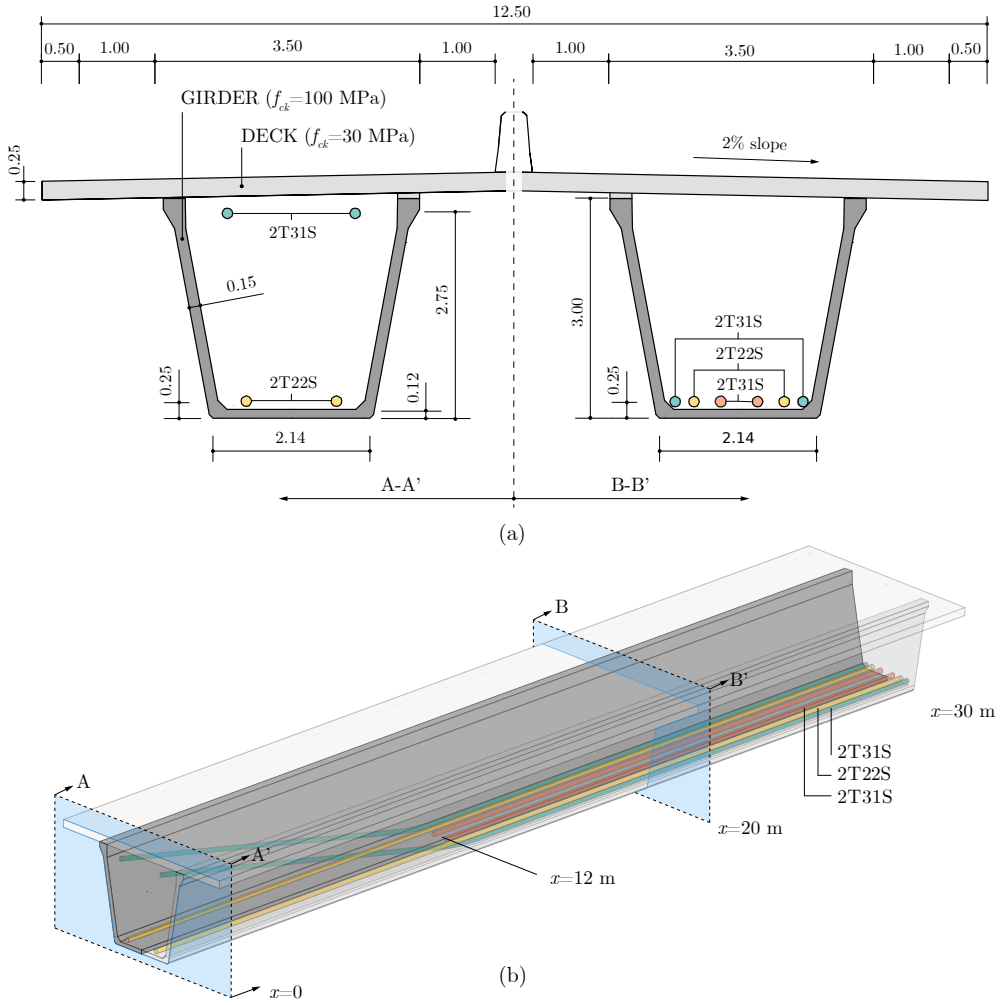

Figure 4.9: (a) Cross-section of the proposed alternative with HPFRC U-girders and conventional deck; (b) 3D representation of half HPFRC proposed bridge.

This HPFRC-based solution is compared with three reference projects of road bridges, all in Spain, where conventional concrete, C40/50 (f_{ck}=40 MPa) and C50/60 (f_{ck}=50 MPa), is used. Specifically, the first two case studies are the Molvizar and the Engaño bridges, whose cross-sections are represented in Figures 4.10 and 4.11. The Molvizar bridge has a span of 51.90 m with a slenderness of 18.9, while the Engaño bridge has a span of 70 m with a slenderness of 21.9. The box girders of these reference projects are continuous over several supports. Both are road bridges, and they have an average depth of 620 and 640 mm. Their passive steel quantity is 122 kg/m^3 and 124 kg/m^3, respectively.

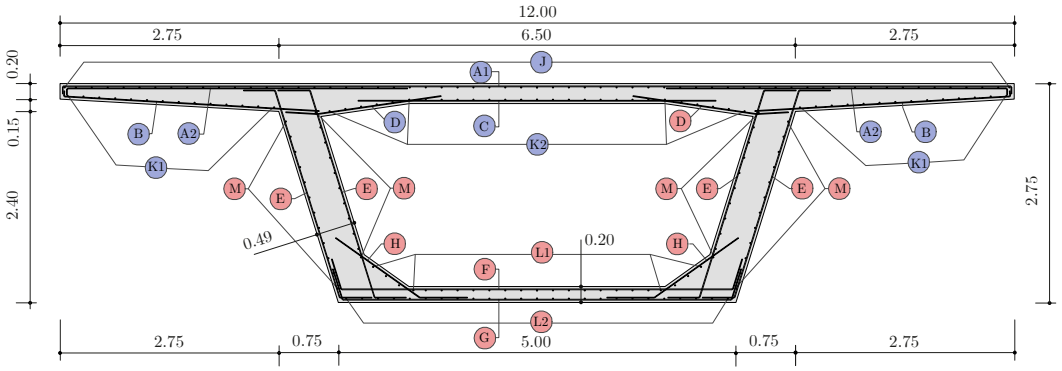

Figure 4.10: Cross-section of the Molvizar bridge.

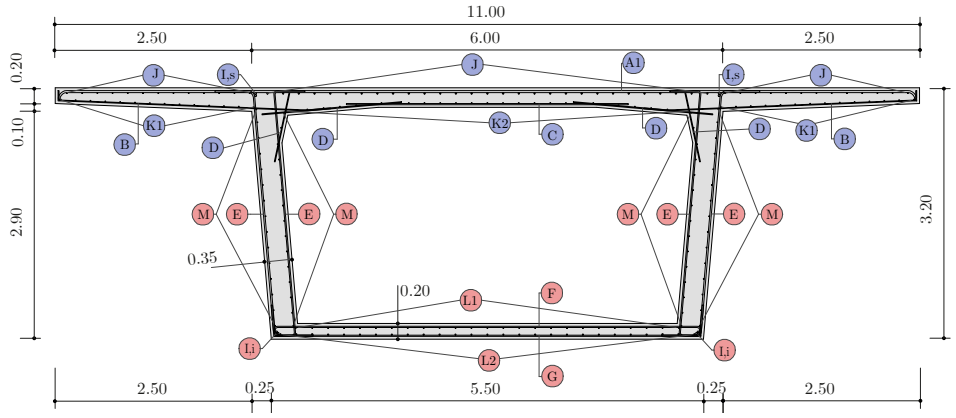

Figure 4.11: Cross-section of the Engaño Bridge in the C550 road.

Tables 4.5 and 4.6 show the quantity of each reinforcement type of the reference bridges according to the labels described in Figures 4.10 and 4.11. The total steel reinforcement of the box girders has been classified into two groups according to the location in the cross-section. The first one, referred as beam reinforcement, includes the webs and the lower slab. The second group, referred as deck reinforcement, accounts for the remaining passive reinforcement of the top slab. The Molvizar bridge has 21,086 kg of beam reinforcement and 23,116 kg of deck reinforcement. The Engaño bridge is characterized by, 32,142 and 29,014 kg, respectively, in the beam and in the deck. Table 4.5 shows that the shear reinforcement steel in the webs is, respectively, 7,845 and 15,823 kg, representing the 18% and 26% of the total. In the HPFRC-based solution, if hardening behaviour is achieved, the longitudinal reinforcement used to control cracking can be totally replaced by metallic fibres [57]. This would save 5,607 kg and 7,475 kg, respectively, which represents about 12% of the total passive steel in both cases.

Table 4.5: Reinforcement for the girders or web/bottom slabs.

Reinforcement [kg]	E	F	G	H	L1	L2	M	I,s	Total
G Molvizar	7,845	3,430	3,430	774	1,534	1,786	2,287	0	21,086
G Engaño	15,823	3,344	4,205	0	1,617	1,872	3,986	1,295	32,142

Table 4.6: Reinforcement for the top slabs or decks.

Reinforcement [kg]	A1	A2	B	C	D	J	K1	K2	Total
D Molvizar	7,665	3,597	1,527	1,572	915	4,179	1,392	2,269	23,116
D Engaño	14,835	0	25,951	1,923	1,114	3,764	,1845	1,647	29,014

The third reference project is the Fuentespina bridge, which has three U-girders to support a conventional in-situ C30/37 (f_{ck}=30 MPa) slab. This road bridge span 44.25 m in a simply supported manner, and it presents a span-to-depth ratio of 18.06. Table 4.7 collects the material consumption for each alternative to ease the comparison of the HPFRC U-girders with the reference projects girders. To estimate the t_{eff} for the Molvizar and Engaño bridges, its decks are supposed to have a t_{eff}=200 mm. Furthermore, the passive reinforcement considered for these reference projects is collected in Table 4.5. Regarding the Fuentespina bridge, only the material corresponding to the U-girders has been considered. The HPFRC-based alternative presents a reduction of t_{eff} of 48%, and 20% respect to the box girders, and the conventional U-girders of the Fuentespina project. Regarding the passive reinforcement, the HPFRC solution has a quantity of 12.49 kg/m^2, which is approximately 1/3 of the reference projects. The active reinforcement comparison should be carefully addressed as its quantity is strongly dependent on the typology of the bridge. For example, the Molvizar and Engaño bridges are continuous supported on the studied span, which significantly reduces its design bending moment at ULS. As the Fuentespina girders are simply supported, and they present a similar span-to-depth ratio, it is more realistic to compare the active reinforcement of this project with the HPFRC-based alternative. Considering that the proposed solution has a span 35.6% longer, while its active reinforcement is only 12.5% higher, it can be stated that the reduction in self-weight, together with the polygonal profile of the proposed solution, reduces significantly the prestressed required for this typology. Table 4.7 also shows the material cost for each project under study. The following unitary cost are used: C40/50=85 €/m^3, C50/60=90 €/m^3, HPFRC100/115=200 €/m^3 (including the cost of the steel fibres), passive steel=0.83 €/kg, prestressing steel of the strands of pre-tensioning=0.90 €/kg, and prestressing steel of the strands of post-tensioning=1.10 €/kg. It can be concluded that the proposed solution is economically competitive compared with the reference projects of

similar spans, as its material cost is 6-20% lower than the reference projects. In addition to the material savings achieved in the superstructure, the savings owing to easier fabrication, transportation and erection must be considered in the overall comparison.

Table 4.7: Comparison of material consumption for the girders of the three bridges under study.

Bridge	Span [m]	Deck width [m]	Typology -	Effective depth [mm]	Passive reinforcement [kg/m^2]	Active reinforcement [kg/m^2]	Material cost [€/m^2]
Molvizar	51.90	12.00	C	420	33.86	20	85.8
Engaño	70.00	11.00	C	440	42.24	26	101.06
Fuentespina	44.25	17.50	SS	250	31.63	24	70.35
HPFRC-based alternative	60.00	12.50	SS	200	12.49	27	80.07

4.5 Conclusions and further research

4.5.1 Conclusions

This Chapter presented a conceptual analysis of the potential implementation of HPFRC in girders of road bridges. For this purpose, the differences in the dosages of FRC, coarse aggregate HPFRC, fine aggregate HPFRC, and UHPFRC have been studied; and the trends observed in a database compiled from the scientific literature have been analysed. The advantages of HPFRCs applied to bridge projects have been then discussed. Also, international precedents have been briefly illustrated. A HPFRC-based girder for a bridge spanning 60 m has been developed, and then compared with two reference existing bridges. The main findings of this study are the following:

- It is possible to develop a cost-competitive HPFRC that reaches class C100/115 (f_{ck}=100 MPa) using a cement content of 500 kg/m^3 and 50 kg/m^3 silica fume with a D_{Max} of 12 mm. Furthermore, by adding 80 kg/m^3 of 4D metallic fibres, ductility can be added to the concrete to remove passive reinforcement from the webs of girders of road bridges.
- There are several international examples of implementation of FRC and UHPFRC. However, there are very few applications of HPFRC in bridge design. This lack of

precedents is partially caused by an absence of normative or recommendations for this material.

- According to authors' experience and recent case of studies, the main field of application for the HPFRC is the construction of precast girders. The execution of these elements in precast factories guarantees adequate control of casting and curing.
- It is possible to cover a span of 60 m with HPFRC through a precast U-girder solution and a conventional deck. When comparing the proposed girders with two conventional box girders, a 48% reduction in concrete consumption and a 66% reduction in passive steel in the beams were observed.
- Furthermore, a comparison with a conventional U-girder of similar features, but with a span of 44.25 m, reveals that the reduction in self-weight, together with the polygonal profile of the proposed solution, reduces significantly the prestressed required for this typology.
- A comparison of the material cost of the HPFRC U-girders with the reference projects girders shows the competitiveness of the proposed solution, with a reduction in cost ranging between 5-20% when compared with the box-girder solutions.

5

Mix development, material characterization and constructability aspects

5.1 Introduction

High-Performance Fibre Reinforced Concrete (HPFRC) has the potential to achieve a high post-cracking tensile strength for structural design, and to reduce the quantity of conventional steel reinforcement as discussed in Chapter 2. Previous studies of the authors have proved that a 60 meter-span road bridge can be designed using precast simply-supported U-girders made of HPFRC, without stirrups in the webs. This HPFRC-based alternative reduces material consumption, labour hours, and production time compared to solutions based on conventional concrete as mentioned in previous Chapters. The HPFRC-based alternative, shown in Figure 5.1, is made of 3 segments with a length of 20 m each, and combines HPFRC100/115 (f_{ck}=100 MPa) precast U-girders with a deck made of a conventional reinforced concrete C30/37 (f_{ck}=30 MPa). The layout of the external prestressing, shown for half of the bridge in Figure 5.1 (b), follows a polygonal profile that, creating an uplift force near the supports, reduces the design shear force. In Section 2.3 the shear strength in elements without stirrups of HPFRC have been applied using various analytical formulations [99]. The study revealed a significant variability in the shear strength according to the different formulations. In view of this, the exact required value of f_{R3k} strongly depends on the adopted shear formulation. For the above mentioned application, a f_{R3k} of around 8-10 MPa should be achieved. This goal

should be fulfilled without comprising the workability of the concrete, while also ensuring that the material cost does not exceed three times that of C70/85.

It is well-known that the structural performance of fibre reinforced concretes (FRC) is significantly affected by the casting technique [100]. Therefore, the execution aspects should be carefully investigated to prevent the occurrence of cold joints or unexpected distribution of fibres. These potential construction issues promote the use of a design-by-testing approach when studying FRC, as outlined in Model Code 2010 [49] and NF P-18 [32]. This design-by-testing procedure has been followed, for example, by di Prisco et al. when conducting an extensive experimental campaign of 40 prestressed roof FRC elements, including material's characterization [85], assessment of the casting process [101], testing and extraction of specimens from the elements [102]. Similarly, other investigations on Steel Fibre Reinforced Concrete (SFRC) floors [103], [67] and on foundation walls using Self-compacting FRC with recycled aggregates [104] involved the extraction of cylinder cores for the purpose of analysing the content and orientation of fibres. This was achieved by measuring the inductance in different directions utilizing a technique developed by Calavaro et al. [105] [106]. Recent publications have adopted a design-by-testing methodology for HPFRC structural elements. For example, Walraven et al. [58] described the experimental verification and design considerations of foundations made of self-compacting HPFRC. Additionaly, Grünewald et al. [107] conducted digital analysis of photographs of extracted cores from the tested elements to obtain the fibre distribution and orientation. Finally, another example is presented in the work of Mendes de Andrade et al. [108], who compared various methods for determining the fibre orientation factor of an HPFRC bridge box girder. Specifically, these authors performed bending tests of prismatic specimens, counting of fibres through digital analysis of photographs, and computed tomography.

The design-by-testing methodology has been also implemented in this work, which investigates the use of coarse aggregate HPFRC to a 60 m-span precast U-girder without stirrups. According to the authors, the experimental evidence represents an essential step when dealing with FRC. The careful analysis of the execution process is essential to characterize the mix, ensure adequate distribution and orientation of the fibres, and verify the structural response through testing of reduced-scale elements.

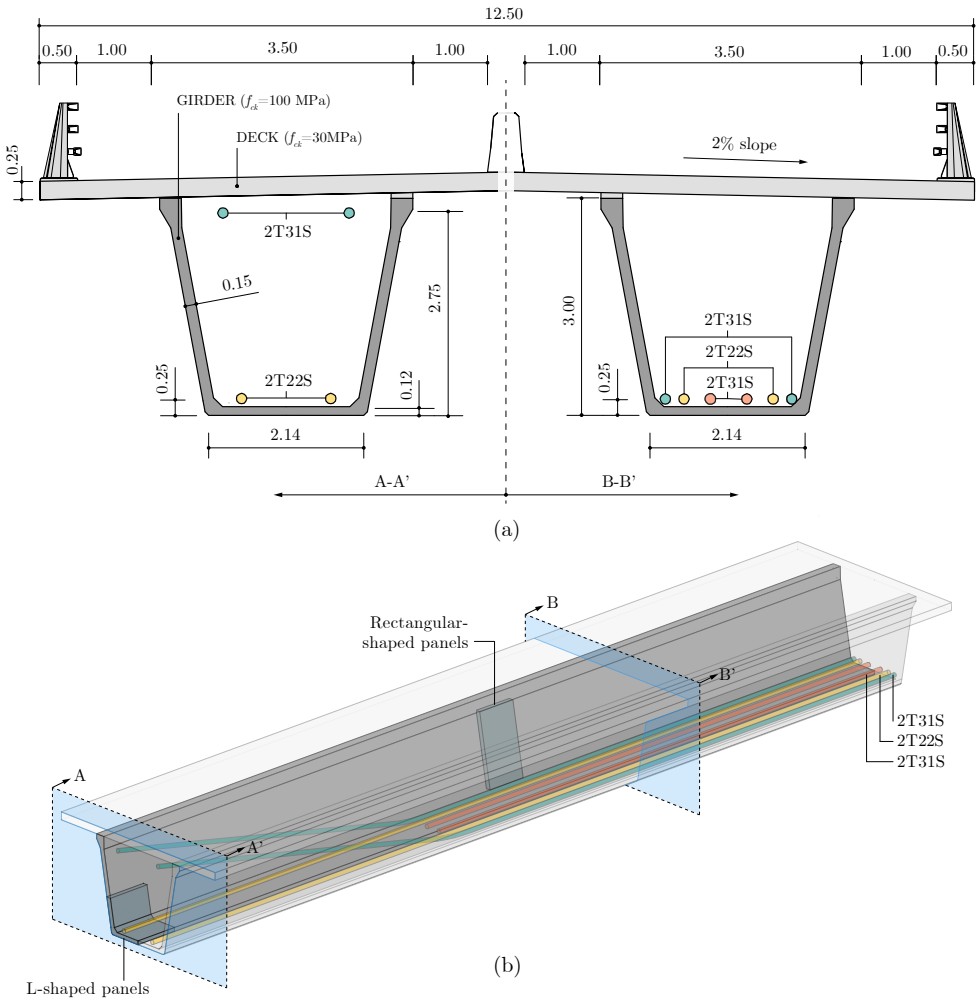

Figure 5.1: HPFRC-based alternative for a road bridge spanning 60 meters. (a) cross-sections with HPFRC U-girder and conventional RC deck at midspan and supports; (b) 3D representation of half HPFRC-based bridge.

5.2 Research significance

Despite the good balance between remarkable mechanical properties and reasonable cost, up-to-date HPFRC is scarcely employed in the construction of bridges. This work is part of a larger research project that explores potential applications of this material to the construction sector. This Chapter focuses on the experimental characterization of a tailor-made HPFRC mix design to be used for the construction of segmental road bridge made of 3 externally post-tensioned U-girders covering a total span of 60 m. Specifically, the strength requirements for the design are: f_{ck}=100 MPa and f_{R3k}≈8-10 MPa. To guarantee the cost-effectivity of

the HPFRC-based solution, these requirements must be fulfilled limiting the cost of HPFRC to 2.5-3.0 times the cost of a conventional high strength concrete (C70/85). The first research stage consists in develop a tailor-made HPFRC mix (definition of the cementitious matrix, type, and quantity of fibres, etc.) fulfilling these material and economic requirements. This has been achieved producing nine different HPFRC mixes with various types and contents of fibres, all based on the same concrete mix. The second stage consists of experimentally validating the potential application of this material to U-girder sections with a segment length of 20 m. This validation represents a challenging stage and involves the construction and testing of several panels with different shapes (L-shaped and rectangular-shaped panels). Referring to Figure 5.1 (b), the rectangular-shaped panels simulate the response of the web, while the L-shaped panels simulate the web-bottom flange connection. Several specimens extracted from these panels are then used to evaluate the influence of several aspects (e.g., construction joints between subsequent concrete pours, and fibres' distribution and orientation) on the structural response.

Figure 5.2 provide a graphical abstract of the research presented in this Chapter: it combines mix design development, laboratory tests to assess strength and workability requirements, and, finally, the study of the panels to investigate possible problems associated with the construction process (cold joints, fibre distribution and orientation, etc.). The Chapter is organized as follows: Section 5.3 illustrates the design of the concrete mix, including the testing of three different types of cement and two types of additions. The mixes' strength and workability are assessed in accordance with the relevant standards. Next, Section 5.4 focuses on the experimental campaigns carried out to investigate the particularities associated with the casting of the proposed U-girders. Finally, the main conclusions are drawn and further research is described in Section 5.5.

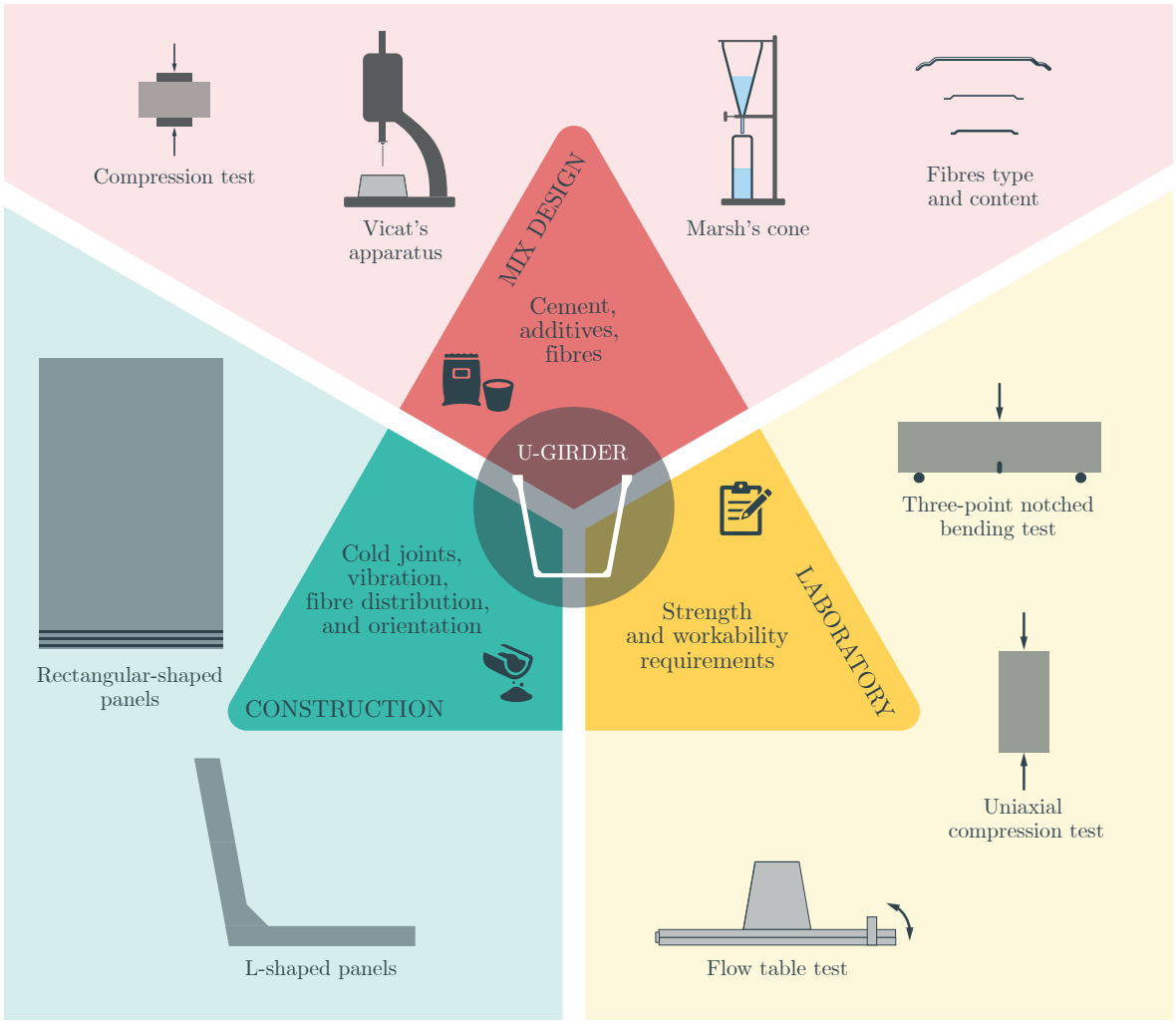

Figure 5.2: Graphical abstract of the research.

5.3 Material characterization

5.3.1 Concrete mix development

The starting point to develop the concrete mix was the previous experience of the second author with the fabrication of high-performance (C90/105) and ultra high-performance (C130/145) concretes (both without fibres). This know-how was combined with the data collected in the database presented in Section 4.3 including the specifications of several steel fibre reinforced cementitious materials. As mentioned before, the tailor-made HPFRC has to fulfil requirements of different types: structural design, workability, execution, and cost. To

maintain an affordable cost of the concrete, some mix component quantities were limited: (i) a maximum cement content of 500 kg/m^3, and (ii) a maximum silica fume content of 50 kg/m^3. Furthermore, the maximum fibre content needed to achieve the structural requirements was pursued without compromising the workability of the mix.

As a first step, an experimental campaign was conducted to select the appropriate cement for the mix. The selection criteria were the highest compressive strength and the longest and most gradual setting time. This second criterion is important to decrease the heat generated by the hydration of the high cement content in the HPFRC, which can lead to cracks due to the significant temperature gradients in the concrete volumes. Therefore, a more gradual setting process was preferred to prevent early-age cracking caused by excessive hydration heat [109].

The development of the compressive strength of three different mortars (each one using a different cement) was investigated according to EN 196-1 [110]. The strength at three ages (1, 7 and 28 days) was evaluated by testing six specimens of 40x40x80 mm for each age and mortar type. The average compressive strengths for these mixes at different ages are shown in Figure 5.3 (a). The highest strength was achieved by the mortar with the CEM I 52.5R SR3, while the fastest strength development was obtained by the one with the CEM I 52.5R. Next, the Vicat apparatus, in accordance with EN 196-3 [111], was used to evaluate the setting time of cement pastes for the three cements under investigation. The start of setting was defined as the time at which the distance between the needle and the bottom plate reached a value of 6±3 mm according to EN196-3 [111]. The results, depicted in Figure 5.3 (b), were as follows: 92, 190, and 235 minutes for, cement pastes with, respectively, CEM I 52.5R, CEM I 52.5R SR5, and CEM I 52.5R SR3. Additionally, the first two cement pastes exhibited a sudden decrease in penetration depth, while the last one showed a smoother setting development. Based on its higher compressive strength at 28 days, as well as its slower and more gradual setting behaviour, the CEM I 52.5R SR3 was selected as the optimal choice. Next, in order to enhance the workability of the HPFRC mix, two superplasticizers were investigated using the Marsh cone, according to the ASTM C939/87 standard [112]. Figure 5.3 (c) illustrates the results, with the horizontal axis representing the admixture content of the tested cement pastes and the vertical axis representing the time required for cement pastes to flow through the Marsh cone. The SikaviscoCrete-90 NG was selected over Masterease 3690, to achieve a higher fluidity with the same content. This first stage research led to the mixture proportions shown in Table 5.1.

Table 5.1: Mix of a coarse-grained HPFRC by Acciona in partnership with authors.

Component	Content [kg/m^3]
Cement (CEM I 52.5R)	500
Silica fume	50
Quartzite sand (0-6 mm)	984
Quartzite coarse (6-12 mm)	800
Superplasticizer (Sikaviscocrete 90 NG)	9
Plasticizer (Sikament 3003 NG)	4
Water	150
Steel fibre (Bekaert 4D Plus 80/60)	80

The maximum contents of cement and silica fume imposed to limit the affordable cost of the mix were strictly fulfilled. Additionally, the water-to-cement ratio was 0.30, and the maximum aggregate size was 12 mm. An additional plasticizer, Sikament 3003 NG, was added to improve the workability of the HPFRC mix.

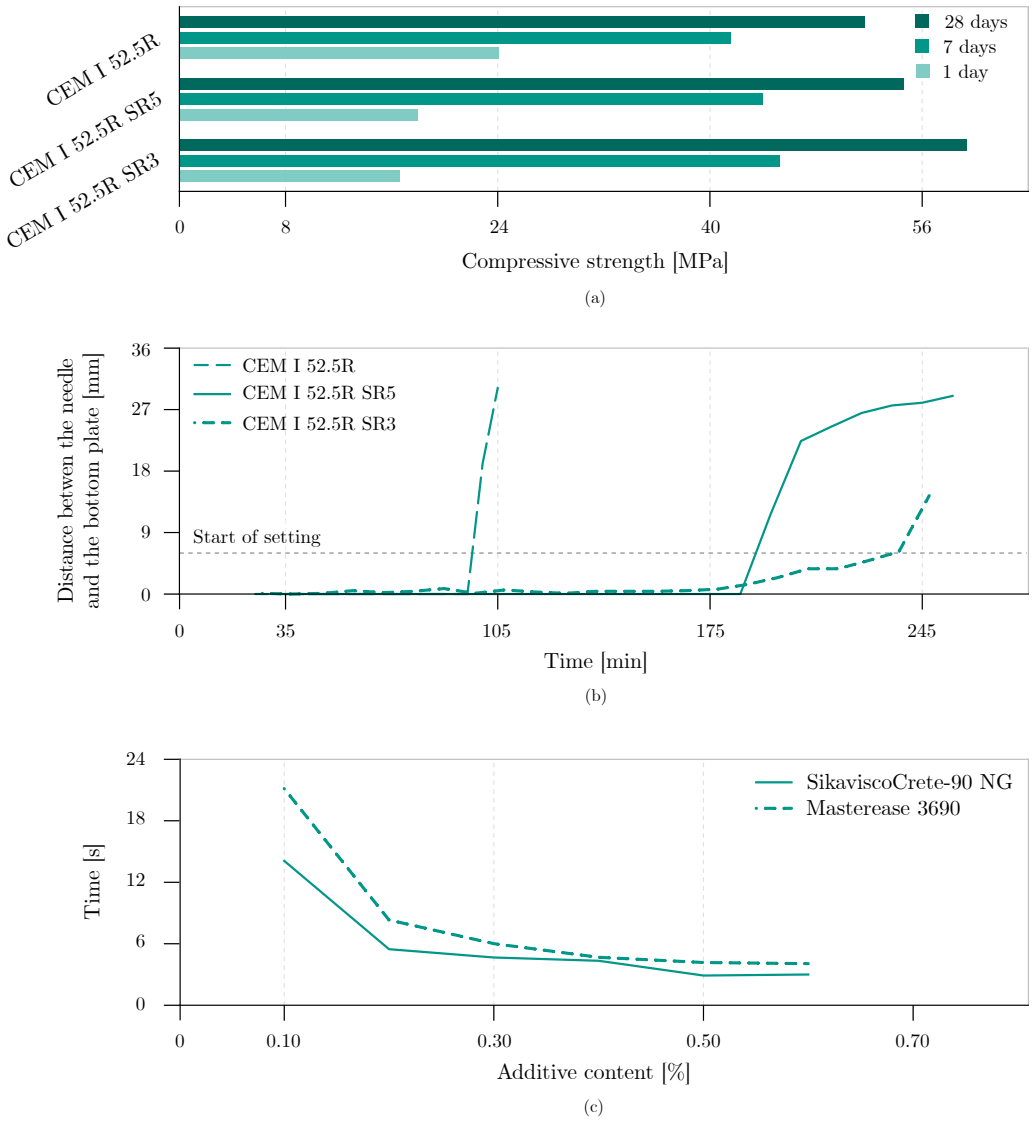

Figure 5.3: Tests results to define the cementitious matrix: (a) compressive strength at three ages of three different mortars, (b) penetration depth over time for three different cement pastes (results from the Vicat's apparatus), and (c) time for cement pastes to flow through the Marsh cone to study two different additives and the optimum additive content.

5.3.2 Reinforcing steel fibres

Using the concrete mix described in Table 5.1, nine different HPFRC mixes were prepared with various fibre types and contents. Specifically, five types of steel fibres were used (for geometrical and mechanical characteristics refer to Table 5.2). Four out of five are long fibres with a l_f ranging from 35 to 60 mm, and the other type (Masterfibre 482) is a short fibre

with l_f=13 mm. Three types of fibres have a direct tensile strength (σ_{fu}) between 1900 and 2200 MPa, while the other two have a σ_{fu} higher than 3000 MPa.

Table 5.2: Properties of steel fibres used in the HPFRC mixes.

Fibres	Length l_f [mm]	Diameter d_f [mm]	Aspect ratio λ_f [-]	Tensile strength σ_{fu} [MPa]
Bekaert 4D Plus 80/60 (4D+60)	60	0.75	80	2200
Masterfibre 482 (M482)	13	0.20	65	3100
Arcelor HE ++ 75-50 (HE+50)	50	0.75	67	1900
Arcelor HE ++ 55-35 (HE+35)	35	0.55	64	1900
Bekaert 3D 80/30 GGP (3DGGP)	30	0.38	80	3070

Table 5.3 presents the main characteristics of the nine different mixes, including the results from their mechanical characterization. In particular, the first three rows describe, respectively, their nomenclature, fibre type, and content (V_f). Next, the table includes the diameter of the flow table test (f) performed on a concrete mix sample as described in EN 12350-5 [113]. Finally, the table includes the mean compressive strength (f_{cm}) obtained from 3 cylinder specimens tested according to EN 12390-3 [114], the mean and average values of the residual strengths (f_{R1m}) and (f_{R3m}) obtained from 3 specimens tested using a 3-point notched bending test following the EN 14651 [4] are also reported.

Table 5.3: Definition of mix characteristics and results of mechanical characterization.

Mix	M1	M2	M3	M4	M5	M 6	M7	M8	M9
Fibres	4D+60	M482	4D+60	4D+60	HE+50	4D+60 HE+35	HE+35	HE+35	3DGGP
V_f [%]	1.00	1.00	0.88	0.75	0.75	0.44/0.44	1.00	1.50	1.50
f [mm]	590	600	500	570	420	430	480	380	310
f_{cm} [MPa]	126	137	136	136	109	113	128	163	130*
f_{R1m} [MPa]	17.81	9.99	17.38	14.64	16.26	13.69	16.08	18.50	18.04
f_{R3m} [MPa]	15.96	5.63	13.17	10.06	12.01	8.84	8.14	10.09	17.00
f_{R1k} [MPa]	13.82	6.67	12.76	11.65	14.50	5.92	12.96	15.61	9.40
f_{R3k} [MPa]	8.45	3.74	4.56	6.95	7.29	0.97	1.92	4.10	7.29

*Refers to the compressive strength at 7 days.

Figure 5.4 graphically illustrates the mechanical performances of the mixes in terms of f_{cm} (a), f_{R3k} (b) and f (c). The discontinuous line and the red area indicate the design requirements. Specifically, Figure 5.4 (a) shows that all mixes exceed the minimum compressive strength

(f_{cm}=108 MPa). It should be mentioned that M9, differently to all the other specimens, was tested at 7 days achieving the desired f_{cm}. This particularity is showed in the figure with a lighter colour in Figure 5.4 (a). Next, Figure 5.4 (b) presents the result of the bending tests in terms of f_{R3k}. The number of tests performed for each concrete mix is shown above the bars. The mix M1 reaches a f_{R3k}=8.45 MPa, which makes it the only mix achieving an acceptable post-cracking strength for the HPFRC-based alternative. Regarding the workability test, Figure 5.4 (c) depicts the flow value (f) obtained for each mixture, and the ranges for each workability class; these results are discussed later.

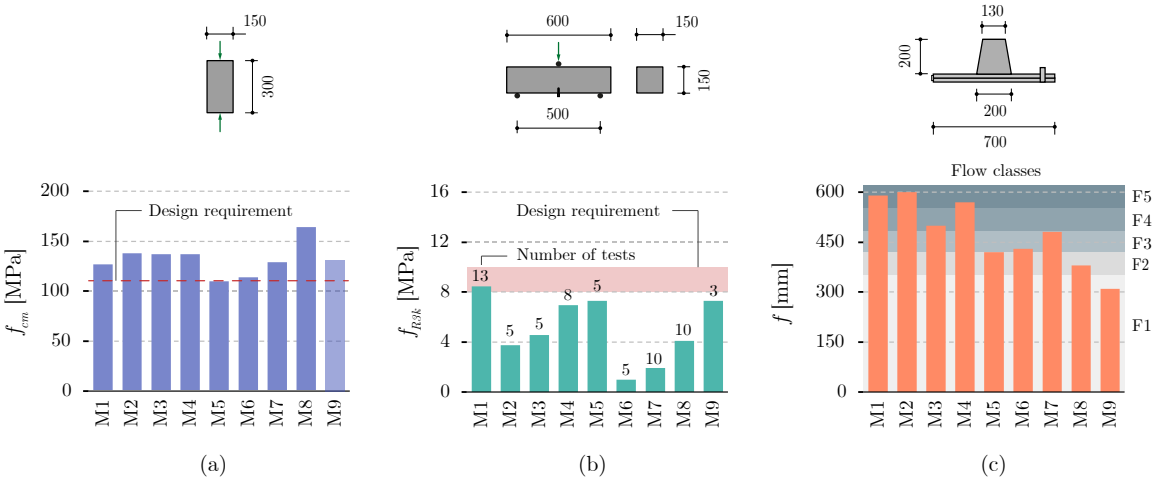

Figure 5.4: Comparison among nine concrete mixes developed with different type and content of fibres: (a) average compressive strength, (b) characteristic value of the residual tensile strength at CMOD=2.5 mm, and (c) diameter of the spread on the flow table test.

Figure 5.5 presents the experimental results obtained from the bending tests carried out on prismatic specimens (refer to Figure 5.4 (b) and EN 14651 [4]) with a notch at midspan to locate crack initiation. These experimental tests are essential to evaluate the residual bending strength of the concrete mixes. The experimental measurements during the test include the applied load (vertical axis) and the crack mouth opening displacement (CMOD) in the notch (horizonal axis).

Figure 5.5 depicts the results of the most significant mixes, those which provide insights into the relationship between the fibres used and their nominal bending strength: Figure 5.5 (a) corresponds to M1, Figure 5.5 (b) to M4, Figure 5.5 (c) to M8, and Figure 5.5 (d) to M7. The plots represent with a light line the result of the individual test, with a dark solid line the average curve, and with a dark discontinuous line the characteristic curve. The two parameters used in the design, f_{R1k} (CMOD=0.5 mm) and f_{R3k} (CMOD=2.5 mm), are

plotted with red dots and their values are shown in the graphs.

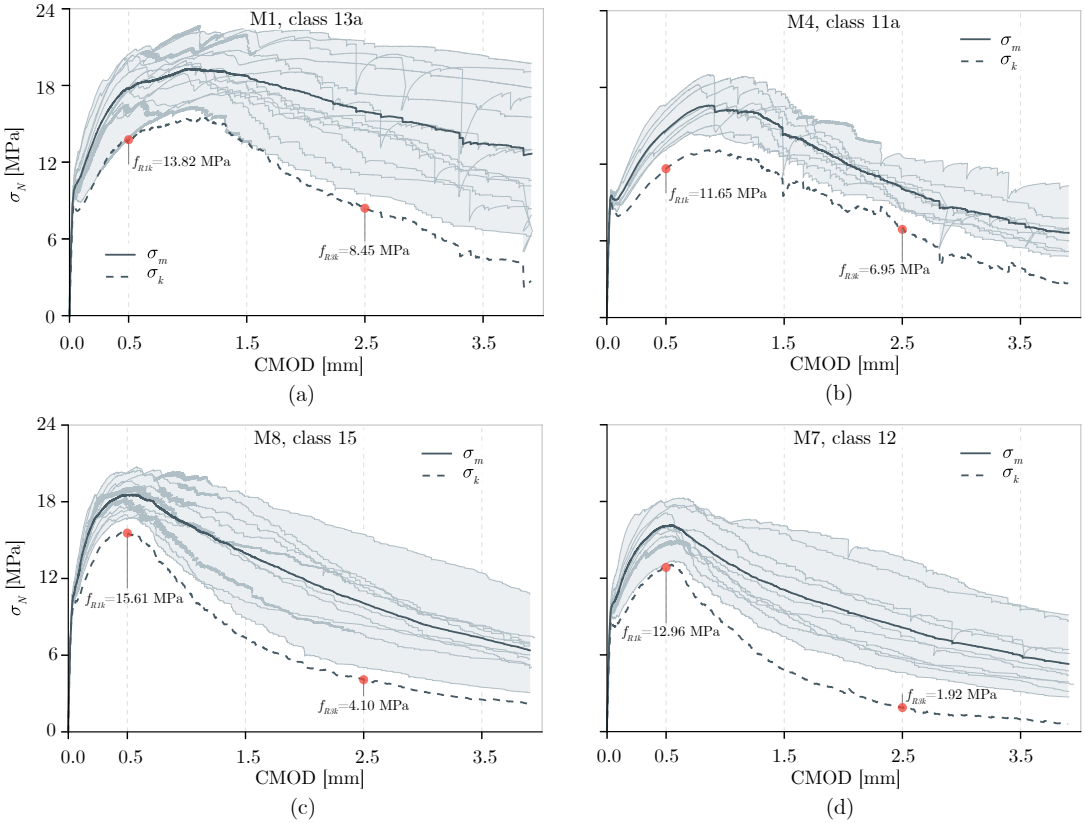

Figure 5.5: Results from the experimental characterization of the residual bending strength of the concrete mixes: (a) M1, (b) M4, (c) M8, (d) M9.

To shed light on the impact of fibre type and content on post-cracking bending behaviour, the average and characteristic curves for five different concrete mixes (M1, M4, M7, M8, and M9) are illustrated in Figures 5.6 (a) and (b). This set of mixes is characterized by three types of fibres (B 4 80/60+, HE++55-35, and B 3D 80/30GGP), and three fibre contents (60, 80, and 120 kg/m^3), as shown by the graphical legend on the right side.

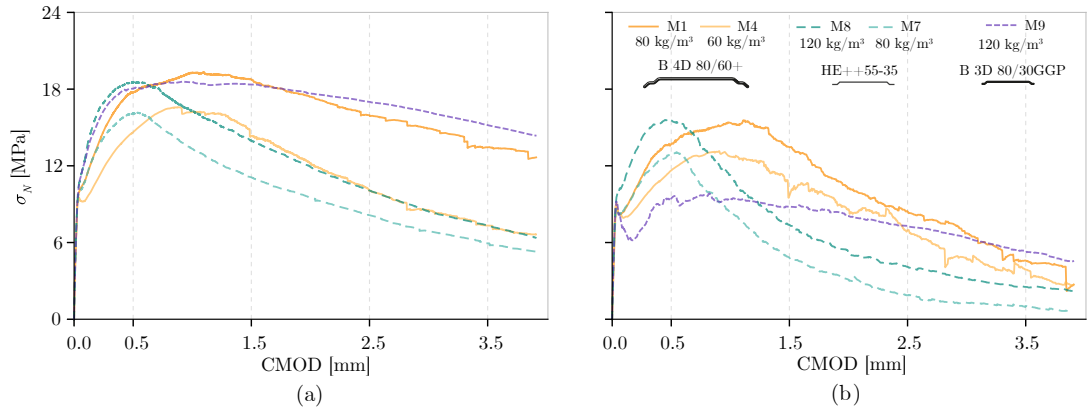

Figure 5.6: Results from the experimental characterization of the residual bending strength of the concrete mixes: (a) average curves from the mixes, and (b) characteristic curve from the mixes.

It should be noted that, although M1 has a 33% lower V_f than M8 and M9, the average curves of these mixes reached similar maximum nominal strengths. This can be attributed to the better anchorage provided by the plastic anchors available for the additional angle at the ends of the B 4D 80/60+ steel fibres. Similar conclusions can be drawn also from the comparison between M4 and M7. Furthermore, longer fibres provide more ductility to the mixes, which can also be deduced from the comparisons of curves between M1 with M8, and M4 with M7. The coefficient of variation (CV) of f_{R1} is the lowest for M8 (7.44%) and the highest for M9 (15.22%). Regarding the CV of f_{R3}, M4 and M7 presented, respectively, minimum (14.10%) and maximum values (36.41%). From this comparison, it can be concluded that M1 presented better flexural behaviour due to a higher f_{R3k} and ductility, with 80 kg/m^3 of fibre content. Furthermore, it showed an intermediate CV with values for f_{R1} and f_{R3} equal to 10.92% and 22.97%, respectively.

The flow table test is capable of detecting the segregation of a concrete mix batch. As an example, Figure 5.7 (a) and (b) illustrate an adequate and a segregated batch, respectively. The former exhibits uniform consistency of the concrete throughout the spread, while the latter lost most of the coarse fraction in the central area.

For the tailor-made HPFRC developed in this research appropriate workability was demonstrated. Moreover, the concrete mix exhibited good compatibility with various fibre types and quantities. However, for M9, the formation of 'fibre balls' occurred (Figure 5.7 (c)). As the concrete mix was well-designed, the authors attributed the appearance of these balls to an excessive number of fibres in the mix. Due to the high viscosity of the concrete mix,